INFORMATION TO USERS

This manuscript has been reproduced from the microfilm master. UMI films the text directly from the original or copy submitted. Thus, some thesis and dissertation copies are in typewriter face, while others may be from any type of computer printer.

The quality of this reproduction is dependent upon the quality of the copy submitted. Broken or indistinct print, colored or poor quality illustrations and photographs, print bleedthrough, substandard margins, and improper alignment can adversely affect reproduction.

In the unlikely event that the author did not send UMI a complete manuscript and there are missing pages, these will be noted. Also, if unauthorized copyright material had to be removed, a note will indicate the deletion.

Oversize materials (e.g., maps, drawings, charts) are reproduced by sectioning the original, beginning at the upper left-hand corner and continuing from left to right in equal sections with small overlaps.

Photographs included in the original manuscript have been reproduced xerographically in this copy. Higher quality 6" x 9" black and white photographic prints are available for any photographs or illustrations appearing in this copy for an additional charge. Contact UMI directly to order.

Bell & Howell Information and Learning
300 North Zeeb Road, Ann Arbor, MI 48106-1346 USA
800-521-0600

Study of the dynamics of driven periodic systems: Charge-density waves and superconducting rings

Mikko Karttunen
Centre for the Physics of Materials
Department of Physics
McGill University
Montréal, Québec
Canada

A Thesis submitted to the
Faculty of Graduate Studies and Research
in partial fulfillment of the requirements for the degree of
Doctor of Philosophy

Dedicated to Mom, Dad, Merja and Eemil.

CONTENTS

List of Figures

List of Tables

Abstract

We study the dynamics of two closely related periodic systems, superconducting rings and charge-density waves, using an approach based on pattern formation.

In the first part of the thesis, we concentrate on the onset of instability in a thin superconducting ring. A periodic instability appears when current is driven by an applied external voltage to the point of instability at temperatures below the critical temperature. The main contribution of this study is to investigate how the new state is selected when the system reaches the point of instability. That is, how the selection process is affected by different factors, such as the rate at which the system is driven. In addition, the generation of Ohmic resistance due to the dissipative phase slip state at the point of instability is studied. The problem of state selection at the onset of instability is a generic problem in pattern formation systems. Our results show that the onset of dissipation leads to strong non-linear effects in the state selection process.

In the second part of this thesis, we study the nonequilibrium behavior of driven charge-density waves in random media in two spatial dimensions. We propose a novel model for charge-density wave dynamics based on the Swift-Hohenberg equation. The advantage of our model is that it includes both amplitude and phase fluctuations of the condensate. We derive the model and show its formal relation to the almost universally used elastic models for charge-density waves. We demonstrate that phase slips proliferate close to the depinning transition thereby rendering a phase-only description invalid. Finally, using our model, we explain two recent experiments that cannot be captured by the traditional elastic approximation; the dynamical x-ray scattering experiments by Ringland et al. [99b], and low temperature transport experiments by Lemay et al. [99].

Résumé

On a étudié la dynamique de deux systèmes périodiques semblables, un anneau supraconducteur et une onde de densité de charges, en utilisant une méthode qui se base sur la formation de motifs ("pattern formation").

Dans la première partie de la thèse, on se concentre sur la formation d'instabilités dans un anneau mince supraconducteur. Une instabilité périodique apparaît lorsqu'une différence de potentiel externe est appliquée aux points d'instabilité à une température en-dessous de la température critique. Cette thèse cherche principalement à comprendre comment le nouvel état est choisi lorsque le système atteint le point d'instabilité. C'est-à-dire, comment le processus de sélection est affecté par différents facteurs, tel que le taux auquel le système est forcé. De plus, la résistance ohmique, généré par l'état dissipatif du glissement de la phase au point d'instabilité, est étudiée. Le problème de la sélection d'état au point d'instabilité est générique dans les systèmes avec formation de motifs. Nos résultats démontrent que le début de la dissipation est accompagné d'effets non-linéaires prononcés dans le processus de sélection d'état.

Dans la seconde partie de la thèse, nous étudions le comportement hors d'équilibre d'ondes de densité de charges dans un milieu aléatoire en deux dimensions. Nous proposons un modèle original, basé sur l'équation de Swift-Hohenberg, pour la dynamique d'ondes de densité de charges. L'avantage de notre modèle est qu'il inclut les fluctuations de l'amplitude et de la phase de l'état condensé. Nous effectuons la dérivation du modèle et nous démontrons formellement sa relation au modèle élastique qui est presqu'accepté universellement pour décrire les ondes de densité de charges. Nous démontrons qu'il y a prolifération du glissement de la phase près de la transistion de désancrage invalidant ainsi la description du glissement de la phase. Finalement, en utilisant notre modèle, nous expliquons deux récentes expériences qui ne sont pas bien décrites par l'approximation élastique traditionnelle; les expériences de diffusion dynamique avec des rayons-X de Ringland et al. [99b], et les expériences de transport à basse température par Lemay et al. [99].

Acknowledgments

First and foremost I would like to thank my supervisor, Professor Martin Grant, for providing me guidance, support, encouragement and freedom throughout my studies at McGill. I would also like to thank Professor Ken Elder of Oakland University. He has been, both directly and indirectly, involved in many stages of this research. It has been very enjoyable to collaborate with him. In addition, I would like to thank Professor Hong Guo for his enthusiastic and encouraging attitude and inspiring teaching.

During my final year I had the great pleasure to work with Mikko Haataja, a fellow graduate student. His tough questions led to countless discussions and debates, and they greatly helped to clarify many questions related to this work and to other physics problems. I also wish to thank to Nick Provatas and François Drolet for many fruitful discussions during the early stages of this study.

Furthermore, I wish to thank Juan Gallego for his help in computer related questions, and Paula, Diane, Joanne, and Lynda for administrative help. In addition, I would like to acknowledge the invaluable financial support from the Academy of Finland, the Finnish Cultural Foundation, the Finnish Academy of Science and Letters, and the Kordelin Foundation (Finland). The Center for Scientific Computing in Espoo, Finland provided part of the computational resources.

On a personal level, these years in Montreal have been eventful, to say the least. A lot has happened and many people have, one way or another, touched my life. I apologize for not mentioning you all by name, but please accept my heartfelt thanks.

Finally, I want to thank my parents for their unconditional support, and Merja and Eemil just for being there. This would not have been possible without you.

Study of the dynamics of driven periodic systems: Charge-density waves and superconducting rings

1

Introduction

1.1 *Pattern formation in physical systems*

The emergence of patterns in physical systems is an intriguing phenomenon displayed by diverse non-equilibrium systems, ranging from chemical reactions, to fluid flow, to optics and to superconductivity[1]. Pattern formation is generally a result of complex dynamical phenomena. In particular, the formation of macroscopic patterns is intimately related to symmetry breaking and instabilities in the system. Due to the non-equilibrium nature of pattern forming systems, the application of external driving forces and constraints may lead to spatially static, or spatio-temporal generation of patterns. Understanding the underlying selection mechanisms is a major task in all pattern formation problems. Perhaps the most well known, and studied, such system is Rayleigh-Bénard convection[2]; the primary instability leads from a uniform state to a convective roll pattern. Another well known example is the Mullins-Sekerka instability of solidification fronts[3].

The theoretical approach to pattern formation often takes the route of considering nonlinear partial differential equations. In most systems, these equations are complicated, and the exact analytical solution of the equations is impossible. These equations are often phenomenological and based on general symmetry considerations. A well know example is the Swift-Hohenberg equation[4] describing Rayleigh-Bénard convection. The difficulty in finding exact analytical solutions has lead to development of approximation techniques. A prime example are amplitude equations, i.e.,

[1] Langer [80]; Cross and Hohenberg [93] provide an excellent reviews.
[2] See e.g. Koschmieder [66]; Newell, Passot and Lega [93]
[3] See e.g. Langer [80].
[4] Swift and Hohenberg [77].

a method to find an equation of motion for the most unstable mode. In addition, in many cases there is an analogy between equilibrium phase transitions and the dynamical instabilities exhibited by pattern forming systems. This approach seems natural since both cases can involve a symmetry breakdown. However, there are important differences, and one should be careful in drawing too hasty analogies between equilibrium and dynamical properties.

In addition to the intrinsic properties of the pattern forming systems, i.e., emergence of instabilities and symmetry breakdown, the effect of randomness can have dramatic effects on their behavior. In the next section we review some central concepts related to quenched randomness, and after that we will provide the overview of this thesis.

1.2 Disordered systems

The effect of randomness on the dynamics of an ordered state is a generic problem arising in many different contexts. Examples of such system are diverse. They include charge-density waves (CDW)[1], flux line lattices in type-II superconductors[2], magnetic bubble arrays[3], flame front propagation[4] and fluid flow in porous media[5], to mention a few. Gaining insight into the rich phenomena displayed by these systems requires understanding the interplay between the internal degrees of freedom and randomness.

1.2.1 Randomness

Typically, disorder is classified as *quenched* or *annealed* randomness. Quenched disorder refers to imperfections whose motions are much slower than any relevant time scale in the problem at hand. Annealed disorder refers to the opposite case. Here, we will concentrate exclusively on the effects of quenched disorder. The effect of quenched randomness on ordered states has been the subject of increasingly intense study during the past decade. This is easily understandable: all real materials contain imperfections to a varying degree, and the imperfections, i.e., dislocations, vacancies,

[1] E.g. Fukuyama [76]; Fukuyama and Lee [78]; Lee and Rice [79]; Balents and Fisher [95]
[2] E.g. Fisher, Fisher and Huse [91]; Koshelev and Vinokur [94]
[3] Hu and Westervelt [95].
[4] Provatas et al. [95]; Karttunen et al. [98].
[5] Kessler, Levine and Tu [91].

interstitials, etc., can have drastic effects on the physical properties such as transport, mechanical properties and strength. Often, the effect of quenched disorder is to destroy long-range spatial order, e.g., periodicity, by pinning the system. Once a strong enough force is applied, the system can depin, and as the system, e.g., an interface, is set in motion, the effect of quenched disorder is effectively reduced to that of thermal noise.

Determining the effects of quenched randomness, i.e., random pinning, on ordered states has proven to be a formidable task. Qualitatively this can be seen as follows. Depending on the degree and strength of disorder, pinning may induce continuous elastic distortions or it may induce topological defects, e.g., dislocations and vortices. Whereas the former problem can be treated (at least to some extent) using the theory of elasticity, the latter needs a different treatment since topological defects are not continuous distortions of the ideal elastic state and cannot therefore be treated perturbatively. Even in the most simplified cell models[1], plastic deformations lead to unexpected behavior, rendering the mean-field treatment inadequate.

In the following we will give two examples that demonstrate the effect of disorder. First, we will discuss percolation, and in the second example we will demonstrate the existence of a depinning transition.

1.2.2 *Percolation: The effect of disorder on slow combustion*

We illustrate of the effect of quenched disorder by looking at slow combustion[2] in a random medium. The system is shown in Fig. 1.1.

On the coarse grained level, slow combustion can be modeled by a set of reaction-diffusion equations for the temperature field, coupled to a background of reactants and augmented by a term describing random temperature fluctuations for ignition. Physically, as the exothermic burning reaction generates heat, it is diffused away to the neighborhood and dissipated in the air due to (Newtonian) cooling. If the diffused heat is enough to cross the activation barrier and to ignite unburned reactants, the interface propagates. However, if the concentration of reactants is low, the heat that reaches the nearest neighbors of a burning area, is not necessarily enough to ignite

[1] Alava, Karttunen and Niskanen [95].
[2] Provatas et al. [95]; Karttunen et al. [98].

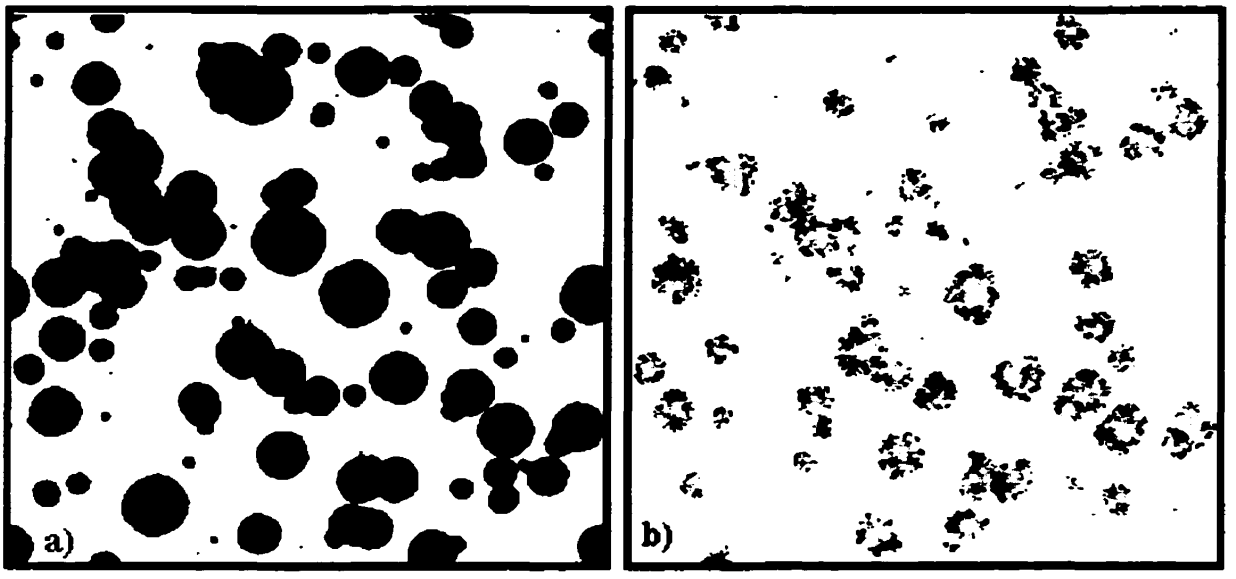

Figure 1.1: The effect of quenched disorder on nucleation and propagation of 'flame fronts' in slow combustion. The grayscale denotes the temperature with black being the hottest region. The systems in a) and b) are otherwise identical, except in a) the system has a uniform concentration of reactants and in b) each lattice site is filled with probability of 0.5. The patches of different size have been nucleated at different times. The fronts in the disordered case become rough and they propagate much more slowly as in the uniform case. From Karttunen et al. [98].

them and the front may stop. This is an example of a percolation transition, i.e., the velocity of the front approaches zero as the concentration of reactants approaches some non-zero limit — below that limit, the system is not connected anymore. This is a direct consequence of the presence of quenched disorder: when heat lost to thermal dissipation exactly balances that due to thermal reaction - that is dependent in the reactant concentration - the velocity of the interface becomes zero. Similar phenomena occurs in wide variety of systems.

The percolation transition is not the only effect of quenched randomness. For non-zero velocity, the randomness causes the interface to roughen[1] as it propagates. In a general sense, this can be thought of as a propagation of stable phase into an unstable phase; the interface separates the two phases, and thus knowing how the interface behaves gives insight into the physics of the phase transformation. A great number of problems ranging from flame front propagation, to biological problems, and charge-density waves (in the elastic limit) can be described in terms of interface propagation.

[1]See e.g. Krug and Spohn [90]; Barabási and Stanley [95]; Kuittu et al. [98].

The dynamics of driven interfaces are often described by the Kardar-Parisi-Zhang[1] equation, a generic equation of motion for driven interfaces.

1.2.3 *Depinning transition*

In addition to percolation and roughening, the presence of disorder can lead to pinning. To get a qualitative picture of this, we take a look at a very simple system: a small pointlike particle on a rough horizontal plane[2]. This is illustrated in Fig. 1.2. The roughness of the tabletop can be considered as quenched disorder since it does not change in time scales of interest here. The equation of motion for the particle is simply

$$m\frac{d^2r}{dt^2} = -\beta\frac{dr}{dt} + F_a - F_c, \tag{1.1}$$

where the first term on the right hand side is the dynamic friction, or the viscous force, the second term the applied driving force, and the last term the static friction. We will assume that inertial effects are negligible, i.e., the term on the left hand side becomes zero. When a small force $F_a < F_c$ is applied, the object remains stationary due to static friction, we say that the object is in the *pinned phase*; it remains stationary due to pinning by the randomness. However, a larger force $F_a > F_c$ will set the object in motion. After the transients die out, the object attains a static nonzero velocity $v \propto (F_a - F_c)$.

If we generalize the above to a system with many degrees of freedom, where instead of depinning a single particle, a collective system with internal interactions is considered, depinning becomes complicated. We have to modify Eq. (1.1) appropriately by adding the internal elastic interactions. Again, we assume that inertial effects are negligible. We can now write the equation of motion as

$$\beta\frac{dr}{dt} = F_a - f_p + \kappa[r], \tag{1.2}$$

where $\kappa[r]$ stands for internal elastic interactions. We have also replaced the static friction by a quenched random pinning force f_p. The form of $\kappa[r]$ depends on the nature of the interactions; for short-range interactions it is possible to use a gradient

[1] Kardar, Parisi and Zhang [86]; Krug and Spohn [90]; Barabási and Stanley [95].

[2] This example is adopted from the lectures by M. Kardar in the IX Summer School on Fundamental Problems in Statistical Mechanics, Altenberg, Germany 1997.

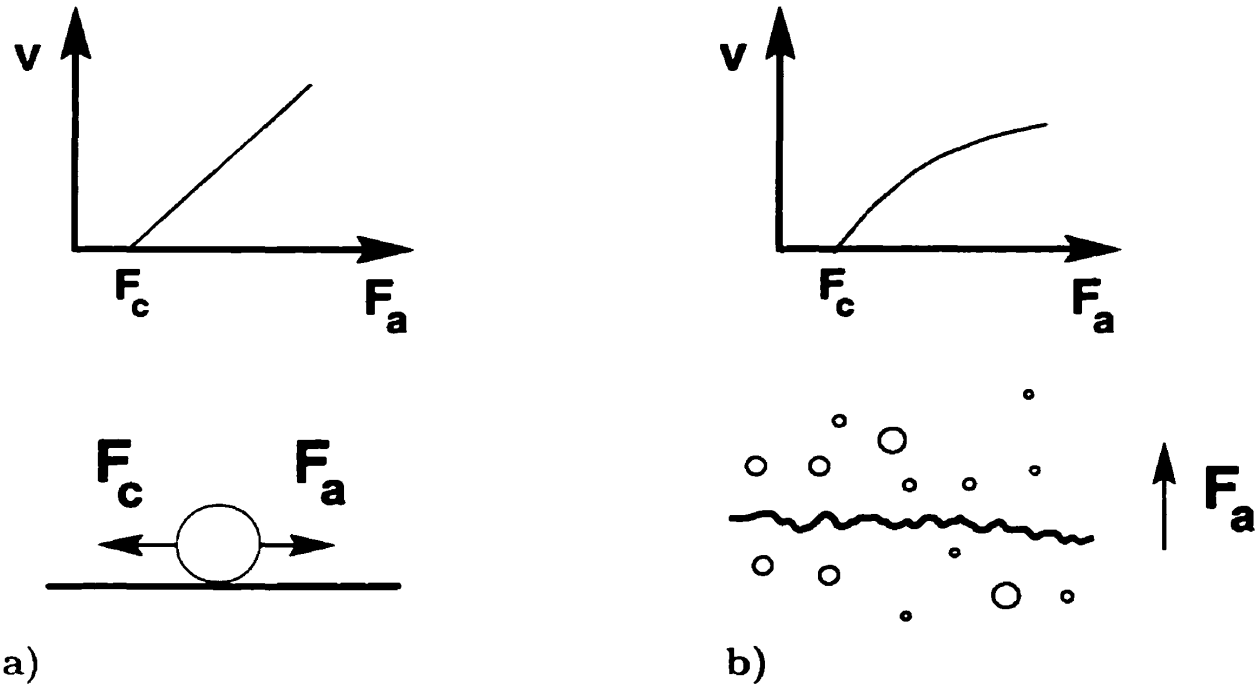

Figure 1.2: The force vs. velocity behavior at depinning transition two different systems. a) In the simplest case we can consider a small ball on a rough surface. b) In a system of many degrees of freedom, such as an interface the behavior becomes much more complicated.

expansion. Using a general formulation for the interactions, we can write the stress due to elasticity of the interface as

$$\kappa[r] = \int dr' \int dt' \{ K(r - r', t - t')[u(r, t) - u(r', t')]\} \tag{1.3}$$

where the kernel $K(r - r', t - t')$ describes the stress transfer. The precise form of the kernel depends on the nature of the elastic force. In the case of line tension, i.e. when $\kappa[r] \propto \nabla^2 u$, the kernel must take the form $\delta(t)\delta(r)\nabla^2$.

As long as the elastic behavior is preserved, the system (i.e., the interface) is singly defined. The interplay between the internal elastic interactions and random pinning leads to very rich physics[1]. In analogy with equilibrium critical phenomena, it has been conjectured[2] that depinning of an elastic interface is an example of novel dynamical critical phenomenon. In particular, the velocity and the correlation length should scale as

$$v \sim (F - F_c)^{\theta} \tag{1.4}$$

[1]See e.g., Barabási and Stanley [95] and references therein.
[2]Fisher [83]; Fisher [85].

$$\xi \sim (F - F_c)^{-\nu}. \tag{1.5}$$

These two formulas have two immediate consequences: Since the correlation length diverges as $F \to F_c$, the system will consist of domains whose length scale is defined by ξ, and secondly, as the system depins, it takes place at a well defined threshold field and it involves the whole system, i.e., it cannot rupture. Whether or not this occurs in experimentally accessible systems has been a subject of intense study over the recent years[1]. This conjecture was first introduced in the context of charge-density waves.

1.2.4 *Imry-Ma argument*

The above examples illustrated that quenched disorder has a profound effect on the static and dynamical properties. Now, we briefly review the so called Imry-Ma[2] argument that provides a qualitative condition for domain formation in the presence of quenched Gaussian random fields. In real systems, the quenched local random fields can be considered as static impurities and other imperfections. For concreteness, consider the random-field XY model with Hamiltonian

$$\mathcal{H}_{RFXY} = -J \sum_{<ij>} \mathbf{S}_i \cdot \mathbf{S}_j - \sum_i \mathbf{h}_i \cdot \mathbf{S}_i. \tag{1.6}$$

The spins $\mathbf{S}_i$ are classical spins restricted to xy-plane with $|\mathbf{S}_i| = 1$. The first sum runs over all nearest-neighbor pairs $\langle ij \rangle$, and the second term describes the coupling of spins to the quenched local random fields $\mathbf{h}_i$. J is the strength of the nearest neighbor interaction, which we will take to be ferromagnetic, i.e. $J > 0$. We assume the local random fields in Eq. (1.6) to be Gaussian, with zero average and short-range correlations, i.e.

$$\langle h_i \rangle = 0 \text{ and } \langle h_i h_j \rangle = h_0 \delta_{i,j}. \tag{1.7}$$

If we consider two neighboring domains of linear dimension L, there be will a domain wall separating the two different configurations. From the Hamiltonian in Eq. (1.6), we can immediately see that the energy cost[3] for creating a domain of volume L^d

[1] E.g. Fisher [83]; Fisher [85]; Robbins, Stokes and Bhattacharya [85]; Middleton and Fisher [91]; Narayan and Fisher [93]

[2] Imry and Ma [75].

[3] The energy argument becomes transparent when we notice that $\mathbf{S}_i \cdot \mathbf{S}_j = \cos\theta_{ij}$ with $\cos\theta_{ij} \approx 1 - \frac{1}{2}\left(\frac{\partial\theta}{\partial x}\right)^2$.

goes as L^{d-2} in d dimensions. Similarly, summing the random fields over a domain of volume L^d gives a contribution to the energy that goes as $L^{d/2}$. Comparison of the two energies shows that the random fields break the system into domains when $d \leq 4$. Since the argument depends only on symmetry and the range of interactions, it is quite general, and we can say that long-range order is not possible for $d \leq 4$ in systems of continuous symmetry in the presence of Gaussian random fields. Thus the presence of quenched randomness raises the lower critical dimension from $d_c = 2$ to $d_c = 4$. In essence, this is a result of competition between surface energy (domain walls) and volume energy (disorder). Furthermore, any non-zero temperature reinforces domain formation since entropy favors disorder (the free energy is the difference between the internal energy and entropy, $F = U - TS$). It is important to notice that the Imry-Ma argument is based on static properties of the system. As we will see in Chapter 4, taking dynamical effects into account may lead to different conclusions.

1.3 About this thesis

In this thesis we study two different nonlinear driven periodic systems using the pattern formation approach. In the first part of the thesis we concentrate on supercurrent flows in mesoscopic quasi-one-dimensional superconducting rings, and in the second part on the dynamics of charge-density waves subjected to quenched random disorder. Both of these systems are examples of periodic mesoscopic systems. Mesoscopic means that the relevant length scales may become of order of the system size. In addition, both systems we study are examples of collective systems where many degrees of freedom interact.

Our approach is based on pattern formation. This is a novel approach to nonequilibrium superconductivity and charge-density wave dynamics. However, as discussed, in pattern formation, the basic problem is to understand how different shapes and morphologies emerge in physical, chemical and biological systems under different conditions. This is exactly what we have in both cases: in the superconducting rings, due to the driving force, the superconducting condensate accelerates until it becomes unstable. The selection of a new state involves generation of topological defects, and it depends on various internal and external properties. This is a typical problem in

pattern formation.

Similar effects occur in charge-density waves. The pattern formation approach provides a novel method to study the dynamics of driven charge-density waves and the emergence of order and disorder in the system. This involves a subtle interplay between the internal degrees of freedom and randomness, and leads to a periodic generation of topological defects.

The above remarks serve as an introduction to the central concepts and phenomenology used in this thesis. An advantage of the pattern formation approach is that topological defects emerge naturally from the physical description of the problem. One of the general aims of the studies presented in this thesis is to gain understanding and insight to the complex macroscopic behavior exhibited by these seemingly simple systems. The hope is that this macroscopic viewpoint will help us to gain understanding the generic features of these, and related systems, despite of the different microscopic origin of them.

This thesis consists of the following chapters. In Chapter 2, we summarize various concepts relevant for the study on nonequilibrium superconductivity, and discuss the Ginzburg-Landau theory of superconductivity in detail. We introduce the general phenomenology and concepts to be used in connection of our original study.

In Chapter 3 we present our original study of state selection and nonequilibrium phenomena in voltage driven quasi-one-dimensional superconducting rings[1]. Despite their apparent simplicity, driven superconducting rings exhibit very rich behavior that can help us to gain more insight into the general problems in nonequilibrium statistical mechanics. In particular, we gain insight into the effect of periodically generated dissipation to state selection.

In Chapter 4 we review the basic concepts underlying the formation of charge-density waves in low-dimensional systems. First, we give a short overview to the microscopic physics behind charge-density waves. After establishing the relevant concepts and quantities, we review the most commonly used approach, and highlight some recent developments in both theoretical and experimental studies of the dynamics of charge-density waves.

[1] Karttunen et al. [99a].

In Chapter 5 we present a novel model[1] to study the dynamics of sliding charge-density waves subjected to quenched disorder. In contrast to the traditional approach based on the Ginzburg-Landau formalism, we have tackled the problem from the pattern formation point of view. Our approach is based on the Swift-Hohenberg equation[2]. First we motivate the model and show formally the connection to the Ginzburg-Landau approach both by perturbation theory and by deriving the corresponding amplitude equation. After that we present a mean-field analysis and numerical results for the system in two dimensions, we compare and contrast them to some recent experimental results. Chapter 6 concludes the thesis.

[1] Karttunen et al. [99b]; Karttunen et al. [99c].
[2] Swift and Hohenberg [77]; Pomeau and Manneville [79]; Cross and Hohenberg [93].

2

Ginzburg-Landau theory of superconductivity

2.1 *Introduction*

In this chapter we first provide a brief review to the developments in superconductivity following roughly the chronological order of discoveries[1]. Rather than attempting to give an extensive summary of the field, we provide a 'roadmap' to the principal concepts by highlighting some of the most important discoveries. Although not all the aspects are directly relevant to this work, it is important to see the relation between the many facets of superconductivity and their relation to nonequilibrium phenomena. We emphasize the issues that are pertinent to the original study in this thesis; after a brief review of the field, we discuss the Ginzburg-Landau theory in detail. The concepts and ideas discussed here will be applied to driven superconducting rings in the next chapter.

There exist a great number of textbooks and reviews covering various aspects of superconductivity. From the point of view of this study, the most useful ones are by de Gennes [66], Tinkham [96] and Tilley and Tilley [90]. This review is based on those books and further references can be found in them. In this chapter, we give references to the original publications only when they are directly relevant to the original work in the next chapter. A very extensive review of various aspects of nonequilibrium superconductivity has been given recently in Tidecks [90].

[1]Seven times the Nobel Prize in physics has been related to superconductivity: In 1913 H. Kammerlingh-Onnes; in 1962 L.D. Landau; in 1972 the Prize went to J. Bardeen, L. Cooper and J.R. Schrieffer; in 1973 the Prize was shared between B.D. Josephson, L. Esaki and I. Gieaver; in 1977 P.W. Anderson, Sir N.F. Mott and J.H. van Vleck were the laureates; in 1987 the Prize was awarded to K.A. Müller and J.G. Bednorz; and finally in 1991 P.-G. de Gennes was the sole recipient.

2.2 Superconductivity: Historical background

The discovery of superconductivity can be traced back to early this century. In 1908 H. Kammerlingh-Onnes managed to liquefy helium in his laboratory in Leiden in the Netherlands. This discovery marks the birth of modern low-temperature physics and led him to study the electrical conductivities of metals at low temperatures. Three years later, in 1911, he observed that, at temperatures below 4.2 K, mercury suddenly lost all dc electrical resistance, i.e., it became superconductive. The temperature where this transition takes place is called the critical temperature T_c, and it is a characteristic of a material. Furthermore, he later discovered that the zero resistance state was destroyed upon application of a sufficiently large magnetic field H_c. Experimental studies of the lifetimes of persistent currents in superconductors indicate very strongly that the perfectly superconducting state is indeed a state of zero resistance, not just a state of very low resistance[1].

However, the absence of electrical resistance alone is not enough to account for perfect superconductivity; magnetic properties have a crucial role. In their landmark experiment in 1933, W. Meissner and R. Ochsenfeld discovered that magnetic field is completely expelled from the interior of a superconductor when it is immersed in a magnetic field smaller than H_c, and then cooled below T_c. This is illustrated in Fig. 2.1. In pure superconductors T_c is typically of order 10K. H_c is temperature dependent, close to T_c it is typically of order 10^3G in pure superconductors. The expulsion of the magnetic field from the bulk of a superconductor is called perfect diamagnetism, i.e., the magnetic susceptibility $\chi = M/B$, where M is the magnetization and B is the intensity of the applied magnetic field, is negative. This is called the Meissner effect. Furthermore, their experiments demonstrated that the superconducting state is a state of thermodynamic equilibrium: it does not depend on whether the sample is first immersed in a field and then cooled, or vice versa. In zero field the phase transition from the normal state to the superconducting state is a continuous one.

Perfect conductivity alone is not sufficient to explain the observations of Meissner and Ochsenfeld. This can be seen for example by considering the Maxwell equation

[1] Experimentally the upper limit for resistivity in copper oxide superconductors has been set to $7 \times 10^{-23}\Omega$cm (Kedves et al. [87]).

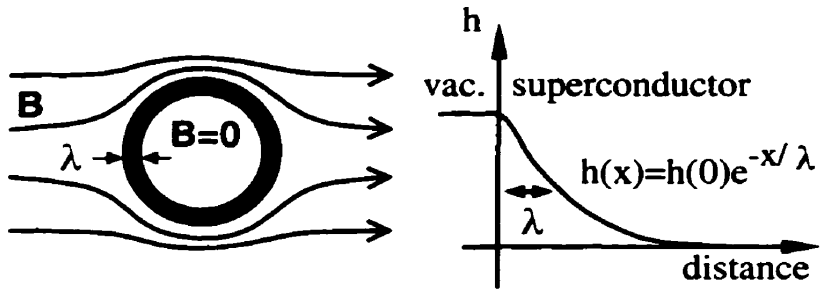

Figure 2.1: a) The Meissner effect. Magnetic field is excluded from the interior of a superconductor. b) The London theory predicts an exponential decay of the penetration length inside superconductor. λ is typically of order 100 Å.

for the electric field $\vec{E}$

$$\nabla \times \vec{E} = -c^{-1}\partial_t \vec{B}. \tag{2.1}$$

Since a superconductor has zero resistance, Ohm's law $\vec{E} = \rho\vec{J}$ indicates that the electric field $\vec{E} \to 0$ as the resistivity $\rho \to 0$. Combining this with Eq. (2.1) shows that there would be a frozen-in magnetic field left inside the superconductor. This is in contradiction with the experimental observations.

In 1935 F. and H. London proposed a phenomenological theory[1] to explain the two distinctive electrodynamic features of superconductivity, namely the zero resistance and perfect diamagnetism. The core of the London theory are two equations, usually referred to as the London equations:

$$\vec{E}(\vec{r}) = \frac{\partial}{\partial t}\left(\Lambda \vec{J}_s(\vec{r})\right), \tag{2.2}$$

and

$$\vec{h}(\vec{r}) = -c\left[\nabla \times \left(\Lambda \vec{J}_s(\vec{r})\right)\right], \text{ where } \Lambda = \frac{4\pi\lambda^2}{c^2} = \frac{m_e}{n_s e^2}. \tag{2.3}$$

In the London equations $\vec{h}$ is the local magnetic flux density[2], $\vec{E}$ is the electric field, $\vec{J}_s$ is the supercurrent density, c is the speed of light in vacuum, n_s is the number of density of superconducting electrons, m_e is the mass of an electron, e is the electron

[1] Originally, the London theory was proposed by postulating that the magnetic field is always identically zero inside a superconductor. That means, using the simple Drude model as an analogy, that the electrons have an infinite mean free path. However, in 1950, F. London showed that the theory can also be derived rigorously starting from the properties of the wave function.

[2] We follow the notation used in de Gennes [66] and Tinkham [96]: $\vec{h}$ is the local magnetic flux density, $\vec{B}$ is the macroscopic average value, and $\vec{H}$ is reserved for the thermodynamical field. In vacuum $\vec{B} = \vec{H}$. Distinction between the local and the average electric fields has no advantage for the present purpose.

charge, and λ is called the magnetic penetration length. Eq. (2.2) describes perfect conductivity; a constant electric field accelerates a current instead of maintaining it at a steady-state. The second London equation, Eq. (2.3), accounts for screening of the magnetic field, i.e., diamagnetism. This can be seen easily when Eq. (2.3) is combined with Maxwell's equations $\nabla \times \vec{h} = (4\pi/c)\vec{J}_s$ and $\nabla \cdot \vec{h} = 0$. This yields $\nabla^2\vec{h} = (1/\lambda^2)\vec{h}$. In a semi-infinite plane where, for example, $x < 0$ is vacuum and $x > 0$ is occupied by a superconductor, the solution is $h(x) = h(0)e^{-x/\lambda}$. This is an important result since it shows that *i)* the magnetic field decays exponentially in a superconductor and *ii)* that λ sets a length scale for $\vec{h}$ and $\vec{J}_s$. The London penetration length is a fundamental length scale that characterizes a superconductor, see Fig. 2.1b.

The magnetic penetration length characterizes the screening of magnetic fields inside a superconductor, but it does not provide information about the quantum mechanical coherence of the superconducting state: a second length scale is needed for that. The London theory describes local electrodynamics, and in 1953 A.B. Pippard suggested a nonlocal generalization of it. The idea behind it is simple: due to the quantum mechanical nature of the system, there must exist a characteristic coherence length for the wave function of the superconducting condensate. An estimate for the coherence length can be obtained easily by using the Heisenberg uncertainty principle: the electrons move with Fermi velocity, and in pure superconductors v_F is typically of order 10^8 cm/s, and the thermal phonon vibrations are characterized by the Debye frequency ω_D. Typically $\omega_D \sim 10^{13}$/s. Therefore, $\xi_0 \approx v_F/\omega_D = 1000$ Å. The reason why the electron-electron interaction does not affect the pair formation is that the screening length is of order of 1Å. ξ_0 is a fundamental length scale characterizing a pure superconductor. Pippard suggested further that, taking scattering into account, the effective coherence length becomes $1/\xi = 1/\xi_0 + 1/l$, where l is the mean free path characterizing scattering.

The major theoretical breakthrough in superconductivity was the microscopic theory by J. Bardeen, L.N. Cooper and J.R. Schrieffer (BCS) in 1957. The essence of the BCS theory is that superconductivity is a result of an attractive interaction between the electrons mediated by phonons. This interaction binds the electrons into Cooper

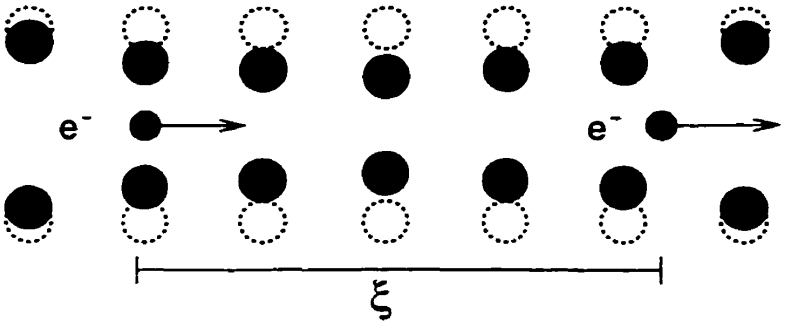

Figure 2.2: A schematic illustration of the electron-electron interaction mediated by the lattice. Propagation of an electron polarizes the lattice, i.e. deforms it. Due to the positive charge of the ions, the second electron sees the deformation as an attractive potential. This mechanism binds electrons into Cooper pairs.

pairs and leads to the formation of an energy gap E_g. The excitation spectrum has a threshold of $2E_g$, since to break a pair, two excitations of energy E_g must be created. The pair formation is due to the fact that the Fermi sea ground state of a metal is unstable against pair formation if there is an attractive interaction between the electrons — no matter how weak the interaction is. This is called the Cooper instability, and it is a direct consequence of the Pauli exclusion principle[1]. The wave function of the Cooper pair is spatially symmetric due to the fact that the electrons are in opposite spin state, i.e., in a spin singlet state. An illustration of Cooper pairing is given in Fig. 2.2.

Even before the BCS theory, there was strong evidence that superconductivity was related to phonons. Experiments had indicated that the critical temperature and the critical field are related to the ionic mass via $T_c \propto M^a$ and $H_c \propto M^b$, where a and b are typically close to 1/2. This is called the isotope effect. The BCS theory predicts $a = b = 1/2$ in the absence of Coulombic interactions between the electrons. In relation to this, H. Fröhlich proposed in 1950 a theory for superconductivity where phonons played an essential role. His theory turned out to be incorrect for superconductors but instead was the description for (incommensurate) charge-density waves. Due to this,

[1]The exclusion principle comes into play via the density of states. The Cooper derivation was based on full occupancy of all electron states below the Fermi level. Then, two electrons above the Fermi level form a bound state if there is even a weak interaction between them. Technically, the calculation involves a self-consistency condition which cannot be fulfilled unless the density of states is nearly constant and the exclusion principle forbids double occupancy of states; due to this, in the case of two classical particles, there exists a threshold for the attractive interaction to be able to form a bound state.

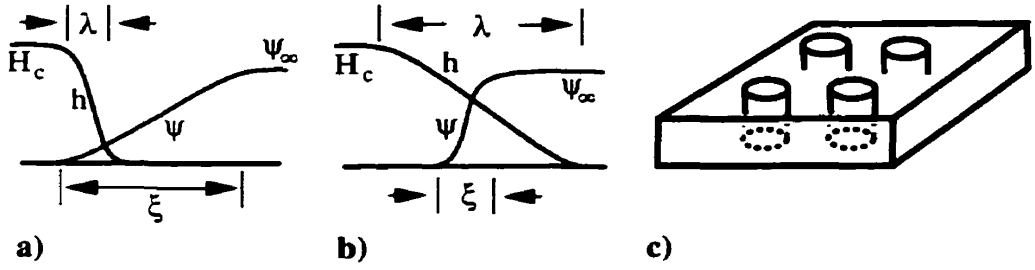

Figure 2.3: a) In type-I superconductors $\lambda(T) \ll \xi(T)$. b) In type-II superconductors the surface energy is negative, with $\lambda(T) \gg \xi(T)$, and therefore it is energetically favorable to create vortices, i.e., to maximize the amount of superconductor-metal interface. c) Vortex state.

charge-density wave conduction is often called Fröhlich conductivity. Charge-density waves and Fröhlich conductivity are discussed in detail in chapter 4.

Even before the BCS theory, V.L. Ginzburg and L.D. Landau (GL) suggested a phenomenological theory of superconductivity based on Landau's theory of continuous phase transitions. A central piece of the theory is the existence of an order parameter Ψ, a quantity that characterizes the emergence of order in the system; $\Psi = 0$ in the disordered phase (i.e., the normal state) and $\Psi \neq 0$ in the ordered state (i.e., the superconducting state). In analogy with quantum mechanics, GL introduced a complex-valued order parameter in such a way that the modulus of it is proportional to the number density of superconducting electrons, i.e., $n_s \propto |\Psi|^2$. The order parameter can be considered as an effective wavefunction for the superconducting condensate.

When it was published, the GL theory received only limited attention. This changed dramatically in 1959, when L.P. Gorkov showed rigorously that close to T_c the GL theory and the BCS theory become equivalent. Furthermore, two years before Gorkov, A. Abrikosov predicted the possibility of two different kinds of superconductors by using the GL theory. He calculated the normal-superconductor surface energy and by comparing the ratio between the coherence length and the magnetic penetration length he showed that the surface energy can become negative. If the surface energy is positive (generally called type-I superconductors,) the amount of interface is minimized. This occurs when $\xi > \lambda$. The interesting result was that when $\xi < \lambda$, the surface energy becomes negative (type-II superconductors), and interface creation is favored, see Fig. 2.3. This leads to creation of a vortex state, where a magnetic flux threads the superconductor, i.e., there are thin lines of normal

state inside the superconductor, Fig. 2.3c. Since the order parameter must be a single valued function, it turns out that the magnetic flux penetrates the superconductor in quantized units called fluxoids, of magnitude $hc/2e \approx 2.07 \times 10^{-7}$ G·cm^2. This was experimentally verified by W.A. Little and R.D. Parks in 1962. The Ginzburg-Landau theory is discussed in detail in the next section.

It is noteworthy that despite the very different behaviors exhibited by the two types of superconductors, the mechanism that leads to superconductivity is the same. It is an interesting anecdote that the London theory is actually applicable to type-II superconductors (in weak fields) and not to the pure superconductors that it was intended for. This is due to the fact that the London theory is local but in pure superconductors the electrodynamics is non-local, i.e., the electronic mean free path is typically quite long. However, in dirty superconductors electrodynamics is local since the mean free path is small.

As a last milestone we mention the discovery of high-T_c superconductivity in copper oxide compounds by J.G. Bednorz and K.A. Müller in 1986. Since then, this field has been one of the most active fields of research in condensed matter physics. However, we will not discuss the developments in that field. Tinkham [96] provides an excellent starting point to understanding various aspects in high-T_c superconductivity.

2.3 *Ginzburg-Landau theory for superconductivity*

In this section we discuss the GL theory of superconductivity in detail, and derive some results that will be used in the next chapter in our study of driven quasi-one-dimensional superconducting rings. Instead of treating superconductivity on the microscopic level like the BCS theory does, the GL theory is phenomenological. The underlying quantum mechanical coherence of the superconducting condensate is characterized by the wave function for the Cooper pairs, and its variations in space and time due to fluctuations and fields. To describe that, a proper order parameter is defined. This makes it suitable to study dynamical properties of the system. The GL approach is based on the phenomenological Landau theory for continuous phase-transitions. In the following, we will briefly review the Landau theory, and then apply it to superconductivity to obtain the Ginzburg-Landau theory.

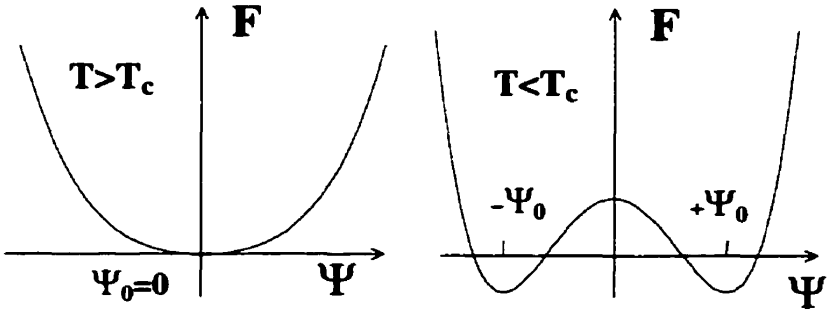

Figure 2.4: Schematic picture of the Landau free energy. Upon cooling below T_c the system undergoes a spontaneous symmetry breaking.

2.3.1 *Landau theory of continuous phase transitions*

The phenomenological Landau theory of continuous phase transitions stresses the importance of overall general symmetry properties and analyticity over microscopic details in determining the macroscopic properties of a system[1]. The validity of it is based on the following assumptions:

1. It is possible to define an order parameter Ψ, that characterizes the order in the system in the following way: $\Psi = 0$ in the disordered state (above T_c), and Ψ is small and finite in the ordered state (below T_c).

2. It is possible to describe the system with a free energy. Close to T_c, it can be expanded in powers of the order parameter, i.e.

$$F(\Psi) = \sum_{n=0}^{\infty} a_{2n} \Psi^{2n}, \tag{2.4}$$

   where F is the free energy, and the expansion coefficients are phenomenological parameters that depend on temperature and the microscopic properties of the system under consideration. Therefore, at least in principle, the a_{2n} can be derived from first principles. The smallness of the order parameter guarantees that the expansion converges, and can be truncated at a finite power.

3. The expansion, Eq. (2.4), of the free energy must be consistent with the high temperature symmetry properties of the system under consideration. Since the Landau theory describes continuous transitions, no odd powers are allowed in

[1] An excellent discussion is given in Goldenfeld [92].

the expansion of the free energy. When the system is cooled down to $T < T_c$ there is a spontaneous symmetry breakdown. This means that the ground state of the system has lower symmetry than the free energy shows: states $+\Psi_0$ and $-\Psi_0$ are equivalent but the system must select one of them, see Fig. 2.4. Mathematically speaking, the Hamiltonian must commute with the symmetry group of the high temperature phase.

4. The free energy must be analytic. In addition to analyticity in Ψ, it is also required that the expansion coefficients must be regular functions of the temperature. Since the second order term is dominant, $a_2(T)$ must vary smoothly from $a_2(T) < 0$ for $T < T_c$, to $a_2(T) > 0$ when $T > T_c$, with $a_2(T = T_c) = 0$. This implies that $a_2(T) \sim (T - T_c)$. To see this, we first minimize the free energy with respect to Ψ,

$$\frac{\partial F}{\partial \Psi} = 2a_2\Psi + 4a_4\Psi^3 = 0. \tag{2.5}$$

The solutions are

$$\Psi_0 = 0 \text{ and } \Psi_0 = \sqrt{-\frac{a_2}{2a_4}}. \tag{2.6}$$

The first is the high temperature solution, while the latter provides the minima for $T < T_c$. From Eq. (2.5) we can see that a_4 must be greater than zero, since otherwise $\Psi \to \infty$ would minimize the free energy rendering the above construction useless. Next, we Taylor expand the expansion coefficients around T_c:

$$a_2(T) \approx a_2(T_c) + (T - T_c)\frac{\partial a(T)}{\partial T}\bigg|_{T=T_c} + \frac{1}{2!}(T - T_c)^2\frac{\partial^2 a(T)}{\partial T^2}\bigg|_{T=T_c} + \dots, \tag{2.7}$$

and

$$a_4(T) \approx a_4(T_c) + (T - T_c)\frac{\partial a_4(T)}{\partial T}\bigg|_{T=T_c} + \frac{1}{2!}(T - T_c)^2\frac{\partial^2 a_4(T)}{\partial T^2}\bigg|_{T=T_c} + \dots . \tag{2.8}$$

As argued above $a_4(T) > 0$, and therefore we can approximate $a_4 = a_4(T_c) = \text{const.}$ This requirement is enough to guarantee the finiteness of the order parameter. Then, $a_2(T)$ must change its sign upon cooling below T_c. Then, $\frac{\partial a_2}{\partial T}\big|_{T=T_c} = const. > 0$, and $a_4(T) \sim (T - T_c)$.

The Landau theory is a mean-field theory since it does not take into account spatial inhomogeneities or thermal fluctuations. To take account of inhomogeneities, we have to let the order parameter become space dependent, i.e., $\Psi \equiv \Psi(\vec{x})$. Conceptually, we should think of Ψ as a coarse-grained order parameter, i.e., Ψ is defined only over a certain length scale. We must define a short wavelength (ultraviolet) cut-off for Ψ in such a way that Ψ varies smoothly in space; the order parameter cannot fluctuate on smaller length scales than the cut-off. In practice, the cut-off may often be thought of as the lattice spacing.

The response of the system to spatial inhomogeneities can be internal 'rigidity'[1]. Physically, it is clear that large differences between neighboring points are unfavorable. In other words, rigidity is a generic property of the system, and therefore there must an energy cost associated with spatial inhomogeneities. Since the order parameter is a smooth and slowly varying function, we can take the rigidity of the system into account by making a gradient expansion and retaining only the lowest order term compatible with the symmetry properties. The validity of the truncation of the gradient expansion depends on the smoothness and slowness of the order parameter variations.

Since the order parameter is now a local variable, the free energy in Eq. (2.4) becomes a functional of Ψ,

$$\mathcal{F}[\Psi] = \int d^d\vec{x} \left[F(\Psi) + \frac{1}{2} K (\nabla\Psi)^2 \right], \tag{2.9}$$

where K is a phenomenological parameter describing the rigidity of the system, and $F(\Psi)$ is the free energy defined in Eq. (2.4). Clearly, K must be positive for the free energy to be bounded from below.

2.3.2 *Ginzburg-Landau theory of superconductivity*

Now, let us apply the above to superconductivity. Our starting point is the free-energy functional in Eq. (2.9). The system is charged, and therefore we must transform Eq. (2.9) into a gauge invariant form. In practice this means that we have to include the vector potential $\vec{A}$ and replace the momentum term by the gauge invariant momentum.

[1] Anderson [84] provides an in-depth discussion about emergence and importance of rigidity in physical systems.

In analogy to the definition of the wave function in quantum mechanics, the superconducting state is characterized by a complex valued order-parameter $\Psi \equiv \Psi(\vec{x}, t)$ representing the underlying quantum mechanical coherence of the system. The order-parameter can be related to the density of the superconducting electrons via $n_s \propto |\Psi(\vec{x}, t)|^2$. It should be noted that $\Psi(\vec{x}, t)$ is not the wavefunction of the whole system, but can be considered as an effective wavefunction for the superconducting condensate.

The total free energy functional can be written as

$$\mathcal{F}\left[\Psi, \vec{A}\right] = \int d\vec{x} \left\{ \frac{\hbar^2}{2m_e} \left| \left(\nabla - i\frac{2e}{\hbar c}\vec{A} \right) \Psi \right|^2 + \alpha |\Psi|^2 + \frac{\beta}{2} |\Psi|^4 \right\} + (8\pi)^{-1} \int d\vec{x} (\nabla \times \vec{A})^2. \tag{2.10}$$

The first term is the gauge invariant kinetic energy term where $\vec{A}$ is the vector potential. It is followed by expansion of the free energy in terms of the order-parameter, and the last term is the magnetic field ($\vec{B} = \nabla \times \vec{A}$). The factor $2e$ is due to Cooper pairing, e being the electron charge, m_e the electron mass, c the speed of light and $\hbar$ Planck's constant. As above, the transition (to the superconducting state) is characterized by a change of sign in $\alpha(T)$, i.e., $\alpha(T) < 0$ for the superconducting state and $\alpha(T) > 0$ for the normal state. The other expansion coefficient β is assumed to be temperature independent. Here, we will always be working in the regime below T_c, i.e., $\alpha(T) > 0$. Since all the microscopics is buried in the coefficients, it is the overall symmetry properties that are most important. By analogy, universality classes in equilibrium critical phenomena are determined by symmetry properties and dimensionality.

The so-called GL equations are obtained from the free energy functional in Eq. (2.10) by requiring that variations $\delta F/\delta \Psi^*$ and $\delta F/\delta \vec{A}^*$ vanish. These are known as the stationarity conditions for the free energy. The additional condition that the variation $\delta F/\delta \vec{A}^*$ must vanish is due to the fact that the electromagnetic fields interact with the superconducting condensate. A straightforward calculation yields

$$-\frac{\hbar^2}{2m_e}\left[\nabla - i\frac{2e}{\hbar c}\vec{A}\right]^2 \Psi + \alpha\Psi + \beta\Psi|\Psi|^2 = 0, \tag{2.11}$$

$$\nabla \times (\nabla \times \vec{A}) = \frac{4\pi}{c}\vec{J}, \tag{2.12}$$

with

$$\vec{J} = \frac{e\hbar}{im_e}(\Psi^*\nabla\Psi - \Psi\nabla\Psi^*) - \frac{4e^2}{m_e c}\vec{A}|\Psi|^2. \tag{2.13}$$

As we shall see below, the GL equations provide the two characteristic length scales of superconductors, i.e., the magnetic penetration length λ and the coherence length ξ. However, since the GL equations are nonlinear, we can only solve them in certain special cases. An obvious solution is $\Psi = 0$, i.e., the high temperature solution for the normal state. It does not provide us with any information about length scales, and we have to look for a nontrivial solution. To find the solution for $T < T_c$, we assume that electromagnetic fields are absent and fix the gauge to $\vec{A} = 0$. With these assumptions and conventions, we can take Ψ to be real. Similar to the case discussed in connection with the London equation, we look for a solution in the case of a semi-infinite superconductor filling the area $x > 0$. This provides boundary conditions $\Psi(0) = 0$ and $\Psi(\infty) = 1$. Using Eq. (2.11) yields $\Psi(x) = \sqrt{n_s}\tanh(x/\xi)$ with $n_s = -\alpha/\beta$ and

$$\xi^2(T) = -\frac{\hbar^2}{2m_e\alpha}. \tag{2.14}$$

From this, we can see that ξ is a temperature dependent measure of the variations of the order parameter, and of the thickness of the surface layer in a superconductor. By using Eq. (2.13), we see that the supercurrents do not penetrate the interior of the superconductor, but flow only at the surface. At temperatures well below T_c in type-I superconductors, $\xi(T)$ is equal to the coherence length defined in the previous section. However, in general, that is not the case.

The second GL equation provides a measure for the range of variations of the magnetic field. Substituting Eq. (2.13) into Eq. (2.12), and taking a curl of both sides, yields a solution of type $B(x) = B(0)\exp(-x/\lambda)$ with

$$\lambda(T) = \left[\frac{m_e c^2}{16\pi e^2\Psi_0^2}\right]^{1/2}. \tag{2.15}$$

Therefore, $\lambda(T)$ determines the range of the variation for the magnetic field inside a superconductor. This is the magnetic penetration length discussed in connection with the London equations. In addition, Eq. (2.13) shows that variations in the supercurrent are due to variations in the phase of the order parameter, since the gradients of the amplitude cancel out.

The above discussion shows that the fundamental length scales arise naturally from the GL description. The possibility for the two types of superconductors discussed in the previous section can be seen by defining the surface energy per unit area for the normal-superconducting interface as

$$\sigma = \frac{1}{Area}\left(\mathcal{F} - \frac{1}{8\pi}\int d\vec{x} H_c^2\right), \tag{2.16}$$

and using a dimensionless ratio $\kappa(T) = \lambda(T)/\xi(T)$ called the Ginzburg-Landau parameter. The first term is the free energy of the superconductor and the second term is the condensation energy. Inspection[1] of Eq. (2.16) shows that there are two limits: when $\kappa(T) \ll 1$ the surface energy is positive and the amount of surface is minimized — this is the solution for type-I superconductors. However, when $\kappa(T) \gg 1$ the surface energy becomes negative and creation of vortices is preferred, see Fig 2.3.

2.3.3 *Existence of a critical current*

Before closing this chapter, we discuss the existence of a critical current in thin superconducting filaments. We assume that the thickness of the wire is much smaller than $\xi(T)$ and $\lambda(T)$. With this approximation, the amplitude of the order parameter ($\Psi = |\Psi|\exp(i\phi)$) can be considered constant. From the first London equation, Eq. (2.2), we see that the application of a field accelerates the supercurrent. However, an unlimited acceleration is clearly unphysical and there exists a critical current at which the superconducting condensate must make a jump to a new state of lower current, or undergo a transition to the normal state. The existence of a critical current can be seen using a thermodynamical argument known as Silsbee's criterion: The critical current can be associated with a thermodynamical critical magnetic field H_c. At I_c the current produces a magnetic field equal to H_c and the system must make a transition to a new state. It is noteworthy that the critical current determined by Silsbee's criterion comes from purely thermodynamical, i.e., equilibrium, considerations.

[1] The trick is to rescale the variables into a dimensionless form. After that, the only parameter that enters the calculation is κ. Similar rescaling will be done in the next chapter in connection with our model. Although it is straightforward, it is lengthy, so we omit the details of the rescaling and surface energy calculation here.

Next, we derive the critical current using the GL theory. Substitution of the order parameter into Eq. (2.13) yields

$$J_x = 2e|\Psi|^2 v_x, \tag{2.17}$$

where the velocity is

$$v_x = \frac{1}{m_e}\left(\hbar\nabla\phi - \frac{2e}{c}A_x\right). \tag{2.18}$$

Eq. (2.11) gives the minimum of the free energy with respect to $|\Psi|$ as

$$\frac{1}{2}m_e v_x^2 + \alpha + \beta|\Psi|^2 = 0. \tag{2.19}$$

Eliminating the velocity between the two equations, and finding the extrema for J_x with respect to $|\Psi|$ gives

$$J_c = \frac{4}{3\sqrt{3}}\frac{\hbar}{\xi(T)m_e}. \tag{2.20}$$

When the supercurrent reaches the critical current, various phenomena can occur depending on such factors as the driving force and the effect of fluctuations. That is one of the main aspects of our study in the next chapter.

2.4 Summary

In this chapter we have briefly reviewed some of the central concepts in superconductivity and discussed the Ginzburg-Landau theory in detail. We showed that the GL theory contains the fundamental length scales, i.e., the coherence length and the magnetic penetration length, and we demonstrated the existence of the critical current. These, and the other results derived here, will be put in use in the next chapter, where we present our original results for driven quasi-one-dimensional superconducting rings.

3

Non-equilibrium behavior of driven 1D superconducting rings

3.1 Introduction

In this chapter, we present our original study[1] of non-equilibrium behavior in voltage driven quasi-one-dimensional superconducting rings. The system consists of a thin superconducting ring of finite length driven by a voltage source. The electric field accelerates the supercurrent by acting as a smooth ramp. Eventually, the system reaches the critical current, becomes unstable, undergoes a dissipative phase slip state and makes a transition to a state of lower current. How the new state is selected, and how dissipation affects the state selection process, are some of the questions we address here. Despite the apparent simplicity of the system, it displays very rich and complex physics.

The system we study is mesoscopic, i.e., the superconducting ring has a finite circumference with a finite number of accessible states. This is how we define a mesoscopic system in this context. In other words, the mesoscopic character means that there is a finite number of metastable current-carrying states available. This is illustrated in Fig. 3.1. In addition to providing a prototype system to study various aspects involving driven systems in general, non-equilibrium superconductivity is of great interest *per se*. Indeed, the current-induced transitions in superconducting filaments have been a subject of intense experimental and theoretical study for almost three decades[2]. We have concentrated on current-induced phenomena, and in particular, on the emergence of the dissipative phase-slip state[3] in mesoscopic systems.

[1] Karttunen et al. [99a].
[2] Tidecks [90] provides a comprehensive review of the field.
[3] Rieger, Scalapino and Mercereau [72]; Skocpol, Beasley and Tinkham [74]; Kramer and Baratoff [77]; Kramer and Rangel [84]; Tarlie and Elder [98].

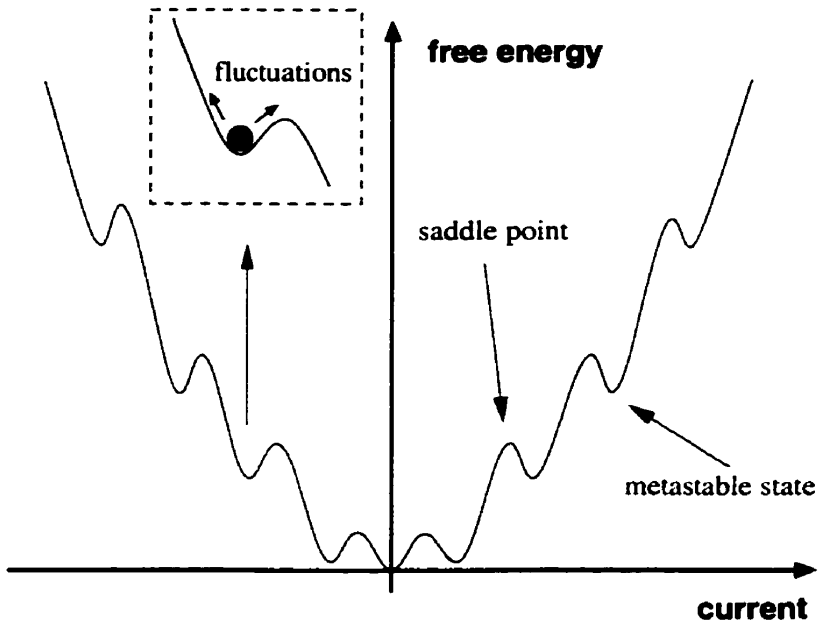

Figure 3.1: A schematic illustration of the free energy landscape in a superconducting ring. There are many metastable states available for a mesoscopic superconductor. If at some moment of time the system resides is one of the metastable states, it can make a transition to new state provided it can jump over the energy barrier. This can occur via thermal fluctuations (inset), or due to an application of an external driving force.

When a superconductor (below T_c) is driven (by voltage or current source) to the critical current, several interesting phenomena may occur: the system will enter the dissipative phase-slip state, Joule heating can take place, mode locking, as well as other phenomena, may occur. Here, we concentrate on the onset of dissipation, and its effect on the dynamics of the superconducting state.

The transitions between the current-carrying states can take place via two fundamentally different routes: *i)* by a nucleation process involving thermal fluctuations and an Arrhenius activation energy barrier, or *ii)* the system may be driven to an instability by an external driving force. In the context of nucleation and metastability, the decay of persistent currents in thin superconductors is an old and extensively studied problem[1]. However, the latter[2] involves a decay from a point of instability, and even in the general context of nonequilibrium dynamics it is a relatively poorly understood problem. One of the major difficulties is this: whereas in the case of nucleation the decay is from a metastable state involving thermal activation and a

[1] Little [67]; Langer and Ambegaokar [67]; McCumber [68]; McCumber and Halperin [70].
[2] Tarlie and Elder [98].

saddle point, in the latter case the external force drives the system to a point of instability where there is no energy barrier left, i.e., the energy landscape looks locally flat. Then, the decay and the final state depend on various factors, such as how fast the system was driven, the relative strength of fluctuations, internal excitations, and so on. This makes precise theoretical formulation of the problem difficult; it is not possible to use the free energy formulation as in the case of metastability.

In the previous chapter we discussed equilibrium properties of superconductors in terms of the Ginzburg-Landau theory. Here, we use the GL theory to study the dynamics of superconducting rings. We emphasize that many of the phenomena observed here are by no means limited to superconducting rings, but appear in many other physical systems ranging from pattern forming systems[1] to lasers[2]. The hope is that the simplicity of our system makes it possible to obtain information about some of the general questions in driven non-linear systems such as state selection and the effect of dissipation on the state selection process itself.

This chapter consists of the following sections. In the next section we introduce the system. After that, we discuss some general issues related to the critical current and the dissipative state. In Section 3.4 we study the stability of the current-carrying state by linear stability analysis with the aim of gaining insight into the subtle effects of dissipation to the state selection process. In Section 3.6 we present results from numerical simulations using the stochastic time-dependent Ginzburg-Landau equation and compare them to the predictions from the linear analysis. Finally, we discuss the relation of our results to experiments and to related problems in non-linear dynamics.

3.2 *The system*

As already mentioned in the previous section, the physical system we have considered is a thin superconducting ring of finite circumference. The driving force can be thought of being coupled to the system in the following manner. Consider an infinitely long solenoid carrying a linearly time-dependent current passing through the center of the ring. By Faraday's law of induction, there is a constant electromotive force acting

[1] See e.g. Kramer and Zimmermann [85]; Ben-Jacob et al. [85]; Kramer, Schober and Zimmermann [88]; Caroli, Caroli and Roulet [92]; Hernández-García et al. [93]

[2] Torrent and San Miguel [88].

on the superconducting condensate. From the first London equation, Eq. (2.2), we can see that this leads to a time-dependent increasing current. We now incorporate the driving force in the GL theory.

Since the current is induced in the loop by a time varying magnetic flux, we first include the effect of the induced electromotive force (emf) in the GL description. A schematic picture of the system is shown in Fig. 3.2. We now apply the Ginzburg-Landau theory of superconductivity to study this system. By Faraday's law of induction, the electrons in the loop are subjected to an emf

$$\mathcal{E} = -\frac{d\Phi(t)}{dt} = \oint \vec{E} \cdot d\vec{l}, \tag{3.1}$$

where $\mathcal{E}$ is the induced emf, $\Phi(t)$ is magnetic flux through the loop, and $\vec{E}$ is the electric field. The magnetic flux and the magnetic field are related by

$$\Phi = \int_{area} \vec{B} \cdot d\vec{S}_l, \tag{3.2}$$

where $\vec{S}_l$ is the area of the loop. We combine Eqs. (3.1) and (3.2), use the relation between the magnetic field and the vector potential, i.e., $\vec{B} = \nabla \times \vec{A}$, and Stokes'[1] theorem in order to obtain a relation between the vector potential and the induced electric field. We denote the tangential (i.e., the longitudinal) component of the field by E_x. This yields

$$E_x = -\frac{A_x}{ct}, \tag{3.3}$$

where A_x is the tangential component of the vector potential, c is the speed of light and t is the time. Since the induced emf is $\mathcal{E} = E_x L$, where L is the length of the wire, we obtain the vector potential in terms of the emf as

$$A_x = -\frac{\mathcal{E}}{L} ct. \tag{3.4}$$

The system we consider is quasi-one-dimensional, i.e., the radius of the cross-section of the superconducting filament is much smaller than coherence length and magnetic penetration length: $\sqrt{S} \ll \xi(T)$ and $\sqrt{S} \ll \lambda(T)$, respectively. The one-dimensional nature of the problem allows several helpful simplifications. First, since

[1] Stokes' theorem relates the rotation of a function in a region to its value at the boundary, i.e., $\int_{area} (\nabla \times \vec{V}) \cdot d\vec{S} = \oint \vec{V} \cdot d\vec{l}$ for an arbitrary vector function $\vec{V}$.

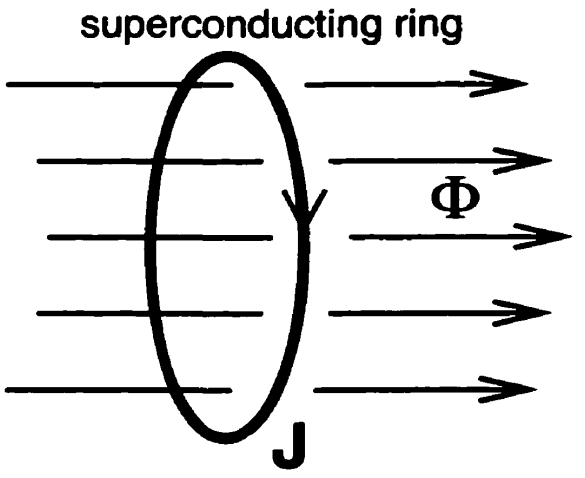

Figure 3.2: A current can be induced in a superconducting wire by subjecting it to a time dependent magnetic flux. For practical purposes one can imagine the magnetic flux to be due to an infinitely long solenoid passing through the center of the loop. That generates a magnetic flux as shown in the figure.

we are dealing with a narrow wire, the magnetic field generated by the supercurrent does not significantly influence the order parameter. This allows us to treat the vector potential A_x as a parameter instead of as a dynamical variable. In addition, since the magnetic field energy due to the supercurrent is much smaller than the energy associated with the order parameter, we drop the magnetic field term from the free energy[1]. It is possible to make one further simplification. Since we have a narrow wire, the order parameter does not change in the perpendicular directions and we can integrate them out from the GL free energy functional, Eq. (2.10). The integration yields a one-dimensional equation

$$\mathcal{F}[\Psi] = S \int dx \left\{ \frac{\hbar^2}{2m_e} \left| \left(\partial_x - i \frac{2e}{\hbar c} A_x \right) \Psi \right|^2 + \alpha |\Psi|^2 + \frac{\beta}{2} |\Psi|^4 \right\}, \tag{3.5}$$

where S is the cross-sectional area of the wire.

Thus far, we have not made any use of the circular shape of the system. Since the order parameter for superconducting condensate must be single valued, periodic boundary conditions emerge naturally, i.e.,

$$\Psi(x) = \Psi(x + L). \tag{3.6}$$

For further analysis and computational efficiency it is convenient to move into dimen-

[1] Langer and Ambegaokar [67].

sionless units. For that we use the following transformations:

$$\begin{cases} \Psi' & \equiv & (\beta/|\alpha|)^{1/2}\,\Psi \\ x' & \equiv & x/\xi \\ A' & \equiv & 2e\xi A/\hbar c \\ v'_{ec} & \equiv & v_{ec}2e\tau_{GL}/\hbar, \end{cases} \tag{3.7}$$

where $\xi^2 = \hbar^2/(2m|\alpha|)$. We have used $|\alpha|$ instead of α since we are always below T_c. τ_{GL} is the Ginzburg-Landau time defined as

$$\tau_{GL} = \frac{\pi\hbar}{8k_B(T_c - T)}. \tag{3.8}$$

The last transformation involves v_{ec}, the electrochemical potential generated by the normal current. It will be introduced in the next section where the GL theory is extended to include phase slips and normal current generation. We have defined the transformation here for consistency.

Performing the transformations defined in Eqs. (3.7) on the one-dimensional GL free energy functional in Eq. (3.5), we obtain

$$\mathcal{F}[\Psi] = \frac{S\xi H_c^2}{4\pi}\mathcal{F}'[\Psi'] = \frac{S\xi H_c^2}{4\pi}\int dx' \left\{ |(\partial_{x'} - iA'_{x'})\,\Psi'|^2 - |\Psi'|^2 + \frac{1}{2}|\Psi'|^4 \right\}. \tag{3.9}$$

We now drop the primes from the transformed quantities, and in the following use the dimensionless quantities and free energy unless otherwise mentioned.

Following the scalings in Eqs. (3.7), it is natural to measure the length in units of the coherence length as

$$\ell = L/\xi. \tag{3.10}$$

Then, the rescaled boundary condition in Eq. (3.6) reads

$$\Psi(x) = \Psi(x + \ell), \tag{3.11}$$

and the free energy in Eq. (3.9) becomes

$$\mathcal{F} = \int_{-\ell/2}^{\ell/2} dx \left\{ |(\partial_x - iA_x)\,\Psi|^2 - |\Psi|^2 + \frac{1}{2}|\Psi|^4 \right\}. \tag{3.12}$$

Now, we need a dynamical description for the condensate. We use relaxational dynamics to obtain a stochastic time-dependent Ginzburg-Landau (STDGL) equation of motion, i.e.,

$$\frac{\partial\Psi}{\partial t} = -\frac{\delta\mathcal{F}}{\delta\Psi^*} + \eta, \tag{3.13}$$

with $\eta \equiv \eta(x,t)$ being an uncorrelated Gaussian noise source as a function of position x and time t

$$\begin{cases} \langle \eta(x,t) \rangle = 0 \\ \langle \eta(x,t)\eta(x',t') \rangle = 2D\delta(x-x')\delta(t-t'). \end{cases} \tag{3.14}$$

The angular brackets denote an average, and D is the intensity of the noise determined by the fluctuation-dissipation[1] theorem as

$$D = \frac{2\pi k_B T}{S H_c^2 \xi}. \tag{3.15}$$

Time is measured in the units of the Ginzburg-Landau time (Eq. (3.8)), i.e., $t \to t/\tau_{GL}$.

To make the model numerically more tractable, we will make the transformation[2] $\Psi \to \Psi e^{iq(t)x}$, with

$$q(t) = q_0 + A_x = q_0 + \omega \ell^{-1} t, \tag{3.16}$$

q_0 being an arbitrary constant and

$$A_x = -\frac{2eV}{\hbar \ell} t = \frac{\omega}{\ell} t. \tag{3.17}$$

This transformation twists, or winds, the order parameter along the wire. The effect of the transformation is to map the current carrying states to twisted plane waves as illustrated in Fig. 3.3. After the transformation, the periodic boundary condition becomes

$$\Psi(\ell + x, t) = \Psi(x,t) e^{iq(t)\ell}, \tag{3.18}$$

and the equation of motion obtained from Eq. (3.13) reads as

$$\partial_t \Psi = \partial_x^2 \Psi + \Psi - \Psi |\Psi|^2 + i\ell^{-1}\omega x \Psi + \eta. \tag{3.19}$$

This formulation still neglects the electrochemical potential due to normal current generation at a phase slip center. The inclusion of it is discussed in the next section.

[1] McCumber and Halperin [70].
[2] Byers and Yang [61]; McCumber and Halperin [70].

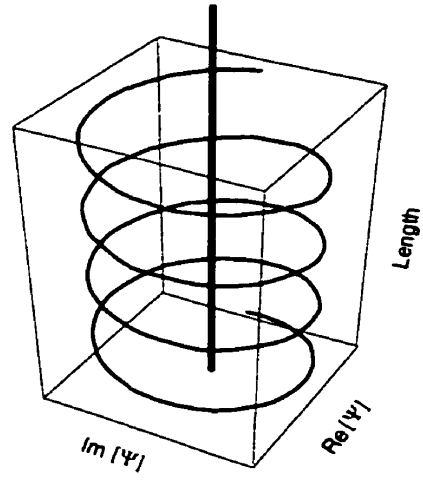

Figure 3.3: Illustration of the current carrying states as uniformly twisted plane waves. At a phase slip the amplitude of the helix approaches zero, and it reduces the current by removing one loop. The line through the center of the helix represents the superconducting wire.

3.2.1 *Electrochemical potential*

Eq. (3.19) would be a sufficient description if we could neglect the generation of a normal current at a phase slip. While this is a valid approximation in a certain limit[1], (this will be discussed in 3.4) our aim is to study the effect of the resistive normal current to the process, and therefore we want to generalize the equation of motion in Eq. (3.19) by including the electrochemical potential.

A phase slip is a point where the system locally loses superconductivity and becomes a normal Ohmic conductor. As discussed above, below T_c the system retains the fully superconducting state after making a transition to a state of lower current. The effect of the generation of normal current on the dynamics is an important question. If the system is driven by a current source, the current is an independent variable. However, to study state selection, it is more convenient to drive the system using a voltage source; the system is periodically driven to the critical current, where it encounters an instability and makes a spontaneous transition to a new state of lower current.

Here, we consider only the voltage driven case. Apart from fluctuations, the normal current is zero between the phase slip events. Because the appearance of a phase slip introduces a (quasi) periodically appearing differential resistance, it is difficult to

[1] McCumber and Halperin [70]; Tarlie and Elder [98].

use qualitative arguments about the importance of the normal current. We will now include the electrochemical potential generated by the normal current in the equation of motion, and in the following sections we study its effects by linear stability analysis and numerical simulations.

To take the generation of normal current into account, we have to replace ∂_t in the STDGL equation of motion in Eq. (3.19) by $\partial_t + iv_{ec}$, where $v_{ec} \equiv v_{ec}(x,t)$ is the electrochemical potential generated by the normal current[1]. With that substitution, our final dimensionless equation of motion becomes

$$\left(\partial_t + iv_{ec}(x,t)\right)\Psi = \partial_x^2\Psi + \Psi - \Psi\left|\Psi\right|^2 + i\ell^{-1}\omega x\Psi + \eta. \tag{3.20}$$

Physically, the appearance of the electrochemical potential is due to local charge imbalance in a superconductor. Gorkov[2] was the first to point out that in a superconductor the Fermi level, and thus the electrochemical potential, is a local time-dependent variable related to the coherence of the superconducting state[3]. Qualitatively, if the local charge balance is disturbed, the Fermi level experiences a local time-dependent perturbation. This in turn affects the local energy gap. Gorkov showed that gauge invariance is preserved, if the order parameter depends on time as $\exp(-2i\mu_F t/\hbar)$ where μ_F is the Fermi energy. This leads to the second term on the left hand side in Eq. (3.20).

Since we have a closed superconducting ring into which the current is induced, the total charge is conserved, i.e.,

$$\partial_x(J_n + J_s) = 0, \tag{3.21}$$

where J_n is the normal current and J_s is the supercurrent, the total current being $J = J_s + J_n$. Using Ohm's law for the normal current we obtain,

$$J_n = \frac{1}{\alpha}\frac{\partial v_{ec}}{\partial x}, \tag{3.22}$$

where α is a measure for Ohmic resistance and v_{ec} is the electrochemical potential.

[1]Stephen and Suhl [64]; Anderson, Werthamer and Luttinger [65]; Schmid [66]; Abrahams and Tsuneto [66]; McCumber and Halperin [70].
[2]Gorkov [58].
[3]Historically, this led Josephson to study coherence in superconductors.

Combining Eqs. (3.21) and (3.22) gives[1]

$$\frac{\partial^2 v_{ec}}{\partial x^2} = -\alpha \frac{\partial J_s}{\partial x}, \tag{3.23}$$

Our final equations that we use in the calculations are Eqs. (3.20) and (3.23).

3.3 *Critical current and phase slip revisited*

Before giving our results, we discuss the critical current and phase slip further, and introduce two useful quantities that will be used in our analysis: the spatially averaged supercurrent and the winding number.

Kramer and Baratoff [77] (KB) studied current-driven quasi-one-dimensional superconducting rings, and pointed out that the thermodynamical critical current (as derived in the previous chapter) provides only a limit of metastability for the zero-voltage superconducting state. How dissipation and non-equilibrium effects affect that picture is not clear. The nature of the driving force is of importance; in the current-driven case the system is maintained at a constant current, but in the voltage-driven case — that we study — the current increases up to the critical current, where it becomes unstable and has to make a transition to a new state of lower current. KB used a current driven system and discovered that in the vicinity of the thermodynamical critical current there exists a narrow range where a stable state of spontaneous oscillations of phase slips exists. This is an important result. Due to the nonlinear and dynamical nature of the problem, it is difficult to prove analytically the existence of a stable phase slip solution for the equation of motion. The numerical results of KB were the first theoretical or computational proof for such a solution.

Experimentally[2], the signature of a stable phase slip state is the appearance of voltage steps in the current-voltage characteristics. When a state with a phase slip center is stable, an increase in current produces only a very small increase in voltage, but when the current again reaches the critical current there is an abrupt jump in voltage to a state with two active phase slip centers. Depending on the length of the sample, there can be several active phase slip centers, each corresponding to a step

[1] There should be no danger in mixing α from the GL equation to α as defined here. We have transformed the equation of motion to make it dimensionless, and α, as defined in connection with the GL equations was scaled away.

[2] Webb and Warburton [68]; Skocpol, Beasley and Tinkham [74]; Dolan and Jackel [77]; Tidecks [90].

in the I-V characteristics. However, as the length of the sample increases, the fine structure of the steps is gradually washed away; a mesoscopic sample can support only a finite number of phase slip centers, but in an infinite sample the number of phase slips, i.e., the density, can vary smoothly as a function of the current.

Our system is driven by a voltage source, and some of the phenomena that we observe are qualitatively different from KB; here, the driving force accelerates the supercurrent leading to an instability, and to a subsequent recovery of the perfectly superconducting state. This cycle is repeated (quasi) periodically. This is very different from the current driven case[1], and from the decay of supercurrents via spontaneous fluctuations[2].

At the phase slip, the system becomes locally metallic and has Ohmic resistance. Due to the resistance, heat is generated. If the heat generated is not large enough to destroy the superconducting state, the system will make a jump to a state of lower current carrying state; this is possible when $T < T_c$. Generally, these kinds of transitions are called current-induced transitions.

A demonstration of the phase slip can be given by using a Josephson junction. If there is an accelerating supercurrent, then the rate of change for the phase difference between the two ends of the superconducting wire is given by the Josephson relation

$$\frac{d(\Delta\phi)}{dt} = \frac{2eV}{\hbar}, \tag{3.24}$$

where ϕ is the phase of the order parameter, and V is the voltage difference between the two ends of the wire. This follows from gauge invariance. The phase is related to the velocity ($\Delta\phi = qL$) of the condensate, and since the supercurrent is related locally to the phase via $J_s \sim |\Psi(x)|^2 \partial_x \phi$ (from Eq. (2.13)), the phase difference must grow as $|\Psi(x)|^2$ becomes smaller, in order to maintain a constant current. Then, as $|\Psi(x)|^2 \to 0$, the system can remove a loop in order to relax[3] — the phase difference is reduced allowing the amplitude to recover. Phase slip reestablishes the phase coherence in the system. The jump can only take place in integral multiples of 2π: persistent current in a ring can only exist if $\oint \nabla\phi dx = 2n\pi$, where n is an integral

[1] Rieger, Scalapino and Mercereau [72]; Skocpol, Beasley and Tinkham [74]; Kramer and Baratoff [77]; Kramer and Rangel [84].
[2] Little [67]; Langer and Ambegaokar [67]; McCumber [68]; McCumber and Halperin [70].
[3] Little [67]; Langer and Ambegaokar [67].

number. This is the reason for the name 'phase slip'. The situation is illustrated in Fig. 3.3; since the helix describes the real and imaginary parts of the order parameter, the local amplitude of the helix is given by $|\Psi(x)|$, and $2\pi/q$ is the pitch.

Due to dissipation, this analogy to a Josephson junction is not exact. Phase slip is, by definition, a dissipative process where a finite amount of condensation energy is lost, thus providing an intrinsic mechanism for dissipation. At the microscopic level, it leads to various subtle charge imbalance effects[1]. The above analogy neglects that.

One method to characterize the phase slip is to measure the supercurrent. In our dimensionless notation the supercurrent, Eq. (2.13), is

$$J_s(\Psi) = -\frac{i}{2}\left[\Psi^*\left(\partial_x - iA_x\right)\Psi - c.c.\right]. \tag{3.25}$$

Instead of using the local instantaneous supercurrent, the spatially averaged supercurrent at time t is the quantity that provides information about the dynamics of the condensate,

$$J_s(t) = \frac{1}{2\ell}\int_0^\ell J_s(\Psi)dx. \tag{3.26}$$

Another useful quantity is the winding number. It is a measure of how much the phase changes along the system. The winding number is defined as

$$W(t) = \frac{1}{2\pi}\int_0^\ell dx \frac{\partial\left[\arg\left(\Psi(x,t)\right)\right]}{\partial x}. \tag{3.27}$$

As described above, the order-parameter can change its winding number by $2\pi n$, where $n = \pm 1, \pm 2...$ Only changes by an integral multiple of 2π are possible in order to preserve the continuity of the order-parameter. This also implies that at a single (multiple) phase slip, the system removes exactly one (integral multiple) fluxoid.

3.4 *Linear stability analysis*

In this section we will study the Eckhaus instability[2] by linear stability analysis. The Eckhaus instability is a longitudinal secondary instability that appears in many systems exhibiting spatially periodic patterns[3], when transverse variations can be neglected. In systems with higher dimensionality, several other instabilities may become

[1] Tidecks [90].
[2] Eckhaus [65]; Kramer and Zimmermann [85]; Kramer, Schober and Zimmermann [88]; Tuckerman and Barkley [90].
[3] Dominquez-Lerma, Cannell and Ahlers [86].

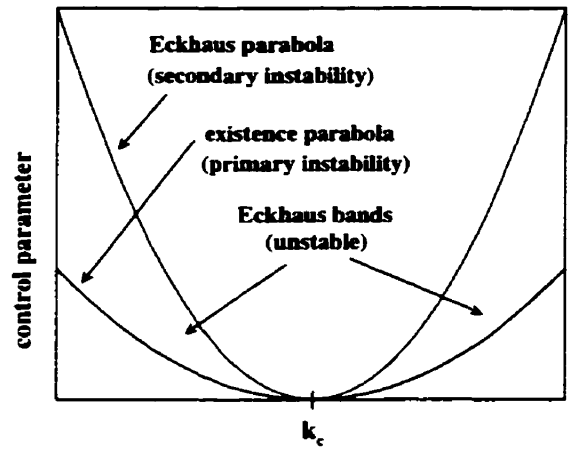

Figure 3.4: The uniform state becomes unstable against perturbation of the critical wavenumber q_c on the existence parabola. In the Eckhaus bands a solution exists, but it is not stable. In the central region the solutions are stable.

active[1]. By secondary instability we mean the following: the primary instability leads from a uniform state to a periodic one, with a family of solutions of form $\exp(ikx)$, where k is the wavevector of the pattern. However, it may occur that only some of the allowed wavelengths are stable. This is the reason for the name secondary instability. The Eckhaus instability is of this type and it is summarized in Fig. 3.4.

The aim of the linear stability analysis is to gain insight into the stability of the current carrying state against small perturbations, how the perturbations grow or decay in time, and how different modes are selected. The superconducting ring we study, has a quasi-one-dimensional geometry, and thus the instability is of necessity of Eckhaus type. In analogy to our system, the instability of the roll pattern in Rayleigh-Bénard convection[2] against certain wavelengths is of Eckhaus type. Fig. 3.4 illustrates that if the wavelength of a pattern is inside the Eckhaus bands, it must change its wavelength in order to reach a stable state. In superconducting rings this occurs via phase slip.

The order parameter in a superconducting ring is periodic as demonstrated in Fig. 3.3 (and as we will see in connection with numerical results in the following sections). As the current increases, the current carrying state becomes unstable against perturbations of some finite wavelength k_c, and it will relax to a state of lower current

[1] Cross and Hohenberg [93].

[2] Rayleigh-Bénard convection is discussed more extensively in connection with charge-density waves in Chapter 5.

via phase slip. In the case of roll patterns in Rayleigh-Bénard convection the analog would be the following: suppose that the system is prepared so that it has 'too many rolls'. Then, it has to find a way to reduce the number of them in order to attain a stable state. That process involves spontaneous generation of dislocations due to the instability, i.e., locations where the amplitude of the pattern goes to zero. That process provides a route to 'get rid of extra wavelengths'. In a superconducting ring dislocations appear as phase slips where the amplitude of the order parameter goes locally to zero, thus providing a mechanism for relaxation. Phase slips are generated (quasi) periodically due to the driving force.

3.4.1 *Eigenvalues*

To study the Eckhaus instability in superconducting rings, we linearize the equation of motion in Eq. (3.20) around a current carrying state by setting

$$\Psi(x,t) = \Psi_0 + \delta\Psi(x,t) \tag{3.28}$$

in the limit of $\omega \to 0$. The electrochemical potential is obtained from Eq. (3.23), and $q \equiv q(t) = q_0 + \omega\ell^{-1}t$ as defined in Eq. (3.16). The current carrying states (between the phase slips, in the limit of $\omega \to 0$) are uniformly twisted plane waves

$$\Psi_0 = \sqrt{1-q^2}e^{iqx}, \tag{3.29}$$

This solution of the equation of motion describes a stable state until the system reaches the instability. Since the system possesses translational invariance and admits plane wave solutions, the perturbation is given in terms of its Fourier expansion

$$\delta\Psi(x,t) = \left(a_{k_n}(t)e^{ik_nx} + a_{-k_n}(t)e^{-ik_nx}\right)e^{iqx}, \tag{3.30}$$

where $a_{k_n}(t)$ is the amplitude of mode n associated with wavevector $k_n = 2\pi n/\ell$. The index n corresponds to the order of the phase slip. To find the eigenvalues we use standard Floquet analysis with $\delta\Psi \equiv \delta\Psi(x)\exp(\lambda t)$. We can solve v_{ec} by Fourier transforming

$$\frac{\partial^2 v_{ec}}{\partial x^2} = -\alpha\frac{\partial J_s}{\partial x} \tag{3.31}$$

The eigenvalue matrix is

$$\begin{bmatrix} -1+2q^2-(k_n+q)^2+\frac{\alpha C(2q+k_n)}{2k_n} & \frac{\alpha C(2q-k_n)}{2k_n}-1+q^2 \\ -\frac{\alpha C(2q+k_n)}{2k_n}-1+q^2 & -1+2q^2-(k_n-q)^2-\frac{\alpha C(2q-k_n)}{2k_n} \end{bmatrix}, \tag{3.32}$$

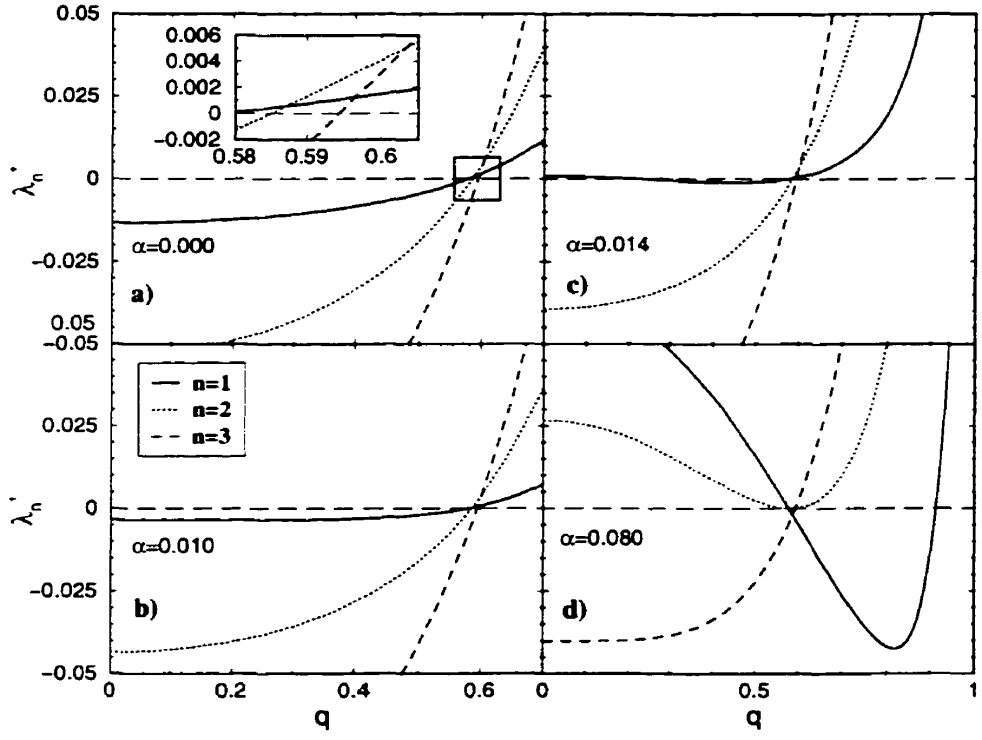

Figure 3.5: The eigenvalues as a function $q(t) = \omega t/\ell$ for different α's. The solid line is the $n = 1$ mode, dotted line $n = 2$, and dashed line $n = 3$ mode. In a) and b) all the modes are initially (i.e., at $q = 0$) stable. In c) the first mode has just become linearly unstable and in d) the first two modes are linearly unstable. The caption in a) shows the boxed area.

where $C = 1 - q^2$. The eigenvalues are

$$\lambda_n^{\pm}(q,\alpha) = -C(1-\alpha/2) - k_n^2 \pm \sqrt{C^2(1+\alpha+\alpha^2/4) + 4q^2(k_n^2 - \alpha C)}. \qquad (3.33)$$

To study the relative growth of different modes, we first examine the behavior of $\lambda_n^{\pm}$. When $\lambda_n^{\pm}$ is negative, the corresponding mode is stable, and thus fluctuations decay back to the superconducting state. However, as $\lambda_n^{\pm}$ becomes positive, the current carrying state becomes unstable against fluctuations of finite wavevector k_n. Since λ_n^{-} is negative definite, we neglect it and concentrate on λ_n^{+}.

Fig. 3.5 shows how the first three modes develop as a function of the driving force for different values of α. For small α, all the modes are initially stable, i.e. $\lambda_n^{+} < 0$. The inset in Fig. 3.5a shows that the modes become unstable sequentially; the lowest mode first, then the mode $n = 2$, and so on. The inset in Fig. 3.5a also shows that there is a competition between the modes. The lower order modes becomes

unstable first, but the higher order modes grow faster, i.e., $\partial\lambda_n^+/\partial q$ is larger for larger n. This indicates that they become dominant over the lower order modes; there is not enough time for the lower order mode to grow and become unstable. For the intermediate region where several modes are active this leads to crossover effects. This is of fundamental importance for the state selection. We will return to this issue again in connection with the numerical results.

In Figs. 3.5b-d we see that α (the constant that characterizes dissipation at a phase slip) has a strong effect on the mode structure. As we see from the figures, upon increasing α, some of the modes may be initially unstable. This is an indication that the simple plane wave solution in Eq. (3.29) is not valid any more, but higher harmonics should be taken into account.

Since several modes can be positive at the same time, and since there is a competition between the modes, we need an estimate for the characteristic time at which the n^{th} mode becomes unstable. This is the time defined by $\lambda_n^+ = 0$, i.e., by the time that the nth mode becomes positive (unstable). The characteristic time together with the growth rate, i.e., the slope of λ_n^+, can be used the estimate the relative probability for phase slips of order n. The characteristic time is obtained from Eq. (3.33) by requiring $\lambda_n^+ = 0$ and using $q = q_0 + \omega\ell^{-1}t$ from Eq. (3.16). We obtain

$$t_n = \frac{\ell}{\omega}\sqrt{1/3 + k_n^2/6}. \tag{3.34}$$

For a wire of infinite length the Eckhaus analysis gives $k_c = 1/\sqrt{3}$ — this first term under the square root. Eq. (3.34) shows that the mesoscopic nature of the system has an effect on the selection process since the instability, and thus the characteristic time, is encountered at wavevectors higher that k_c, with the correction depending on ℓ. It is also rather surprising that t_n in Eq. (3.34) is independent of α. To see the effect of α, we estimate the slope at time t_n. To first order this gives

$$\lambda_n^{+\prime}(q,\alpha) = \lambda_n^{+\prime}(q,0)[1 + \alpha(k_n^2 - 4)(k_n^2 + 2)/(3k_n^2[5k_n^2 + 4])]. \tag{3.35}$$

The correction due to α has the largest effect on the lowest mode, i.e., $n = 1$. This is also clearly visible from Fig. 3.5. By using the same parameters as in the simulations we obtain

$$\lambda_n^{+\prime}(q,\alpha) = \lambda_n^{+\prime}(q,\alpha = 0)(1 - 50\alpha) \tag{3.36}$$

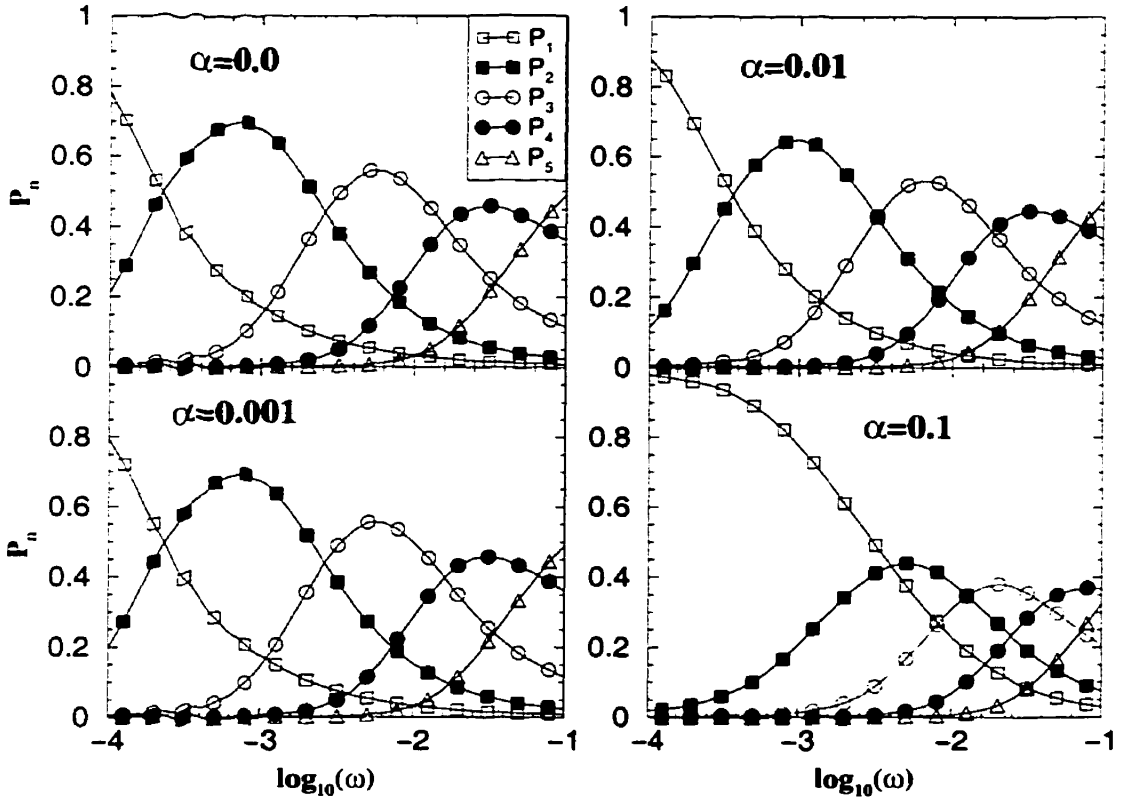

Figure 3.6: State selection probabilities from the linear stability analysis as a function of α

for the first mode ($k_n = 2\pi n/\ell$, $\ell = 54.4$; details are given in connection with the numerical results). Thus $\alpha \ll 0.02$ for the normal current to be negligible.

3.4.2 *Mode analysis*

As the preceding discussion pointed out, the competition between different modes is due to their different growth rates and the different times when they become unstable. To gain more insight into this process, we write a stochastic equation of motion for the modes as

$$\frac{da_n(t)}{dt} = \lambda_n^+(k_n, q(t), \alpha)a_n(t) + \eta_n(t), \tag{3.37}$$

where η is a Gaussian distributed random process. This equation describes a time-dependent Ornstein-Uhlenbeck process[1], i.e., it is a linear equation of motion supplemented with a Gaussian noise source.

The reason for approximating the state selection process by Eq. (3.37) is that

[1] Gardiner [90].

$\langle|a_n(t)|^2\rangle$ can be used to estimate the relative probability of mode $a_n(t)$ being selected as a function of the driving force and the noise strength as

$$P_n = \frac{\langle|a_n(t)|^2\rangle}{\sum_{n=1}^{n_\ell}\langle|a_n(t)|^2\rangle}, \tag{3.38}$$

where n_ℓ is the number of modes allowed in a system of length ℓ. The quantity we have to calculate is the autocorrelator $\langle|a_n(t)|^2\rangle$. We do that by using the Itô calculus[1] integrals. The calculation yields

$$\langle|a_n(t)|^2\rangle = \frac{2D}{\ell}\exp\left[2\int_0^t dt_1\lambda_n^+(t_1,\alpha)\right]\int_0^t dt'\exp\left[-2\int_0^{t'} dt_1\lambda_n^+(t_1,\alpha)\right]. \tag{3.39}$$

The calculation of the state selection probabilities for different α are shown in Fig. 3.6. For $\alpha < 0.001$ the influence of the normal state resistivity is very small. However, for higher α, the modes start to overlap more, suggesting strong crossover effects. The result in Fig. 3.6 also show that, independent of α, the state selection probabilities depend very strongly on the strength of the driving force, that is, how rapidly the system is swept through the instability. Eq. (3.39) also shows another interesting feature: the probability of state n being selected depends on the noise strength. Physically, the noise strength depends on the temperature of the system via the fluctuation-dissipation theorem. The intensity of thermal noise increases as $T \to T_c$. Thus, close to T_c the relative importance the noise becomes increasingly important, whereas away for T_c the driving force is dominant. Since α has no time dependence, the expansion of $\int_0^t dt_1\lambda_n^+(t_1,\alpha)$ leads to the same result as obtained by Tarlie and Elder [98], i.e., in terms of the intrinsic and extrinsic parameters, the instability of order n becomes active at time $\tau_n = \ell(\partial_q\lambda_n^+\omega\ell)^{-1/2}$. To summarize, the linear analysis shows that the state selection has a subtle dependence on both the applied driving force and on the intrinsic properties of the system. We will compare these results to numerical simulations of the stochastic time-dependent GL equation in Section 3.6.

[1] Gardiner [90] provides an excellent discussion of Itô calculus. In essence, the Itô calculus provides rules for transforming differential equations involving Gaussian random processes into a tractable form. The need for it arises from the non-differentiability of these processes. Itô calculus provides a consistent way of treating them.

3.5 Simulation method and parameters

Before moving forward to the results, we estimate our quantities in terms of typical experimental values. We use $T_c = 3\text{K}$, $T = 0.93T_c$, $H_c = 300G$, and $\xi(0) = \sqrt{S} = 1000\text{Å}$. With these values, the intensity of the noise $D = 10^{-3}$ and the GL time $\tau_{GL} = 1.4 \times 10^{-11}$ and $\omega \approx \mathcal{E}/23\mu\text{V}$. In the simulations we always kept the temperature constant, and thus the intensity of noise is fixed. ω was varied between 0.0001 to 0.1. This corresponds to electromotive forces from 2nV to 2μV. The parameter that couples the Ohmic resistance to the system, α, can be related to experimental quantities as follows. Since the phase slip is a resistive state, it is possible to use Ohm's law $R = (\rho L_n/S) = (V/I_n)$, where ρ is the normal state resistivity, L_n is the quasiparticle diffusion length, S is the cross-sectional area of the wire, V is the voltage drop, and I_n is the normal current. Using this, $\alpha = (\rho L_n/S)$. The quasiparticle diffusion length is related to the charge imbalance due to generation of normal current[1], and it is given as $L_n = \sqrt{l v_F \tau_n/3}$, where l is the mean free path, v_F the Fermi velocity, and τ_n is the relaxation time for charge imbalance[2]. Typically[3], $l \approx 0.01 - 1\mu\text{m}$, $v_F \approx 10^6\text{m/s}$, $\tau \approx 10^{-10} - 10^{-9}\text{s}$, and $\rho \approx 0.01 - 0.001\mu\Omega\text{m}$. Using these values $\alpha \approx 10^{-4} - 1.0$, depending on the dimensions and the material. We varied from 0.0 to 0.01. We also performed simulations with higher values of α, but they were hampered by numerical instabilities.

We have used the simple Euler algorithm for the time integration of Eq. (3.20), and Eq. (3.23) was solved in Fourier space. The complex order parameter was separated into its real and imaginary parts. The simulation parameters were: $L = 64$, $dx = 0.85$, $dt = 0.2$, where dx and dt are the smallest discrete elements of space and time respectively. The length of the system was chosen in such a way that $n_\ell \equiv \ell q_c/2\pi$, where $q_c = 1/\sqrt{3}$ from the Eckhaus analysis of the GL equation as discussed above. We have used $n_\ell = 5$. This allows enough complexity due to interaction between different modes, while remaining numerically tractable. When computing the probability of an n^{th} order phase slip, P_n, the averaging was typically from 2000

[1] Skocpol, Beasley and Tinkham [74]; Dolan and Jackel [77].
[2] Tidecks [90]. However, as discussed in this reference, this serves as a first approximation. There may be other relaxation mechanisms that become dominant. Tinkham [96]
[3] Tidecks [90].

phase slip events (small ω) up to 15,000 phase slips (large ω).

3.6 Numerical results

First, we illustrate the dynamics of the order parameter around a phase slip in Figs. 3.7 and 3.8. Fig. 3.7 clearly illustrates that the current carrying state is formed of uniformly twisted plane waves. As the current increases, the helix becomes more tightly wound. Due to fluctuations, there will be 'weak spots' where the local supercurrent reaches the critical current before the rest of the system. This is the point where the amplitude of the order parameter starts to decay rapidly toward zero. When $|\Psi|^2 \to 0$, the phase slip center momentarily disconnects the phases to the left and right of it, the helix looses a loop, and the supercurrent jumps to a lower value. This cycle is repeated periodically.

In Figs. 3.7 and 3.8 the behavior predicted by Eq. (2.13) is clearly visible: as the supercurrent, or superfluid velocity, increases, the absolute value of the order parameter, $|\Psi|^2$, decreases and, at the moment of the phase slip, approaches zero. After the phase slip, the order parameter rapidly recovers. Fig. 3.8 demonstrates this behavior. This allows the amplitude to relax toward equilibrium in the vicinity of the phase slip center (times t_2 and t_3 in Fig. 3.8 and Fig. 3.7c,d). After a moment, the wire obtains a uniform current (t_4 in Fig. 3.8).

Fig. 3.9 displays the time development of the winding number and the supercurrent. They are defined in Eqs. (3.27) and (3.26), respectively. The electric field drives the current to the critical current, where it makes a jump to lower current. As suggested by Fig. 3.9, there can be several modes simultaneously present; in the figure, phase slips of order two dominate, but occasionally there are jumps of order three. Furthermore, every now and then the winding number also displays little dips, as if the total phase slip was a results of a two stage process.

As discussed in connection with the linear stability analysis, the appearance of phase slips of different order is a subtle issue. It is instructive to look at the state selection probabilities in Fig. 3.10 together with the dynamics of the supercurrent and the winding number in Fig. 3.9. As seen from Fig. 3.10, at lower driving forces phase slips of order $n = 1$ always dominate the process. However, as α is increased,

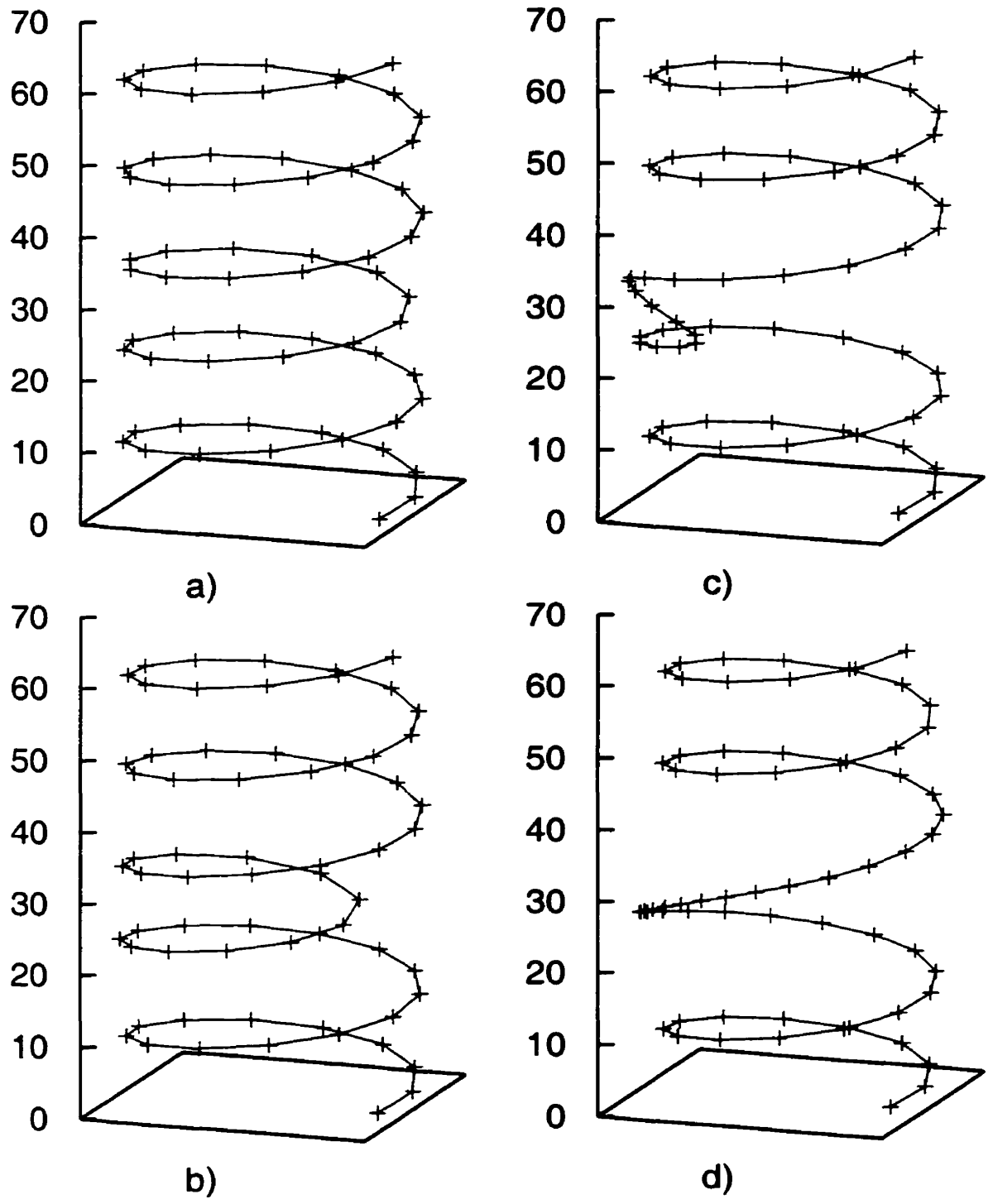

Figure 3.7: A snapshot of a phase slip process, $L = 64$. a) The current carrying states are uniformly twisted plane waves. b) Due to fluctuations, the supercurrent at some location along the wire grows slightly faster than in the rest of the system. c) At a phase slip the system makes a transition back to below the critical current by reducing the number of loops in the helix. d) After the phase slip, the system retains the perfectly superconducting state with $J < J_c$ everywhere. z-axis: length, x-y plane: Re[Ψ] and Im[Ψ].

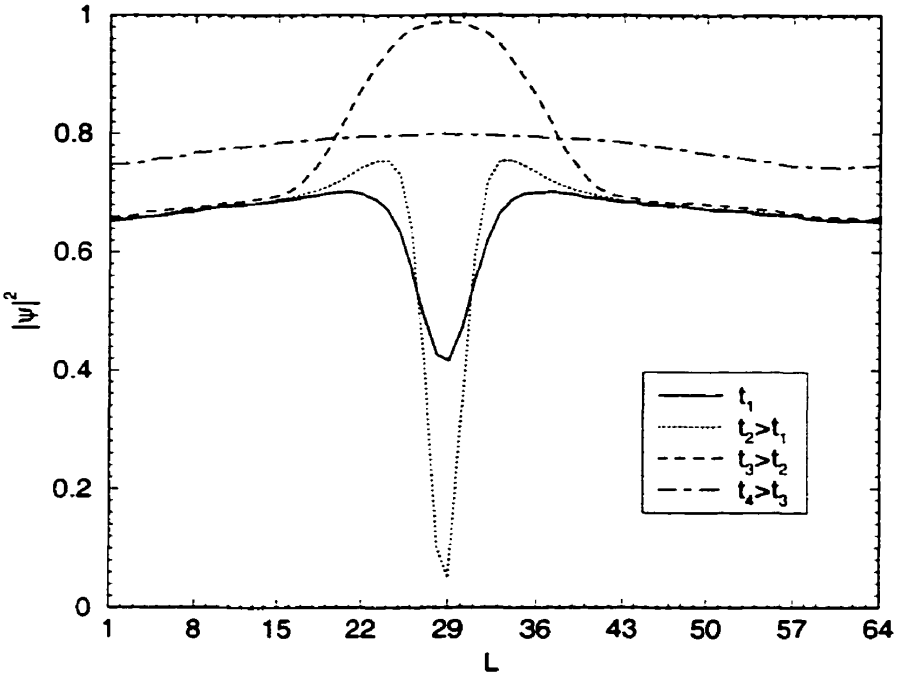

Figure 3.8: Order parameter just before and after the phase slip. As $|\Psi| \to 0$, the phase gradient must grow in order to maintain a constant current. As the amplitude goes to zero, it can 'slip' by a multiple of 2π and relax to a state of lower current.

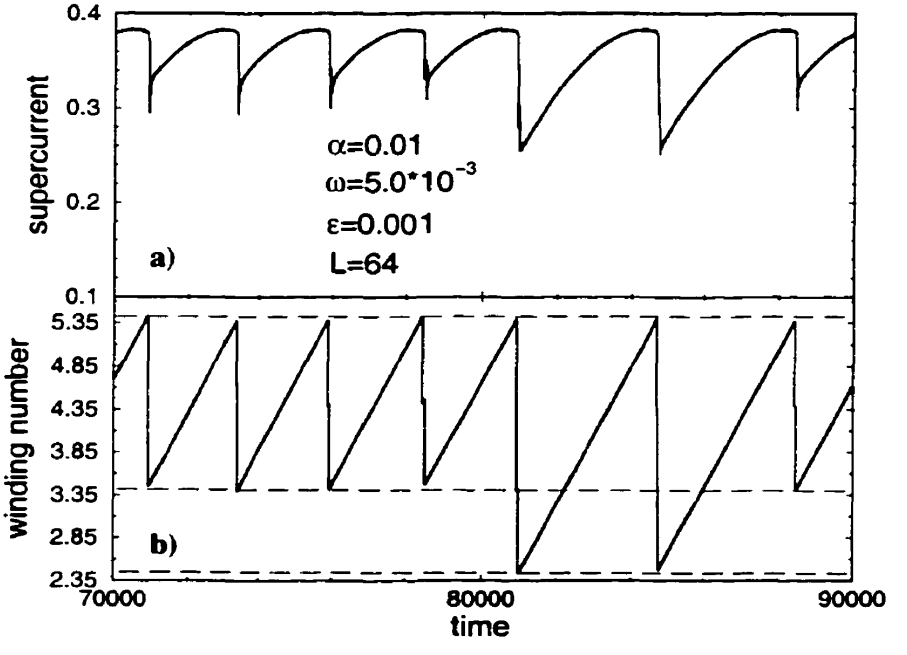

Figure 3.9: a) Supercurrent and b) winding number as a function of time. When this figure is compared to the state selection probabilities in Fig. (3.10), it can be seen that the probabilities of double and triple phase slips are almost equal, but there is still a small probability for single slips.

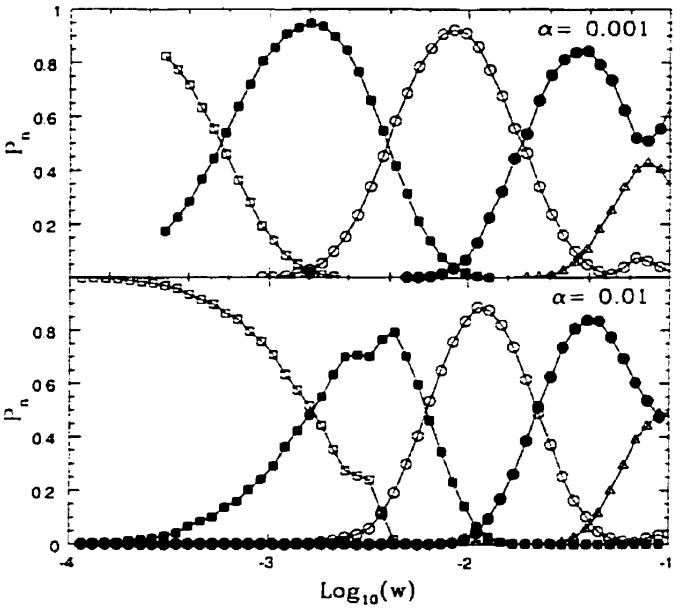

Figure 3.10: State selection probabilities as a function of the driving force. The open squares denote single phase slips, closed squares doubles, open circles triples, closed circles quadruples, and open triangles phase slips of order five.

phase slips of lower order remain dominant to larger driving forces before crossover to higher modes. As the driving force is increased phase slips of order $n = 2$ start to appear (i.e., to have a finite probability), and there is a crossover to regime where phase slips $n = 2$ dominate. Order by order other modes become dominant in a similar manner. The little dips referred to above are a result of competition between the modes. As seen in the linear stability analysis in the previous section, modes of lower order become active first, but the higher order ones grow faster. This leads to competition and crossover effects. This implies that the dips in Fig. 3.9 are not due to a result of a two-stage process where a phase slip of higher order occurs via two lower order processes, but instead due to coexistence of different modes with different growth rates modes. For higher α this picture starts to break down, this is the reason for the 'kink' in Fig. 3.10. Fig. 3.11 illustrates the complicated nature of the phase slip when several modes are simultaneously present. There is a competition between different modes, and it is even possible for several phase slip centers to exist (almost) simultaneously.

Fig. 3.12 shows the behavior of $|\Psi|^2$ and the electrochemical potential at the phase

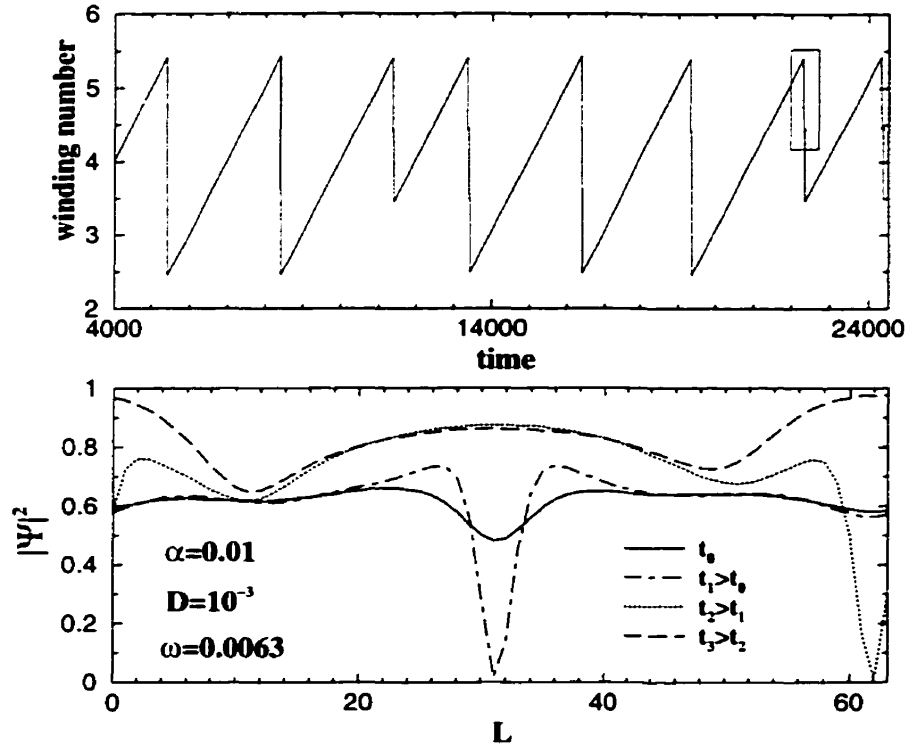

Figure 3.11: The upper figure shows the winding number as a function of time. The lower figure shows the square of amplitude of the order parameter taken at four different times inside the boxed area. As the winding numbers increases, there are spots where the amplitude starts to decay (t_0). This leads to competition and coexistence of several modes, and possible several phase slip centers. The parameters correspond to the case when three modes, $n = 1, 2, 3$, are present.

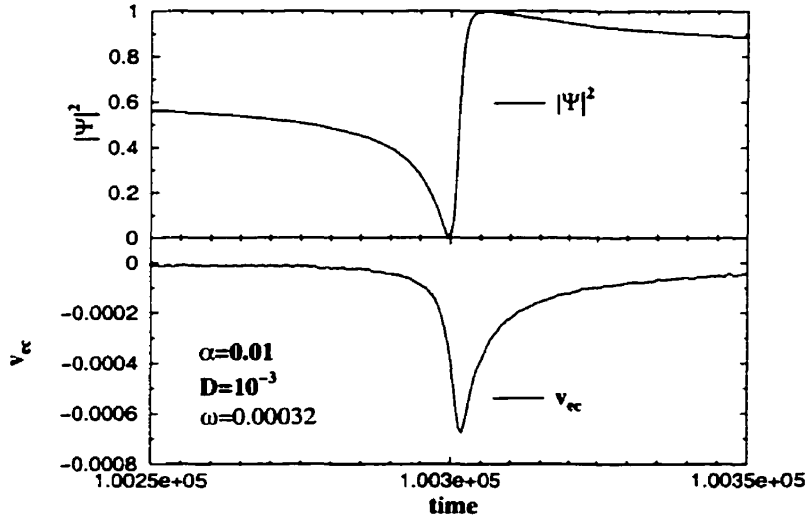

Figure 3.12: Upper figure: $|\Psi|^2$ at the location of the phase slip as a function of time. Lower figure: the electrochemical potential at the phase slip center as a function of time. The simulation parameters correspond to a case when single slips dominate almost completely. The slice runs from immediately before the phase slip to just after it.

slip center as a function of time, when the mode $n = 1$ is dominant. The time frame is selected in such a way that the figures cover the immediate vicinity of the phase slip. At the moment of the phase slip, $|\Psi|^2 = 0$. After the phase slip, Ψ rapidly recovers its equilibrium value. Since there is a constant emf acting on the superconductor, $|\Psi|$ starts to decrease after its recovery. As seen in the lower figure, v_{ec} regains its equilibrium value ($v_{ec} = 0$) at the phase slip center considerably slower than Ψ. This can be seen in the following way. The electrochemical potential is zero, if the current is uniform throughout the sample. However, as seen in Figs. 3.8 and 3.11, the time required to reach a uniform current is much longer than the time required for healing of the order parameter at the phase slip center. Physically, this corresponds to relaxation of the charge imbalance[1] in a superconductor. The relaxation is diffusive[2], with time scales typically of order $10^{-9} - 10^{-10}$s.

3.6.1 *Power dissipated at a phase slip*

The phase slip is a dissipative process, where energy is locally converted into heat. This is due to appearance of Ohmic resistance at the phase slip center. Early experiments[3] showed that the differential resistance related to the phase slip is temperature independent for a wide range of temperatures[4]. A finite amount of heat is generated during the process. In this section we obtain a method to estimate the heat generated at a phase slip. Since at a phase slip exactly one (or any multiple) quantum of flux is lost, we expect that to be reflected in the dissipated power as well. The normal carriers can be assumed to follow Ohm's law. We can use the Joule heating law to estimate the heat generated at a phase slip. The power generated is

$$P = \int_{volume} \vec{J}_n \cdot \vec{E} d\Omega = S \int J_n E_x dx, \tag{3.40}$$

where $d\Omega$ is a volume element, S is the cross sectional area of the ring, J_n is normal current density and E_x is the electric field along the wire. In terms of the electro-

[1] Tinkham [96].
[2] Skocpol, Beasley and Tinkham [74]; Dolan and Jackel [77]; Tidecks [90].
[3] Skocpol, Beasley and Tinkham [74]; Dolan and Jackel [77].
[4] The differential resistance is temperature independent except very close to T_c. This is a delicate issue; heating due to Ohmic resistance changes the local critical current, and issues related to charge imbalance and relaxation also become of importance. Chapter 7 in Tidecks [90] discusses these issues in detail.

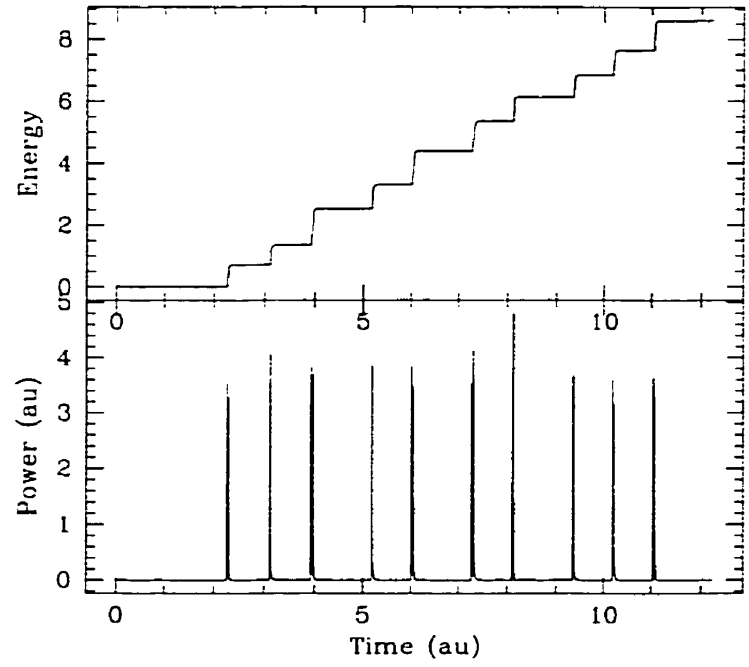

Figure 3.13: Upper figure: Energy (in arbitrary units) dissipated as a function of time. Lower figure: The corresponding power (in arbitrary units) dissipated at phase slips. The figures show clearly the quantized nature of dissipation. The crossover effects are visible in the width of peaks. The simulation parameters were $dx = 0.85$, $dt = 0.2$, $\alpha = 0.01$, $\omega = 0.0064$ and $D = 10^{-3}$. These parameters correspond to a case when three modes ($n = 1, 2, 3$) are active at the same time.

chemical potential, we can write this as

$$P = S \int J_n \frac{\partial v_{ec}}{\partial x} dx = S \rho_n^{-1} \int \left(\frac{\partial v_{ec}}{\partial x} \right)^2 dx, \tag{3.41}$$

where ρ_n is the normal state resistivity. We convert the above equation into a dimensionless form by using the transformations in Eq. (3.7). After removing the primes we obtain

$$P_0 = \frac{16 S k_B T_c^2 (1-t)^2}{\pi^2 e^2 \rho_n \xi} \int_0^{\ell} \left(\frac{\partial v_{ec}}{\partial x} \right)^2 dx. \tag{3.42}$$

The total energy dissipated is then

$$E = \int P dt = P_0 \tau_{GL} \int_0^{\tau} \left[\int_0^{\ell} \left(\frac{\partial v_{ec}}{\partial x} \right)^2 dx \right] d\tau', \tag{3.43}$$

where $\tau = t/\Gamma_{GL}$.

The increase in temperature due to a phase slip can be estimated using the heat capacity. The heat capacity per unit mass is

$$c = \frac{1}{m} \frac{\Delta E}{\Delta T} \tag{3.44}$$

and therefore the change in temperature is

$$\Delta T = \frac{E}{cLS\rho_m} = \Delta T = T_0 \int_0^\tau \left[\int_0^\ell \left(\frac{\partial v_{ec}}{\partial x} \right)^2 dx \right] d\tau', \tag{3.45}$$

where we have used c for the specific heat[1], ρ_m is the density of the material, and

$$T_0 = \frac{2k_B T_c (1-t)\hbar}{c\pi e^2 L \rho_m \rho_n \xi}. \tag{3.46}$$

Eq. (3.45) can be used to estimate the change in temperature due to a phase slip. The linear dependence of T_0 on $1-t$ expresses the well know fact[2] that close to T_c the effects of Joule heating are less significant. Evaluation of ΔT requires information about the time and the length scales involving v_{ec}, and therefore we have not estimated it. Fig. 3.13 shows the accumulated energy and power dissipated as a function of time.

3.7 Conclusion

In this chapter we have studied the dynamics of quasi-one-dimensional superconductors subjected to a constant electromotive force. The emf accelerates the supercurrent until it reaches the critical current, where it has to make a transition to a state of lower current. This transition to a new state is from a point of instability, and it involves generation of a resistive phase slip center that heals after the phase slip. How the state takes place, and what is the effect of the resistive phase slip state were some of the questions we addressed. Our approach was based on voltage driving instead of using current as a driving force. The traditional way is to use current as the driving force. That enables one to study issues such as charge imbalance, relaxation mechanisms, heating due to the resistive state, and so on, i.e., issues related directly to the nature of the superconducting state. On the other hand, using a voltage drive, as we have done, emphasizes different aspects: the relation to the general methods and problems in nonlinear dynamics, statistical mechanics and pattern formation.

We used linear stability analysis to investigate the Eckhaus instability. We found out that within the linear approximation, the state selection process is a competition of two factors: the characteristic time at which a mode $a_n(t)$ becomes unstable, and

[1] Even though we have earlier used c for the speed of light, there should be no danger of misinterpretation. The notational inconvenience is due to using standard conventions.
[2] Skocpol, Beasley and Tinkham [74]; Dolan and Jackel [77].

the growth rates of the other modes. For low driving forces, the low order modes have time to grow and dominate the process, where as for higher driving forces the faster growth rates of high order modes lead to their dominance. In the intermediate region there is a competition between the two cases leading to crossover.

Next, we integrated the stochastic time-dependent Ginzburg-Landau equation and found the behavior to be consistent with the predictions of the linear analysis. Although the behavior was qualitatively similar, nonlinearities and interaction between the phase slips at higher driving forces and higher normal current resistivity lead to differences. Despite of the simplicity of the system it displays rich and complex phenomena, and more analytical and numerical studies are needed. However, to our knowledge, there exists no systematic method to study state selection in accelerated systems. It has been suggested recently[1], that the path integral method of Onsager and Machlup[2] may offer a framework for that. We have not explored that, and it could be a subject of a future work, as could numerical studies of the two-dimensional case.

[1] Tarlie and McKane [98].
[2] Onsager and Machlup [53].

4

Charge density-waves

4.1 Introduction

In Chapter 1, we discussed some general issues of driven and disordered systems. As both experimentally and theoretically accessible, charge-density waves (CDW) provide a prototype system to study the effects of disorder on driven periodic medium. As will become apparent in the following discussion, they display very interesting and diverse physics. As discussed in Section 3.3, driven superconductors exhibit a state where phase slips appear periodically — the current-voltage (I-V) characteristics display abrupt jumps when phase slip centers appear upon increasing driving current. As we will see later in chapter, this phenomenon has an analog in CDW systems.

The objectives of this chapter are threefold. The first goal is to review briefly the basic physical phenomena behind CDWs. The second aspect is to show, by reviewing a well defined and studied theory, how to model mesoscopic aspects of collective transport and dynamics of CDWs. This approach is based on Ginzburg-Landau theory. And last, before presenting the original work in the next chapter, we will discuss the limits of the elastic approach and open questions related to the driven CDWs.

Even though CDWs have been studied extensively for more than two decades, many open questions, even controversies, remain[1]. From the theoretical point of view, one of the main difficulties is the collective and highly nonlinear nature of the system. Almost all the analytical results[2] are based on mean-field type approaches

[1] See e.g. Grüner [94]

[2] Sneddon, Cross and Fisher [82]; Fisher [83]; Fisher [85]; Matsukawa and Takayama [86b]; Matsukawa [86].

and on the assumption that CDWs are perfectly elastic systems with fixed topology[1].

This brief review is by no means intended to be exhaustive, but it concentrates on the points that are of immediate interest to this study. Several extensive reviews covering both theoretical and experimental aspects of CDWs exist[2].

In addition to providing a prototype system to study novel collective effects, CDW systems also have industrial potential. Until now, no commercial products based on CDWs exist, but recent studies point to the direction that in the future CDWs may indeed find their way even to consumer electronics. Field-effect transistors seem at the moment the most prominent candidates[3].

4.2 Microscopic origin of CDWs

4.2.1 Response function of a one-dimensional electron gas

Due to the reduced phase space, fluctuations, impurities and interactions have a strong effect on low dimensional systems. Systems that exhibit CDWs are typically quasi one-dimensional (1D) metals. They become insulators at the phase transition to the CDW state. To see the special nature of 1D systems, consider the response of a free electron gas to a small potential $\phi(\vec{x})$ at $T = 0$. The Fermi surface of a 1D electron gas consists of two points at $\pm k_F$ and the dispersion relation is given as $\epsilon_k = \hbar k^2/2m_e$. k_F denotes the Fermi wavevector, and m_e is the mass of an electron. When the perturbation is weak, we can apply linear response theory. The Fourier transforms of the induced charge density $\rho_{ind}(\vec{q})$ and the total potential $\phi(\vec{q})$ are connected via

$$\rho_{ind}(\vec{q}) = \chi(\vec{q})\phi(\vec{q}), \tag{4.1}$$

where $\chi(\vec{q})$ is the response function. The response function depends on the dimensionality of the system. As we will see, in 1D it has a very distinct character.

[1] Fukuyama and Lee [78]; Lee and Rice [79]; Littlewood [86]; Sibani and Littlewood [90]; Middleton and Fisher [91]; Middleton [92].

[2] Grüner and Zettl [85]; Monceau [85a]; Monceau [85b]; Gorkov and Grüner [89]; Grüner [88]; Grüner [94].

[3] See e.g. Adelman, Zaitsev-Zotov and Thorne [95] and references therein.

Using the Lindhard theory of screening[1], the response function is given as

$$\chi(\vec{q}) = e^2 \int \frac{\mathrm{d}\vec{k}}{(2\pi)^d} \frac{f_{k+q} - f_k}{\epsilon_{k+q} - \epsilon_k}, \tag{4.2}$$

where f_k is the Fermi function, i.e., $f_k = 1/\left[\exp(\epsilon_k - \mu)/k_B T) + 1\right]$, where μ is the chemical potential. At $T = 0$ and in 1D the above integral (integration from $-k_F$ to k_F) yields

$$\chi(q) = -\frac{m_e e^2}{q\hbar^2} \ln \left| \frac{q + 2k_F}{q - 2k_F} \right|, \tag{4.3}$$

and in 3D the evaluation of Eq. (4.2) gives

$$\chi(\vec{q}) = -e^2 \frac{1}{4} \frac{m_e k_F}{\pi^2 \hbar^2} \left[\frac{1}{2} + \frac{4k_F^2 - q^2}{2k_F q} \ln \left| \frac{q + 2k_F}{q - 2k_F} \right| \right]. \tag{4.4}$$

There is clearly a qualitative difference between Eqs. (4.3) and (4.4): The 1D response function becomes divergent as $q \to 2k_F$, whereas the 3D response is logarithmically singular. The divergence is a characteristic of the 1D case; in higher dimensions Eq. (4.2) does not lead to divergences. The result that $\chi(q)$ is divergent suggests that the free electron gas is intrinsically unstable against any perturbation. Furthermore, by substituting Eq. (4.4) into Eq. (4.1) we can see that the screened potential is oscillatory even in the 3D case: $\phi(\vec{x}) \sim r^{-3} \cos(2k_F x)$. These oscillations are called Friedel oscillations. They can be induced by impurities, and that can lead to a subtle interplay between them and the CDW[2]. We calculated the 3D form for Friedel oscillations to show that they are not a special case for 1D systems; even though a CDW systems are typically quasi one-dimensional, the electron gas itself is three dimensional.

The above example shows that low dimensional systems can display rather surprising phenomena. The instability of the free electron system against perturbation is a very real effect, and in a quasi-1D system the interaction between the electron and phonon systems leads to a static modulation of the electron density. The modulation is usually referred to as charge-density wave and the related phase transition is called the Peierls transition, or sometimes the CDW transition.

[1] The Lindhard theory is used because the applicability of the Thomas-Fermi theory is limited to length scales $q \ll k_F$. The Lindhard theory reduces to the Thomas-Fermi theory as $\vec{q} \to 0$. The time-independent response function, Eq. (4.2) can be obtained by direct application of perturbation theory. The time-dependent case is more complicated, and details of the full Lindhard theory of screening (based on the random phase approximation) can be found in Pines and Noziéres [66].

[2] Tüttö and Zawadowski [85].

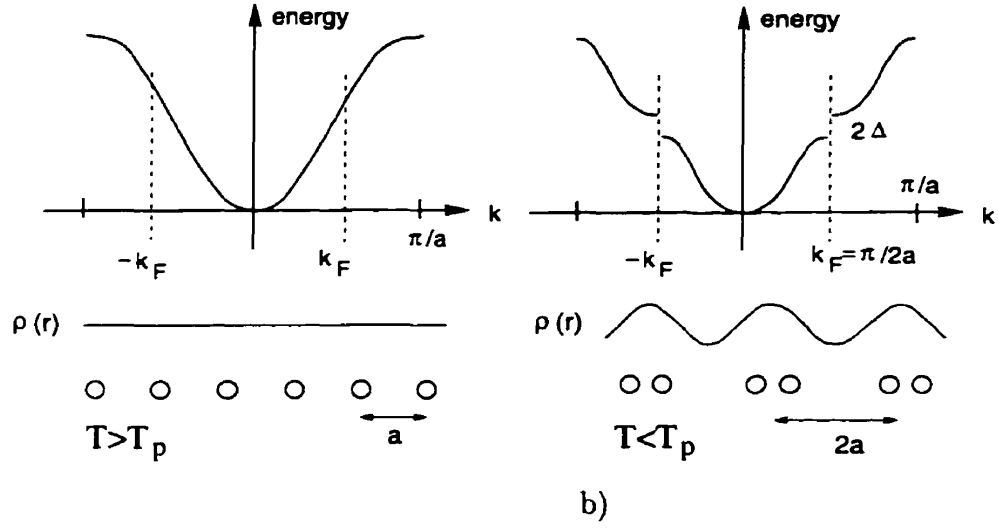

Figure 4.1: The single-particle energy band, and the corresponding electron density $\rho(r)$. a) Above T_P the electron density is uniform and states are filled up to the Fermi level. b) Below T_P a lattice distortion develops with an associated modulation in the electron density, and a gap Δ opens up at k_F.

4.2.2 *Peierls transition*

Almost 40 years ago Peierls [55] and Fröhlich [54] independently suggested[1] that a coupling of the electron and phonon systems in a one dimensional metal at $T = 0$ is unstable with respect to a static lattice deformation of wavevector $Q = 2k_F$.

Due to the periodicity of the lattice deformation, the electron density will also become periodically modulated. This is illustrated in Fig. 4.1. As a result of the modulation, a gap opens up in the single-particle excitation spectrum at the Fermi level, and a spatially periodic charge density modulation is formed with wavevector $2k_F$. The deformation is limited by the corresponding increase in elastic energy. This can be seen by writing down the energies for the lattice distortion and electrons.

The Fröhlich Hamiltonian describes a jellium coupled to noninteracting electrons.

[1]Historically, the mechanism leading to the formation of CDWs was first discussed by Peierls [30] already in 1930. In 1941 Bardeen [41] suggested that for superconductors there is a possibility that a periodic lattice distortion would lead to an energy gap at the Fermi level. In 1954 Fröhlich [54], in his article "On the Theory of Superconductivity: The One-Dimensional Case", discussed in detail the formation of periodic incommensurate modulation in electron density as a mechanism for superconductivity; in a perfect crystal, an applied electric field would lead to infinite conductivity. This is the reason why the sliding CDW motion is sometimes referred to as Fröhlich superconductivity, or as the Fröhlich mode.

It is given as

$$\mathcal{H}_{Fr} = \sum_k \epsilon_k c_k^\dagger c_k + \sum_q \hbar\omega_q b_q^\dagger b_q + \sum_{k,q} g_q \left(b_q + b_{-q}^\dagger\right) c_{k+q}^\dagger c_k, \tag{4.5}$$

where ϵ_k (ω_q) is the electron (phonon) dispersion relation, c_k ($c_k^\dagger$) is the electron annihilation (creation) and b_q ($b_q^\dagger$) the phonon annihilation (creation) operator at the corresponding electron and phonon wavevectors, and $g_q = i\sqrt{\hbar}V_q q/\sqrt{2NM\omega_q}$ is the coupling constant between the electron and phonon systems, where V_q is the interaction potential. N is the number of lattice sites per length and M is the ionic mass. The lattice displacement $U(x)$ and the phonon operators are related via

$$U(x) = \sum_q \sqrt{\frac{\hbar}{2NM\omega_q}} \left(b_q + b_{-q}^\dagger\right) e^{iqx}. \tag{4.6}$$

By assuming g_q is a constant in the Fröhlich Hamiltonian, it is possible to calculate a temperature dependent mean-field dispersion relation for the phonon system. For this, $\chi(\vec{q})$ must also be evaluated at finite temperature. The calculation indicates that there is transition to a state with a frozen lattice distortion (phonon mode), such that the lattice displacement becomes periodically modulated,

$$U_{MF}(x) \propto \Delta \cos(2k_F + \phi), \tag{4.7}$$

where Δ is the energy gap and ϕ is a phase[1]. Next, we will take a look at the energetics and see that it is indeed energetically favorable to have a static lattice deformation.

From Eq. (4.7) we can immediately see that the elastic energy due to the deformation is

$$E_{elastic} = \frac{1}{4} K \Delta^2, \tag{4.8}$$

where K is a stiffness constant. A straightforward calculation shows that small displacements are favored since they lower the energy logarithmically[2] $E_{electr.} \sim U^2(x) \ln U(x)$ and $E_{elastic} \sim U^2(x)$. Therefore, the lattice distortion leads to an associated modulation of the electron density, and thus the formation of a charge-density wave breaks translational symmetry of the electron gas, lowering the symmetry of the system. This is called the Peierls transition.

[1] From here on ϕ is used to denote the phase of the CDW. Even though ϕ was used above to denote the potential, the distinction should be clear. This notational inconvenience is due to using a standard convention from the literature.

[2] Strong electron-electron correlations may lead to the formation of a spin density-wave (Grüner [94]).

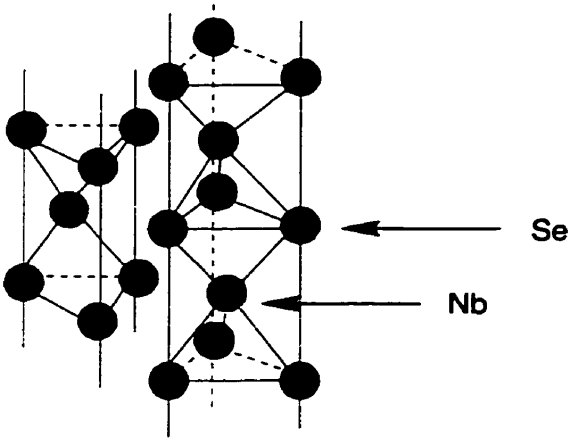

Figure 4.2: Schematic structure of $NbSe_3$. The structure is clearly anisotropic. The chains have weak couplings between each other.

The opening of a gap means that the Peierls transition is a phase transition from a metal to an insulator. The transition is a continuous one, and it occurs at the so called Peierls temperature T_P. This transition has been experimentally observed[1] in many anisotropic transition metal compounds consisting of weakly coupled chains, i.e., in quasi-1D structures. Fig. 4.2 illustrates the structure of $NbSe_3$ which is the most studied CDW material, another very commonly studied material is TaS_3. The transition temperatures are greatly material dependent, and vary from higher than room temperature to liquid nitrogen temperatures. $NbSe_3$ exhibits two Peierls transitions, the first at $T_{P1} = 144$K and the second at $T_{P2} = 59$K[2].

4.2.3 *Sliding conductivity*

In addition to showing that a periodic modulation is energetically favorable, Fröhlich demonstrated that if the CDW is incommensurate with the underlying lattice, that is, if the ratio of the CDW wavelength and the lattice period is not a rational number, then the CDW can slide through the lattice upon application of an infinitesimal electric field. In other words, an incommensurate CDW is translationally invariant, and there is no energy costs associated to the translational ($q = 0$) mode. Since the CDW carries charge, it can contribute to electrical conductivity. Fröhlich suggested that as a possible mechanism for superconductivity. The sliding conductivity of a CDW is

[1] See e.g. Grüner and Zettl [85]; Grüner [88].
[2] Grüner and Zettl [85].

a collective mode, and physically it is a result of a traveling potential produced by oscillating atoms. Many materials, e.g. $NbSe_3$, develop incommensurate CDWs. If the CDW is commensurate with the lattice, or if it is pinned by impurities, the translational invariance is broken. Whether or not the CDW is commensurate depends on the details of the Fermi surface.

4.2.4 *Elementary excitations: phasons and amplitudons*

In their seminal paper in 1974, Lee, Rice and Anderson [74] studied the conductivity of the CDW state. They calculated the elementary excitations for a CDW starting from the Fröhlich Hamiltonian, Eq. (4.5), and established the existence of two normal modes. They identified these modes as phase and amplitude fluctuations of the order parameter, often called phasons and amplitudons, respectively. They found[1] that while the acoustic, or phase, mode is gapless

$$\omega_-^2 = \frac{m_e}{m_e^*} v_F^2 q^2, \tag{4.9}$$

the optical, or amplitude, mode has a gap

$$\omega_+^2 = \lambda \omega_Q^2 + \frac{4}{3}\frac{m_e}{m_e^*} v_F^2 q^2. \tag{4.10}$$

In the above equations, m_e^* is the effective mass and λ is the dimensionless electron-phonon coupling constant. Since $\omega_- \to 0$ as $q \to 0$, the phase mode is a sliding mode, and can, in the absence of imperfections and fluctuations, lead to infinite d.c. conductivity. However, the amplitude mode is gapped and changing the amplitude corresponds roughly to creating a single particle electronic excitation, costing an amount of the order of gap energy.

All real materials contain imperfections to a varying degree, and scattering of electrons with impurities and defects leads to finite resistance. Impurities and defects have a drastic effect on CDWs. Lee, Rice and Anderson showed that the impurity potential couples directly to the order parameter and gives rise to a small gap in the phase mode. This leads to disappearance of translational invariance of the incommensurate CDW (with respect to laboratory frame) and leads to the existence of a finite

[1] The analysis of Lee, Rice and Anderson is based on mean-field arguments, and the phase and amplitude are decoupled only to the first order, i.e. they are not the exact normal coordinates of the CDW.

threshold field for d.c. conductivity. Due to the existence of the gap, it is difficult to distort the amplitude. However, it is possible for the phase to distort arbitrarily slowly at long length scales, thus the phase distortion is a Goldstone mode. This suggests two limits for impurity pinning: *i)* the pinning is strong, so that the energy is minimized when the CDW adjusts locally to each impurity, or *ii)* the pinning is weak, so that the CDW collectively adjusts to the impurity configuration. The former leads to the collapse of the CDW amplitude at the impurity sites, whereas in the latter case the amplitude remains virtually constant, and only the phase is affected by pinning.

These results have far-reaching consequences. Since a CDW is a collective system with many degrees of freedom, pinning by a spatially distributed impurities (or imperfections) leads to a subtle interplay between the internal degrees of freedom and the pinning forces. If the pinning centers are randomly distributed, the CDW has many metastable states. Application of a d.c. driving force can then lead to very strong polarization of the CDW, and as the driving force exceeds the threshold field, the CDW has a strong non-linear contribution to electrical conductivity. The non-linear conductivity due to CDWs, and the existence of a threshold field were experimentally discovered by Monceau et al. [76] and Fleming and Grimes [79], respectively. The competition between the elastic forces, periodic nature of the system, and the presence of random impurity pinning gives rise to very interesting physics. In the next section, we will review an extensively studied model in order to see how to model CDWs on the mesoscopic level.

4.3 Fukuyama-Lee-Rice theory for CDWs

The above review of the microscopic origin of CDWs indicates that the physics related to CDWs has many complex and interesting facets. Since our interests lie in the dynamical properties of CDWs, we will not explore the microscopic aspects any further, but investigate a coarse grained theory instead. The microscopic approach is not convenient for studying the collective dynamics and structural properties of CDWs when driven far from equilibrium. One possible model for the CDW dynam-

ics is the Fukuyama-Lee-Rice (FLR) model[1]. Although several other models exist, the FLR model is by far the most extensively studied and the most successful one. The FLR model is a many-degree-of-freedom model for perfectly elastic medium under the influence of periodic pinning by quenched randomness. It reproduces many experimentally observed phenomena characteristic to CDWs such as non-Ohmic conductivity[2], mode-locking[3], and narrow-band noise (NBN)[4]. In addition to providing a model for CDWs, the FLR model is in some sense a generic model for an elastic periodic medium interacting with random impurities. However, despite the qualitative success of the FLR theory, quantitative comparisons with experimental results have proven to be difficult. In the following, we review the FLR theory and its limitations. The following discussion of the FLR theory and the elastic approximation serves as a starting point for the original work in Chapter 5.

The FLR theory is based on the Ginzburg-Landau theory, and it describes a CDW as a perfectly elastic continuum of fixed topology interacting with quenched impurities and coupled to an externally applied driving field. As the topological constraint indicates, the FLR theory does not allow plastic deformations, i.e., phase slip is not possible, and therefore the amplitude of the CDW is considered to be constant.

As the dispersion relations (in the absence of disorder) for incommensurate CDWs in Eqs. (4.9) and (4.10) show, the amplitude mode is gapped, whereas the phase mode is 'soft' with a linear dispersion relation. Furthermore, Eqs. (4.6) and 4.7) suggest that the modulation of the electron density is a proper order parameter for CDWs; at $T > T_P$ it is zero, and it becomes nonzero when $T < T_P$. The total density of the conduction electrons can be given by a Fourier expansion

$$\rho(\vec{x}, t) = \rho_{ave} + \rho_{CDW}(\vec{x}, t)\cos(\vec{Q} \cdot \vec{x} + \phi(\vec{x}, t)), \tag{4.11}$$

where $Q \equiv 2k_F$ denotes the CDW wave number, ρ_{ave} is the mean conduction electron density, ρ_{CDW} is the CDW condensate density and ϕ is the phase giving the location of the CDW relative to the lattice. If we write the density in Eq. (4.11) in a more

[1] Fukuyama [76]; Fukuyama and Lee [78]; Lee and Rice [79].
[2] Monceau et al. [76]; Fleming and Grimes [79]; Matsukawa and Takayama [86a].
[3] Gill [81]; Sherwin and Zettl [85]; Coppersmith and Littlewood [86].
[4] Fleming and Grimes [79]; Bhattacharya, Higgins and Stokes [39]; Sibani and Littlewood [90].

suggestive form, i.e.,

$$\rho(\vec{x}) = \rho_{ave} + \mathrm{Re}[e^{i\vec{Q}\cdot\vec{x}}\Psi], \tag{4.12}$$

we obtain the following order parameter for CDWs:

$$\Psi = \rho_{CDW}(\vec{x},t)e^{i\phi(\vec{x},t)}, \tag{4.13}$$

where ρ_{CDW} is the amplitude of the CDW condensate and $\phi(\vec{x},t)$ is the phase, as defined above.

If the wavevector $\vec{Q}$ is incommensurate with the underlying lattice wavevector, the free energy of the CDW is independent of the ϕ, implying translational invariance. Then, when acted on by an applied field at $T = 0$, and in the absence of impurities and defects, the CDW should display sliding conductivity with linear response without resistance — in a manner described by Fröhlich. However, coupling to impurities breaks translational invariance. As discussed above, Lee, Rice and Anderson [74] showed that the order parameter couples directly to the impurity potential. Therefore, the interaction energy for an impurity atom with potential $V(\vec{x} - \vec{R}_i)$ located at $\vec{R}_i$ can be written as

$$H_i = \rho_{CDW}(\vec{x},t)V(\vec{x} - \vec{R}_i)\cos(\vec{Q}\cdot\vec{R}_i + \phi(\vec{x},t)), \tag{4.14}$$

where the potential is assumed to be short-ranged. To get the total impurity contribution to the energy, we must take a sum over all impurities, i.e.

$$\mathcal{H}_{imp} = \sum_i H_i = \sum_i \rho_{CDW}(\vec{x},t)V(\vec{x} - \vec{R}_i)\cos(\vec{Q}\cdot\vec{R}_i + \phi(\vec{x},t)). \tag{4.15}$$

Since the FLR theory assumes CDWs to be perfectly elastic systems without plastic deformations or rupture, amplitude fluctuations are completely suppressed, and therefore the phase is the only dynamical variable. Using the GL free energy,

$$F = \int dx \left[\frac{K}{2}|\nabla\Psi(\vec{x},t)|^2 + a|\Psi(\vec{x},t)|^2 + b|\Psi(\vec{x},t)|^4\right] \tag{4.16}$$

and assuming the amplitude in Eq. (4.13) is constant, we add the contribution from the impurities, and the driving force (E is the applied field), to obtain the FLR Hamiltonian

$$\mathcal{H}_{FLR} = \int d\vec{x}\frac{K}{2}(\nabla\phi)^2 + \sum_i \rho_{CDW}V(\vec{x} - \vec{R}_i)\cos(\vec{Q}\cdot\vec{R}_i + \phi) - E\phi. \tag{4.17}$$

Neglecting the applied field, there are two competing energy contributions in the FLR Hamiltonian: the elastic energy and the pinning energy. The interaction between elasticity and impurity pinning has two limits: the weak pinning limit where the phase of the CDW order parameter adjusts collectively to minimize the energy, and the strong pinning limit where the CDW deforms to minimize its energy locally at each impurity site. In the strong pinning limit the phase of the CDW adjusts completely at each impurity site, ultimately leading to the local collapse of the CDW amplitude. At that limit the energy cost per impurity is

$$E_i = V_0 \rho_{CDW}, \tag{4.18}$$

and the elastic energy cost per impurity is,

$$E_{el} = K n_i / 2, \tag{4.19}$$

where n_i the number density of impurities, and impurities are assumed to have short-range potential, $V(x) = V_0 \delta(x)$

The above simple argument shows the existence of two limits, strong ($E_i \gg E_{el}$) and weak pinning ($E_i \ll E_{el}$). The above arguments show that, at the strong pinning limit the phase adjusts itself at each impurity. What happens in the case of weak pinning can be subtle, since there is a competition between the elastic force and the impurity pinning. In the weak pinning case, the phase adjusts itself over a certain length, thus providing a characteristic length scale for phase-phase correlations. It is reasonable to ask how this length scale depends on the other parameters, and on dimensionality. This length is often referred to as the Lee-Rice length, L_{LR}. We use dimensional analysis and the Imry-Ma argument to find it.

From the FLR Hamiltonian in Eq. (4.17) we can see, that in the absence of an applied field, a distortion of the CDW has an elastic energy cost of

$$\epsilon_{el} \sim K L^{-2}, \tag{4.20}$$

per unit volume. The impurity pinning is assumed to follow Gaussian statistics, and thus, by the Imry-Ma argument, the pinning energy per unit volume is

$$\epsilon_{pin} \sim V_0 n_i^{1/2} L^{-d/2}. \tag{4.21}$$

By minimizing the total energy density, i.e.

$$\epsilon_{tot} = \epsilon_{el} - \epsilon_{pin}, \tag{4.22}$$

we obtain the Lee-Rice length,

$$L_{LR} \sim \left(\frac{V_0^2 n_i}{K^2}\right)^{\frac{1}{d-4}}. \tag{4.23}$$

The energy due to impurity pinning is negative in Eq. (4.22) since the energy is gained by adjusting the phase inside a domain of size L_{LR}^d. A domain wall separates two neighboring domains with different preferred phases. This is the source of the elastic energy cost. From this it is also transparent that the Lee-Rice length is the phase-phase correlation length, i.e., $\langle\phi(x)\phi(0)\rangle \sim \exp(-x/L_{LR})$. The Lee-Rice length is an experimentally accessible quantity and it is typically[1] (e.g., in $NbSe_3$) of order 1000Å.

Dynamics in the FLR model is assumed to be relaxational[2]. This assumption is a reasonable one in the presence of impurities, and as long as long-range Coulomb interactions are not important. Then, the equation of motion can be obtained from

$$\frac{\partial\phi}{\partial t} = -\frac{\delta\mathcal{H}_{FLR}}{\delta\phi}. \tag{4.24}$$

4.4 Uniqueness of the sliding state

Quenched impurities pin periodic media, such as a CDW, and destroy long-range positional order[3]. The effect of quenched disorder has two immediate consequences: 1) destruction of long-range order due to domain formation and 2) existence of a finite depinning threshold E_T at which the periodic structure depins and starts to move, i.e. a transition from a stationary state with $v = 0$ to a moving state with $v > 0$ as $E \geq E_T$. Intuitively, one would expect that, once in motion, the structure would become more ordered than in the pinned state, i.e. in the mobile state the impurities would be less effective in destroying the long-range order since the moving system sees them as an effective thermal noise[4], i.e., $T_{eff} \sim 1/v$.

[1] On the other hand, the amplitude correlation length is typically of order 10Å, see e.g. Brock et al. [94]; DiCarlo et al. [94b].

[2] Typically the phase relaxation rate is of order 10^{-11}s. This is much faster than any other time scale in the problem, as noted by Hall, Hundley and Zettl [88]

[3] Imry and Ma [75]; Efetov and Larkin [77].

[4] Koshelev and Vinokur [94] discuss this in the context of vortex lattices.

In some sense, the FLR model is a generic model, providing the simplest way to study driven periodic medium influenced by random forces. Therefore the interest in it is easily understood. The FLR model is highly non-linear, and quite intractable analytically. Because of this, very few analytical results have been obtained. Apart from mean-field analysis, the available analytical results do not apply close to the depinning threshold[1], but are high velocity expansions. Thus they have only limited applicability. One problem, that also has important consequences in real systems, is that the behavior is different above and below E_T. As $E \to E_T^+$, the system exhibits critical behavior. However, below the threshold the system has many metastable states and the behavior is hysteretic. As $E \to E_T^-$, there are domains that become depinned. As a result of this, there are avalanches of different sizes and durations as the field is increased: the correlation length of pinned domains diverges as $E \to E_T^-$. This is manifested by the appearance of broad-band, or $1/f$, noise[2].

The infinite range mean-field theory by Fisher[3] suggested that the transition from the pinned to the sliding state is a novel dynamical critical phenomenon with the velocity and the correlation lengths of the CDW scaling[4] above E_T as

$$v \sim (E - E_T)^{\zeta} \tag{4.25}$$

$$\xi \sim (E - E_T)^{-\nu}. \tag{4.26}$$

Comparison of the mean-field, and experimentally and numerically obtained exponents are given in Table 4.4. Reliable measurements of the exponents have turned out to be quite demanding due to their dependence on determining the threshold field E_T and finite size effects[5]. This is especially true in the case of the correlation length exponent ν.

The critical behavior requires the existence of a well defined threshold field. It is possible to obtain an estimate for E_T by using Eqs. (4.22) and (4.23). We can balance the energy due to the applied field with the energy gain from domain formation. This

[1] Sneddon, Cross and Fisher [82].
[2] Bhattacharya et al. [85]; Bhattacharya, Higgins and Stokes [89].
[3] Fisher [83]; Fisher [85], For experimental considerations, see Robbins, Stokes and Bhattacharya [85].
[4] These are the most accessible exponents.
[5] Littlewood [89]; Myers and Sethna [93a]; Myers and Sethna [93b].

Exponent	Dimension	Theoretical	Experimental	Computational
ζ	mean field:	3/2 [1]	-	-
	$d = 3$	-	1.23 ± 0.07 [2]	1.16 ± 0.04 [3]
		-	-	0.80 ± 0.1 [7]
	$d = 2$	-	-	0.63 ± 0.06 [4,5]
		-	-	0.95 ± 0.05 [3]
		-	-	0.65 ± 0.05 [7]
	d=1	-	-	0.85 ± 0.15 [6]
		-	-	0.45 ± 0.05 [7]
ν	mean field	1/2 [1]	-	-
	$d = 3$	-	-	0.36 ± 0.10 [3]
		-	-	0.5 ± 0.1 [7]
	$d = 2$	-	-	0.38 ± 0.05 [3]
		-	-	0.5 ± 0.1 [7]
	$d = 1$	-	-	0.2 ± 0.1 [6]
		-	-	0.4 ± 0.1 [7]

Table 4.1: Comparison of exponents obtained from CDW experiments, theory and computation. [1]: Fisher [85]; [2]: Bhattacharya, Higgins and Stokes [89], [3]: Sibani and Littlewood [90]; [4]: Middleton [92]; [5]: Middleton and Fisher [93]; [6]: Littlewood [89]; [7]: Myers and Sethna [93a].

yields

$$E_T \sim \left(\frac{n_i V_0^2}{K^{d/2}}\right)^{\frac{2}{4-d}}. \tag{4.27}$$

Middleton and Fisher [91], and Middleton [92] studied the limiting behavior of the sliding state as $t \to \infty$. They showed that, when a perfectly elastic medium is subjected to quenched randomness and a uniform external driving force, that above the depinning threshold the spatial configuration of the system approaches a unique state. Originally, Middleton derived the result in the context of charge-density waves but as he pointed out, the results are quite general provided that the inertial effects are negligible, i.e., the equations of motion are first order in time, the order parameter is scalar, the internal interaction potential is convex, and that thermal noise is absent. This result applies only above the depinning threshold. Below E_T, the behavior is hysteretic and no unique solution exists. Even though the above conditions and the

assumption of perfect elasticity are rather stringent, it shows that at the elastic limit, CDWs exhibit critical behavior.

The argument for the unique sliding state can be summarized as follows. Assume the following discretized equation of motion (from the FLR Hamiltonian)

$$\partial_t \phi_i = \Delta^2 \phi_i - V_i(\phi_i) + E, \tag{4.28}$$

where Δ^2 is the lattice Laplacian and V_i the pinning potential. Clearly, the elastic potential is convex. The convexity leads to monotonic behavior. This is the so called 'no-passing' rule[1]: if there are two solutions with the same driving forces and pinning potentials, then the solution that is initially behind cannot pass the one that is initially in front. This has important consequences: depinning takes place at a sharp threshold E_T, moving and stationary solutions cannot coexist, and the asymptotic velocity is unique for a given impurity potential and driving force. This is easy to see from Eq. (4.28) in the following way: Assume a sliding solution in such a way that $\dot{\phi}_i^{init} > 0$. In addition, assume that at time $t = t^*$ there exists a $\dot{\phi}_j$ such that $\dot{\phi}_j(t = t^*) = 0$. Using this in Eq. (4.28), and taking the derivatives, leads to an immediate contradiction. The existence of a unique solution in the elastic limit is supported by simulations [2]. Experimentally, the uniqueness should be manifested as an appearance of a sharp delta function peak in the conduction noise spectrum of a moving CDW, i.e., $f_0 \propto j_{CDW}/\lambda$, where j_{CDW} is the CDW current density. The linear relation between f_0 and j_{CDW} is observed[3] in pure samples, but more disordered samples show deviations from it. In addition, the the f_0 peak (and harmonics) are always broadened. This narrow-band noise is correlated with the appearance of broad-band, or $1/f$, noise in CDW systems[4].

4.5 Limits of the elastic approximation

Since the FLR theory is an elastic approximation, it is reasonable to ask what are its limitations. In real systems, topological defects exist. They may appear due to

[1] Middleton [92].
[2] Littlewood [86]; Sibani and Littlewood [90]; Middleton and Fisher [93].
[3] Monceau, Richard and Renard [80]; Grüner [88].
[4] Robbins, Stokes and Bhattacharya [85]; Bhattacharya et al. [85]; Bhattacharya, Higgins and Stokes [89]; Bloom, Marley and Weissman [94]; DiCarlo et al. [94a].

strong pinning, thermal fluctuations, or they may be generated dynamically due to competition between the internal degrees of freedom and the pinning forces. Topological defects, whether intrinsic or dynamically generated, involve irreversible plastic deformations.

Coppersmith and Millis[1] studied the self-consistency of the phase-only approach, and demonstrated that even in the case of weak pinning, and below E_T, there will be diverging strains. Coppersmith and Millis argued that there always exist some rare domains where the local depinning threshold is much larger than the threshold field (E_T) needed to set the whole system in motion. The existence of these rare regions leads to diverging strains, i.e., to infinite local energy densities. This shows that the applicability of the elastic approximation is limited. In the following, we will review their argument.

Consider two neighboring domains in a CDW system consisting of many domains. Assume that one of them has no impurity pinning at all and that the other one that is pinned. Assume further that the applied field is below the depinning threshold, i.e., $E < E_T$. Then the net velocity of the system is zero. Pinning is a volume effect, and thus the energy scales as L^d. Since the external field affects every point inside the domain, the energy due to it also scales as L^d. The unpinned domain has a threshold field equal to zero. To prevent it from moving, the pinned domain must exert a force on it. The restoring force from the elastic couplings with the neighboring domains scales as the perimeter area, i.e., as L^{d-1}. Evidently, there is an imbalance between the volume and the surface effects.

Assume that the domains have a distribution of local depinning thresholds E_{loc}. If the impurities are randomly distributed, then by the central limit theorem the distribution of E_{loc} is Gaussian. When $L \to \infty$ there will always exist some rare areas with E_{loc} much greater than the global depinning threshold E_T.

The Coppersmith-Millis scenario leads to several consequences: as pointed out by Lee, Rice, and Anderson, the phase and the amplitude are not the exact normal coordinates of the CDW. There is a weak coupling between them. Therefore, increasing strains can lead to the collapse of the CDW amplitude. Qualitatively we can see

[1] Coppersmith [90]; Coppersmith [91]; Coppersmith and Millis [91].

this as follows: Large phase gradients change the CDW wavevector away from $2k_F$, increasing the energy cost of the distortion with respect to the electronic energy. The overall effect of large strains effects the elastic constants. Related effects occur also in vortex lattices[1]. In addition, Eq. (4.23) together with Eq. (4.22) states that for $d < 4$ the energy will become increasingly negative, i.e., the disorder dominates. This, as suggested by the Coppersmith and Millis scenario, leads to infinite energy densities. Physically, this means that topological defects proliferate on length scales $L \gg L_{LR}$. Indeed, a very recent study[2] strongly suggests that in two dimensions dislocations are energetically favorable.

4.6 Order in driven periodic media

As the Coppersmith and Millis scenario suggests, the elastic approximation breaks down even in the case of weak pinning. It is then natural to ask what are the consequences of that, what are the experimental signatures, and have they been seen. Balents and Fisher [95] discussed these issues and proposed a phase diagram for driven CDWs. We will now review their arguments.

As seen above, the application of the Imry-Ma argument to the static CDW shows that long-range order is not possible for $d < 4$. In terms of the order parameter, that means that the correlations do not converge to a finite nonzero value as the distance grows but instead tend to zero,

$$g(\vec{x}) = \langle \Psi^*(\vec{x}, t)\Psi(\vec{0}, t)\rangle \to 0, \text{ as } |\vec{x}| \to \infty. \tag{4.29}$$

The Imry-Ma argument is valid for a static CDW, but it does not apply to the sliding state, where dynamical processes may change the behavior drastically. This is the essence of the approach of Balents and Fisher. The Coppersmith and Millis scenario suggests that in the case of $0 < E < E_T$ topological defects will emerge in all physical dimensions, dynamical processes may be important and need to be considered separately.

Qualitative features emerge from dimensional analysis similar to the static case, and the formal analysis relies on dynamical renormalization group treatment. Here,

[1] Koshelev and Vinokur [94].
[2] Zeng, Leath and Fisher [99].

we present only the dimensional analysis since it is enough to reveal much of the interesting physics. The starting point is again the FLR Hamiltonian, Eq. (4.17), but with the term involving the applied external field dropped. The equation of motion is

$$\partial_t \phi = D\nabla^2 \phi + V(\vec{x}) \sin(2\vec{Q} \cdot \vec{x} + \phi), \tag{4.30}$$

where D is the diffusion constant. Instead of working directly with this, the equation of motion is coarse grained in such away that the impurities appear only as a Gaussian distributed random term. Furthermore, the driving force is included by taking the total derivative $\partial_t + v\partial_x$ instead of ∂_t, so we have

$$\partial_t \phi = D\nabla^2 \phi - v\partial_x \phi + V(\vec{x}), \tag{4.31}$$

where $\langle V(\vec{x}) \rangle = 0$ and $\langle V(\vec{x}) V(\vec{0}) \rangle = V_0 \delta(x)$.

If the velocity $v = 0$, we recover the results obtained previously in this section. However, using the same arguments for $v \neq 0$, Balents and Fisher found that in 3D there exists a moving solid phase that is stable against the proliferation of topological defects. They argue that the transition is a true nonequilibrium transition, and that there exists a critical velocity v_c, above which temporal long-range order exists. Below v_c, the system is in a plastic flow phase, and thus unstable against the nucleation of dislocations. Also the results (that will be outlined below) shows that the system is unstable against the formation of dislocations when $d < 3$.

The first task is to transform away the convection term $v\partial_x \phi$. This can be done by moving into a moving frame with $x \to x - vt$. Clearly, the elastic term $\nabla^2 \phi$ is invariant under this transformation. However, the quenched noise is transformed so that it appears to be moving with velocity v, i.e., $V(\vec{x}) \to V(x - vt, \vec{x}_\perp)$. As before, the system is now divided into regions of size L. However, unlike above where there was only one time scale present (the time for phase diffusion $t_\phi \sim L^2/D$), there is now a second time scale due to the velocity. This second time scale is $t_0 \sim L/v$, and it is the time it takes for a region of size L to move to reach an area of uncorrelated randomness (i.e., to advance by distance L). In other words, since the system is moving, it samples on the average t_ϕ/t_0 independent samples of randomness. Summing over the random fields gives $\sqrt{V_0 D/v} L^{(d-1)/2}$. Combining the contributions from elasticity and random

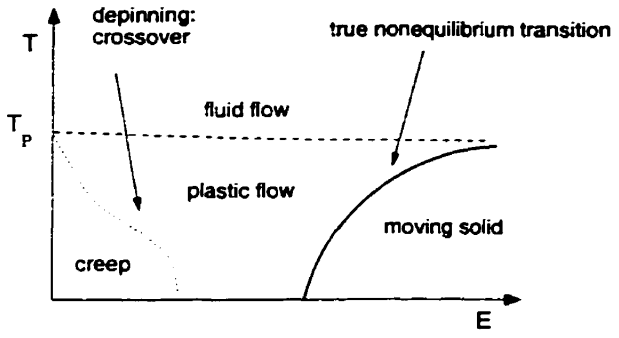

Figure 4.3: The schematic Balents-Fisher phase diagram for the 3D CDW. The solid line is the suggested true nonequilibrium transition and the other lines represent crossovers.

pinning as in Eq. (4.22), leads to

$$\epsilon_{tot} \sim DL^{d-2} - \frac{V_0 D}{v} L^{(d-1)/2}. \tag{4.32}$$

This shows that $d = 3$ is a special dimension, and that the systems becomes ordered as the elastic energy overcomes the pinning forces when $v_c \sim V_0/D$. Below $d = 3$ dislocations always proliferate. This is an important result, and shows that the emergence of order depends on the dynamics of the system. These results imply the following:

1. In 3D: When a strong driving force is applied, there is a dynamical phase transition into a temporally periodic state with quasi-long-range translational order. The ordered state is called a 'moving solid' state. However, the 'moving solid' state does not have the true long-range positional order of a solid in equilibrium does, instead it is characterized by an algebraic power-law dependence for positional correlations (like a 2D crystal). The 'moving solid' state is periodic in time and has long-range temporal correlations. In addition, due to the existence of dislocations, the depinning transition and critical behavior, as described above, are smeared out.

2. In 2D: Impurity induced phase slips will destroy the 'moving solid' state: The moving solid phase driven through quenched impurities is *always* unstable against the proliferation of dislocations. Due to the motion of unbound dislocations (or vortices in 2D), the system attains the symmetry of a driven liquid.

From these conclusions, Balents and Fisher proposed a 3D phase diagram for driven CDWs. It is shown in Fig 4.3, and has the following characteristics:

1. Transition/crossover from fluid flow is a Peierls transition to the CDW state.

2. The line between creep and plastic flow is the depinning line as described by the elastic approximation. Upon proliferation of phase slips, the critical behavior disappears as predicted by Coppersmith and Millis.

3. The line between plastic flow and moving solid is a true nonequilibrium phase transition, with the moving solid phase exhibiting temporal long range order. Translational order is only quasi-long-range.

Thus far, this scenario has not been tested experimentally or theoretically. If the Balents-Fisher scenario is true, one of the experimental signatures that can be experimentally tested is a Kosterlitz-Thouless transition[1] in $d = 3$. The proliferation of dislocations and plastic flow can be interpreted as dynamical generation of topological defects due to periodically appearing phase slips in CDW systems. Since this picture includes topological defects, the standard FLR model becomes inadequate. In the next chapter, we will introduce a novel model for CDWs that can be used to test these ideas.

4.7 Some experimental observations

So far we have mostly discussed theoretical aspects related to charge-density waves. We have mentioned some of the most significant experimental signatures of collective CDW motion (under d.c. drive), namely the non-linear conductivity, existence of a threshold field, generation of narrow-band and broad-band noise, and strong polarization effects upon applied driving force. Here, we will briefly discuss experiments that have a direct relation to the results we will present in the next chapter.

Very recently, time-resolved x-ray scattering measurements by Ringland et al[2]. have provided direct evidence that the dynamics and order of CDWs is a subtle issue. They used both doped and very pure $NbSe_3$ samples in temperatures close to

[1] Kosterlitz and Thouless [72]; Kosterlitz [74].
[2] Ringland et al. [99b].

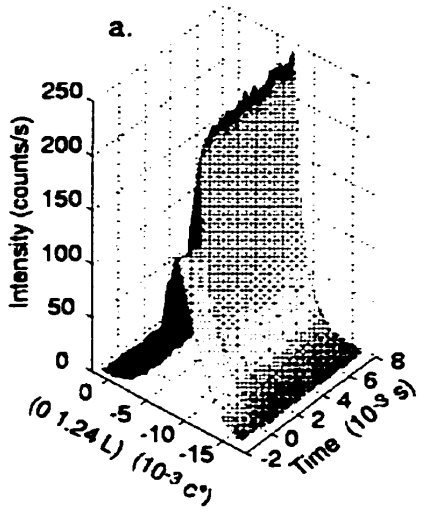

Figure 4.4: At early times ($t < 0$), the CDW is driven and it is in the sliding state. At $t = 0$ the driving field is switched off. After a short transient time the CDW relaxes to pinned state. The measurements are from a pure $NbSe_3$ sample at $T = 100K$. From Ringland et al. [99b].

T_{P1}. The CDW was first driven far above the depinning threshold. After that the driving field was switched off and the system was let to relax. Their striking, and unexpected, observation was that, even in the weak pinning limit, the CDW becomes more ordered when the driving field is turned off, and the CDW has relaxed to a pinned state. This is shown in Fig. 4.4. This observation is surprising since, from the Fukuyama-Lee-Rice theory, and from the theories of motion of interfaces in random medium, one would expect the opposite to occur: intuitively, the pinned state (after relaxing) should be more disordered. However, in the sliding state it would be natural to expect the randomness to have the same effect that quenched disorder has on a moving interface, i.e., it acts as an effective temperature[1], $v \sim 1/T_{eff}$. Thus higher driving force (i.e., velocity), would make the interface more ordered. The fact that the system is more disordered when it is driven suggests that dynamical (periodic) generation of dislocations may take place. Qualitatively, this is in agreement with the the Coppersmith-Millis argument, and the theory by Balents and Fisher. However, at the moment, to our knowledge, no current CDW model produces this behavior. This intriguing scenario is one of the issues we will discuss in the next chapter.

The dynamical x-ray scattering experiments are not the only ones indicating the possible importance of topological defects. Earlier NMR experiments by Ross Jr.,

[1] Koshelev and Vinokur [94]; Provatas et al. [95]; Karttunen et al. [98].

Wang and Slichter [90] strongly suggested that the whole CDW is not set into motion at a sharp threshold field E_T, but that there exist stationary domains even when $\langle v \rangle \neq 0$. Should that be the case, phase slip must occur at the domain boundaries — otherwise unphysical divergent strains would occur at the boundaries, as discussed above. Those experiments, however, were inconclusive since it was impossible to rule out contact effects. Another observation that points in the same direction is the broad-band, or $1/f$, noise above the depinning transition[1]. These, and several other observations, show that the dynamics and dynamical processes involved in connection to sliding CDWs, and other periodic media, is a subtle issue and many open questions remain.

The above remarks imply that dislocations have a subtle effect on the dynamics and order of CDWs. Another interesting aspect is the appearance of switching[2], i.e., hysteresis. Switching refers to bistable behavior of the driving force; upon increasing the driving force from zero, the system abruptly 'switches' from low conductivity state to high conductivity state. Upon decreasing the driving force, the jump take place at a different value of the driving force. Thus, there exist two threshold values. This behavior occurs typically in temperatures much lower than the threshold field, in $NbSe_3$ around 40K. Switching is characteristic of CDW dynamics far away from the transition temperature in CDW materials, yet the standard CDW models are not able to reproduce this behavior. This is one of the aspects we will look into in the next chapter.

4.8 Summary

In this chapter we first discussed the microscopic background of charge-density waves. After that reviewed the most widely studied model for CDW dynamics, namely the Fukuyama-Lee-Rice theory. This is based on the elastic assumption, i.e., the amplitude of the CDW remains constant, and the CDW collectively adjusts to the random pinning in order to minimize its energy. While this approach has been a very fruitful one, we also saw its limitations: Even in the pinned state there may be diverging

[1] Bloom, Marley and Weissman [94].
[2] Zettl and Grüner [82]; Hall and Zettl [84]; Hall, Hundley and Zettl [86]; Sherwin, Zettl and Hall [88]; Lemay et al. [99].

strains in the system due to a random distribution of local pinning strengths. This implies that the elastic approximation becomes inadequate, and that amplitude modulations have to be taken into account. In the static case, the Imry-Ma argument states that the system is disordered below four dimensions. However, in the case of driven CDWs dynamical effects may alter this picture and long-range order may be possible below four dimensions, as discussed in connection with the theory of Balents and Fisher. Whether or not this is the case, requires more theoretical and experimental studies. A related aspect is the appearance of switching, bistable behavior, in low temperatures.

In the next chapter, we will present our original study of charge-density wave dynamics.

5

A novel model for dynamics of driven charge density-waves

5.1 *Introduction*

In the previous chapter we discussed the elastic approach to the dynamics of CDWs. However, the argument by Coppersmith and Millis[1] and the theory by Balents-Fisher[2] clearly showed that dynamically generated topological defects, i.e., dislocations in 3D or vortices in 2D, do exist, and they are likely to change the dynamical behavior of the system drastically from the predictions resulting from assuming a perfectly elastic system.

In this chapter, we propose a novel approach[3] to study the dynamics of charge-density waves (CDW). Instead of looking at the dynamics using the conventional approach, i.e., by using the Fukuyama-Lee-Rice equation or an extension of it, we approach the problem by proposing a phenomenological equation of motion for the CDW condensate itself. In our approach, we consider the formation of the CDW condensate from a pattern formation point of view. As our starting point, we will use the Swift-Hohenberg equation[4]. The Swift-Hohenberg equation is a generic model for pattern formation in rotationally invariant systems, such as Rayleigh-Bénard systems. We show that by using general symmetry arguments, the Swift-Hohenberg equation can be modified in order to model periodic systems of broken translational symmetry subjected to quenched disorder, such as CDWs. This is why we call our model the Modified Swift-Hohenberg model, or MSH. The advantage of our approach is that the model is a generic one including the subtle interplay between elasticity and

[1] Coppersmith [90]; Coppersmith [91]; Coppersmith and Millis [91].
[2] Balents and Fisher [95].
[3] Karttunen et al. [99a].
[4] Swift and Hohenberg [77]; Pomeau and Manneville [79]; Elder, Vinals and Grant [92]; Cross and Hohenberg [93].

pinning forces. It is also worth noticing that topological defects emerge naturally in this picture; they may be generated dynamically or/and they may be present due to strong pinning. This is very important: to our knowledge, no other approach is capable of describing this phenomena.

A legitimate question one should ask is, what is the reason for introducing yet another model for CDWs while the Fukuyama-Lee-Rice model[1] has been quite successful and several others[2] exist? One answer is this: The MSH model we introduce is unique since no other existing dynamical model for CDWs *generically* contains both the elastic limit and generation of dislocations without any *ad hoc* assumptions. In the following, we derive the MSH model and show its relation to the Fukuyama-Lee-Rice model. After that we show the qualitative behavior at different limits, and compare the results to some recent experimental observations.

Much of our interest in CDWs was motivated by the X-ray scattering experiments of Ringland *et al.*[3]. Their results indicated that the sliding CDW above the depinning transition is more *disordered*, than the CDW when it is let to relax to equilibrium from the sliding state. This is in contrast to the predictions of the elastic Fukuyama-Lee-Rice theory. Physically, this may be due to the dynamical generation of dislocations above the depinning transition, i.e., when the average velocity of the CDW condensate is nonzero. Furthermore, in that case, the generation of dislocation is a bulk effect, unlike the often regarded current conversion process in the vicinity of the contacts[4]. Our model generically accounts for topological defects and is able to explain the experimental observations.

5.2 *Model*

As we reviewed in previous chapter, in the conventional approach, one writes down the phenomenological Ginzburg-Landau free-energy for the complex order parameter

[1] Fukuyama and Lee [78]; Lee and Rice [79]. Levy et al. [92] have also proposed an extension of the Fukuyama-Lee-Rice model incorporating the effects of normal carriers.
[2] Grüner, Zawadowski and Chaikin [81]; Ong, Verma and Maki [84]; Myers and Sethna [93a].
[3] Ringland et al. [99b].
[4] Ramakrishna et al. [92]; Ramakrishna [93].

Ψ of the condensate:

$$\mathcal{F}_{GL} = \int d\vec{x} \left(|\nabla\Psi|^2 + \frac{\alpha}{2}|\Psi|^2 + \frac{\beta}{4}|\Psi|^4 \right), \tag{5.1}$$

where $\Psi = A(\vec{x},t)e^{i\phi(\vec{x},t)}$, and the parameters α and β determine the mean field amplitude through $A_{MF} = \sqrt{-\alpha/\beta}$. To study the dynamics of the condensate, one adds terms accounting for the driving force and pinning by imperfections, to the free-energy. When the amplitude fluctuations (and hence phase slips) are neglected, the only dynamic degree of freedom is the local phase, and one arrives at the Fukuyama-Lee-Rice[1] equation of motion. However, as discussed in the previous chapter, the phase-only description has limited validity, due to the possibility diverging strains and phase slip. Therefore, one would like have a model that both incorporates phase slips, and is numerically efficient. Phase slips are certainly taken into account in the full Ginzburg-Landau approach when amplitude fluctuations are included, but we have found a novel, alternative method that we will show is equivalent to the Ginzburg-Landau approach.

5.2.1 *Swift-Hohenberg equation*

Since the Swift-Hohenberg equation is the basis for our model, we will review it briefly before deriving the model. As we discussed in Chapter 3, instabilities in physical systems may arise for various reasons; in a voltage driven superconducting ring, the supercurrent periodically reached the critical current and the system had to make a transition to a new state. This process involved generation of topological defects and led to a complicated state selection problem. This behavior arose naturally from the phenomenological Ginzburg-Landau theory of superconductivity. The Swift-Hohenberg equation was originally developed to study convective flow, and, in particular, the transition from a uniform conductive state to a convective state in simple fluids, within the Boussinesq approximation[2]. The Rayleigh-Bénard experiment is probably the most famous such system, see Fig. 5.1.

In the Rayleigh-Bénard problem, the onset of the convective state is controlled by the ratio between the buoyancy force and the viscosity. This is a dimensionless

[1] Fukuyama and Lee [78]; Lee and Rice [79].

[2] The Boussinesq approximation means that thermal volume expansion of the fluid is negligible.

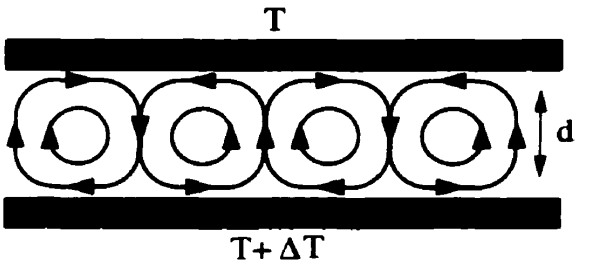

Figure 5.1: In many driven systems there is a transition from a uniform conductive state to a periodic state. In a Rayleigh-Bénard experiment, a viscous liquid is heated from below. When the temperature gradient between the plates becomes large enough, the uniform state breaks as convective rolls emerge. This occurs when the viscosity cannot balance the destabilizing buoyancy force anymore. The arrows indicate the motion of the convecting rolls.

measure and it is called the Rayleigh number R. There exists a critical value R_c at which the instability occurs. Loosely speaking, R_c plays a similar role to the critical temperature in the case of a continuous phase transitions. The Rayleigh-Bénard system is rotationally invariant in the horizontal plane; there is no reason why the rolls should prefer one direction over another. However, the system is characterized by a wavelength, since the emergence of the roll pattern introduces a length scale in the problem, i.e., at the onset of the instability, the growth rate of the most unstable mode becomes positive and a pattern emerges.

By using the analogy to critical phenomena, we can define a control parameter $\epsilon = (R - R_c)/R_c$. If $\epsilon < 0$, the growth rates corresponding to all wavevectors are negative. However, as ϵ passes through zero and becomes positive, the growth rate of the most unstable mode becomes positive and a pattern with $q_c \neq 0$ emerges. q_c is the first wavevector that becomes positive. We use linear analysis and general symmetry principles to obtain a generic equation exhibiting the behavior described above. When that equation is supplemented by the lowest order nonlinear term we obtain the Swift-Hohenberg equation. In addition to rotational symmetry, the system must also exhibit mirror symmetry $x \rightarrow -x$ (and $y \rightarrow -y$). The symmetry requirements forbid odd powers of q from entering the dispersion relation, and the lowest order term that fulfills the symmetry requirements is q^2. Therefore, the dispersion relation must be of form

$$\sigma(q) = \epsilon - (q_c^2 - q^2)^2. \tag{5.2}$$

The behavior of σ vs. q is shown in Fig. 5.2 for different values of the control pa-

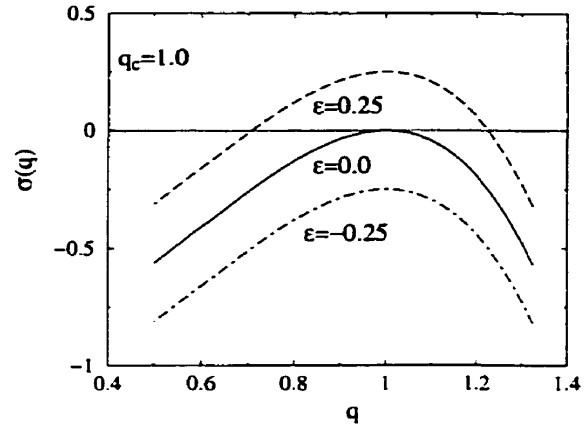

Figure 5.2: Growth rate $\sigma(q)$ for various values of the control parameter ϵ. As ϵ becomes positive the growth rate of the most unstable mode becomes positive and the amplitude of the new pattern becomes nonzero.

rameter. To obtain the equation of motion, we notice that the scalar field must be symmetric under sign reversal, i.e., under $\psi \to -\psi$, and therefore the simplest nonlinear term in the equation of motion is cubic. Combining these considerations, we obtain the Swift-Hohenberg equation. In dimensionless units, the Swift-Hohenberg equation reads

$$\frac{\partial \psi}{\partial t} = \left[\epsilon - \left(q_c^2 + \nabla^2\right)^2\right] \psi - \psi^3, \tag{5.3}$$

where $\psi = \psi(\vec{x}, t)$ is a scalar field. Strictly speaking, the Swift-Hohenberg equation is asymptotically correct in the limit $R \to R_c$, since the equation of motion was derived by considering only the immediate vicinity of the most unstable wavevector q_c. It is also remarkable that it is possible to express the Swift-Hohenberg equation in terms of a Lyapunov functional

$$\mathcal{F}_{SH} = \int d\vec{x} \left(-\psi \left[\epsilon - \left(q_c^2 + \nabla^2\right)^2\right] \frac{\psi}{2} + \frac{\psi^4}{4} \right), \tag{5.4}$$

so that the equation of motion satisfies relaxational dynamics. Fig. 5.3 shows a snapshot from a simulation using a discretized version of the Swift-Hohenberg equation.

5.3 *Modified Swift-Hohenberg equation*

Motivated by the Swift-Hohenberg equation we now derive an equation of motion for CDWs. Due to the motivation, we call it the Modified Swift-Hohenberg (MSH) equa-

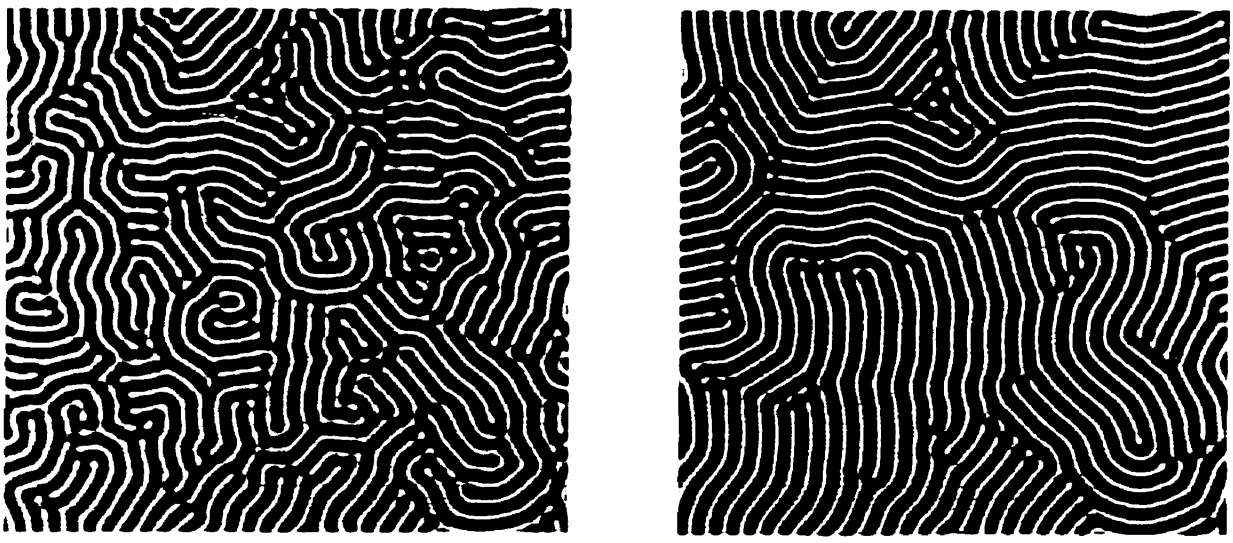

Figure 5.3: Snapshots from a simulation of the Swift-Hohenberg equation, Eq. (5.3). The roll patterns are rotationally invariant and have a characteristic wavelength. The control parameter was set to $\epsilon = 0.25$. The two snapshots are taken at times a) $t = 100$ and b) $t = 1000$. It is clearly visible that the system has not yet reached its steady state since ordering takes place as the time evolves. This can be considered as a top view of the system in Fig. 5.1.

tion. As discussed in the previous chapter, an ideal incommensurate CDW system at rest is a translationally invariant periodic state. The translational invariance is broken if the CDW is pinned by imperfections. In analogy to the Swift-Hohenberg equation, we have to define a control parameter ϵ. In CDWs, the state with $\epsilon < 0$ corresponds to the uniform charge density of the metallic state, and $\epsilon > 0$ should yield the periodic CDW state. Since the periodic CDW state emerges upon cooling the system below T_P, the critical temperature of the Peierls transition, we define $\epsilon \equiv (T_P - T)/T_P$. From the pattern formation point of view, there is one major difference in the symmetry properties of the Rayleigh-Bénard system as compared to CDWs. In contrast to Rayleigh-Bénard system, the ground state of a CDW system does not have rotational symmetry, but has a preferred orientation in the horizontal plane instead. This is due to the highly anisotropic nature of systems exhibiting CDWs. This can be taken into account by modifying the rotationally invariant gradient term in such a way that Eq. (5.3) reads now as

$$\frac{\partial \psi}{\partial t} = \left[\epsilon - \left(q_c^2 + \frac{\partial^2}{\partial x^2}\right)^2 + 4q_c^2 \frac{\partial^2}{\partial y^2}\right] \psi - \psi^3. \tag{5.5}$$

This modification guarantees that the ground state has a preferred orientation, i.e., it is an anisotropic uniformly striped phase in the y-direction.

In the absence of external drive and impurities, the Swift-Hohenberg equation gives rise to a sinusoidal scalar field[1]. This provides a direct analogy to the CDW condensate, where the wavelength $q_c = Q = 2k_F$. q_c is the fastest growing mode, i.e., $\partial_q \sigma(q = q_c) = 0$, where $\sigma(q)$ is the dispersion relation from Eq. (5.2). In the following we will use $q_c = 1$. Therefore, in Eq. (5.5) the scalar field ψ denotes the local CDW condensate density, and $\epsilon \equiv |T - T_P|/T_P$, with T_P denoting the critical temperature of the Peierls transition.

We now add an external drive $E \sim v$, impurity pinning V^i_{imp} that couples directly to the order parameter as in the Fukuyama-Lee-Rice theory, and an uncorrelated Gaussian noise source η , i.e., $\langle \eta(\vec{x}, t) \rangle = 0$ and $\langle \eta(\vec{x}, t)\eta(\vec{x}', t') \rangle = 2\epsilon_{noise}\delta(\vec{x} - \vec{x}')\delta(t - t')$. The angular brackets denote an average, and ϵ_{noise} is the intensity of the noise. With these additions the full MSH equation becomes

$$\frac{\partial \psi}{\partial t} + E\frac{\partial \psi}{\partial x} = \left[\epsilon - \left(1 + \frac{\partial^2}{\partial x^2}\right)^2 + 4\frac{\partial^2}{\partial y^2}\right]\psi - \psi^3 + \sum_i V^i_{imp} + \eta. \qquad (5.6)$$

As in the case of the Swift-Hohenberg equation, we note that the dynamics of the order parameter can be derived (in the absence of external drive) from the following Lyapunov functional:

$$\mathcal{F}_{MSH} = \int d\vec{x} \left(-\psi \left[\epsilon - \left(1 + \frac{\partial^2}{\partial x^2}\right)^2 + 4\frac{\partial^2}{\partial y^2}\right]\frac{\psi}{2} + \frac{\psi^4}{4} + \sum_i \psi V^i_{imp}\right). \qquad (5.7)$$

Even though the MSH equation contains the correct symmetries, we have to establish a formal connection to the traditional Ginzburg-Landau/Fukuyama-Lee-Rice approach.

If the cosine solution is perturbed locally, i.e., $\cos(qx)$ is replaced by $\cos(qx + \phi(x))$, the energy cost goes as $\int d\vec{x}|\nabla\phi|^2$. In other words, there is a 'soft' mode associated with the local modulation of the condensate, just as in the traditional Fukuyama-Lee-Rice theory. As discussed in the previous chapter, the amplitude mode is 'hard' having an energy cost of order of the energy gap. An amplitude excitation in the Ginzburg-Landau model corresponds to local variations of the amplitude of the sinusoidal order

[1] Pomeau and Manneville [79]. Strictly speaking, this is true at the limit when $\epsilon \to 0$. For large ϵ numerical solutions are needed.

parameter in the MSH equation. In the absence of an external driving force and impurities, and in the limit $\epsilon \to 0$, the nonlinearities are weak, and the spatial and temporal modulations of the pattern are slow. Hence we can use perturbation theory to study the dynamics of the most unstable mode q_c, which is the one of most interest; as the growth rate of q_c becomes positive, the periodic CDW state emerges.

Formally, we use the method of multiple scales. The idea is to separate the fast and slow scales by expanding the solution in terms of the control parameter ϵ in the MSH equation. This expansion leads to an equation of motion for the amplitude. The solvability condition yields an equation of motion for the amplitude of the most unstable mode. We introduce a slow time scale $T = \epsilon\, t$, slowly varying spatial scales $X = \epsilon^{1/2}\, x$, $Y = \epsilon^{1/2}\, y$, and expand the solution ψ as a weakly nonlinear expansion in ϵ:

$$\psi = \epsilon^{1/2}\psi_0 + \epsilon\psi_1 + \epsilon^{3/2}\psi_2 + O(\epsilon^2). \tag{5.8}$$

Since we are looking for a solution when $E = 0$, we drop out the second term from the left hand side in Eq. (5.6). In addition, thermal noise η and the impurity term are neglected.

The derivatives in Eq. (5.6) transform as

$$\begin{cases} \frac{\partial}{\partial t} & \to \epsilon \frac{\partial}{\partial T} \\ \frac{\partial}{\partial x} & \to \frac{\partial}{\partial x} + \epsilon^{1/2} \frac{\partial}{\partial X} \\ \frac{\partial}{\partial x} & \to \frac{\partial}{\partial y} + \epsilon^{1/2} \frac{\partial}{\partial Y}, \end{cases} \tag{5.9}$$

and the operators in the MSH equation transform as

$$\begin{cases} \frac{\partial}{\partial t} & \to \epsilon \frac{\partial}{\partial T} \\ \left(q_c^2 + \frac{\partial^2}{\partial x^2}\right)^2 & \to \mathcal{L}^2 + 4\mathcal{L}\epsilon^{1/2} \frac{\partial}{\partial x}\frac{\partial}{\partial X} + \epsilon \left(4\frac{\partial^2}{\partial x^2} + 2\mathcal{L}\right) \frac{\partial^2}{\partial X^2} + 4\epsilon^{3/2} \frac{\partial}{\partial x}\frac{\partial^3}{\partial X^3} + O(\epsilon^2) \\ \frac{\partial}{\partial y^2} & \to \frac{\partial}{\partial y^2} + \epsilon \frac{\partial^2}{\partial Y^2} + 2\epsilon^{1/2} \frac{\partial}{\partial y}\frac{\partial}{\partial Y} \\ \frac{\partial}{\partial x} & \to \epsilon \frac{\partial}{\partial y} + \epsilon^{1/2} \frac{\partial}{\partial Y}, \end{cases} \tag{5.10}$$

where we have defined the linear operator as $\mathcal{L} = q_c^2 + \partial_x^2$. Now, we substitute the transformed operators with Eq. (5.8) into the MSH equation. When we collect the terms order by order in ϵ, we find out that the terms of order $O(\epsilon^{1/2})$ and $O(\epsilon)$ do not provide a constraint for the amplitude of the lowest mode, i.e., A_0. The first

non-trivial case is $O(\epsilon^{3/2})$ yielding

$$-\mathcal{L}^2\psi_2 + 4\frac{\partial^2}{\partial y^2}\psi_2 - A_0^3 e^{3iq_c x} + \left[e^{iq_c x}\left(-\frac{\partial}{\partial T} + 4q_c^2\frac{\partial^2}{\partial X^2} + 4\frac{\partial^2}{\partial Y^2} - 3|A_0|^2 + 1\right)A_0\right] + c.c. = 0. \quad (5.11)$$

By using the Fredholm alternative theorem[1] we obtain the following equation for motion for A_0:

$$\frac{\partial A_0}{\partial T} = 4\left(\frac{\partial^2}{\partial X^2} + \frac{\partial^2}{\partial Y^2}\right)A_0 + A_0 - 3|A_0|^2 A_0. \quad (5.12)$$

This is the time-dependent Ginzburg-Landau equation of motion for a complex order parameter in the absence of a driving force and a pinning potential. Therefore, close to the threshold, i.e., when $\epsilon \to 0$, where only the most unstable mode is important, the MSH and Ginzburg-Landau approaches are equivalent. The scalar MSH order parameter contains both the local amplitude and phase fluctuations of the periodic CDW modulation in the Ginzburg-Landau approach. This equivalence of the two approaches should come as no surprise since the nature of the equation of motion depends only on the universal symmetries.

Away from the threshold ($\epsilon \sim O(1)$), the argument becomes more subtle, since other (linearly) unstable modes are important and cannot be ignored. In particular, we want to make sure that the wavelength of the modulation does not vary too much. In fact, Pomeau and Manneville[2] have established that an approximate steady-state solution of $d = 1$ SH equation can be written as

$$\psi^{d=1}(x) = \sum_{i=0}^{\infty} a_i \sin(q_c[2i+1]x), \quad (5.13)$$

where $a_0(q_c) = \sqrt{4w(q_c)/3}$, $a_1(k_0) = -a_0(q_c)^3/4w(3q_c)$, $w(q_c) = \epsilon - (1-q_c^2)^2$, and $q_c = 1 - \epsilon^2/1024$. This solution shows that the main effect of the other unstable modes is to effectively renormalize the wavelength q_c of the (approximately) sinusoidal solution. Since the wavelength of the CDW condensate does not depend on temperature, we expect that our approach is still valid even for $\epsilon \sim O(1)$, since then $q_c = 2k_F$ has changed by 0.1 per cent. Our numerical results and tests for $\epsilon \gg 0$ and large E

[1] See e.g. Nayfeh [81]
[2] Pomeau and Manneville [79].

strongly support this result. Furthermore, in the case of Rayleigh-Bénard convection, experimental results[1] show similar behavior. Even away from the transition point, the wavenumber of the convection rolls appears to be q_c to a great degree of precision.

We have now established a formal connection to the Ginzburg-Landau/ Fukuyama-Lee-Rice theory, and shown that the MSH approach has the correct symmetries and produces the correct ground state. Before going to the results, we discuss briefly the effect of thermal fluctuations. We will not present a full analysis but refer to the results for the Rayleigh-Bénard instability. Graham[2] studied the effect of thermal fluctuation around R_c in detail. His results show that the convective instability in the presence of thermal fluctuations strongly resembles continuous phase transitions in equilibrium statistical mechanics. However, there is some controversy about this result, since Swift and Hohenberg [77] argued that the transition at R_c is of first order. See also the work of Nelson and Toner [81]. However, this should not be a crucial issue, since we are not interested in the transition to the CDW state but are always below the transition. In addition, we are interested in the properties under an applied driving force. Furthermore, an interesting aspect about fluctuations upon application of an ac drive is mode-locking and freeze-out thermal fluctuations[3]. We have not pursued those aspects in detail.

5.4 Results

5.4.1 Mean-field theory

Before presenting the results from the numerical simulation, we study the effect of dislocations by mean-field analysis. However, the mean-field results, especially the predictions for the nature of the (dynamical) phase transition and critical exponents, should be interpreted with care. This caution is due to the unperturbative nature of topological defects. Nevertheless, the mean-field analysis should be able to display many of the generic features of the process.

Unbound dislocation pairs or loops decrease order in systems with continuous symmetry in equilibrium; a prime example of this is the $d = 2$ XY model, where the

[1] Koschmieder [66].
[2] Graham [73]; Graham [74].
[3] Higgins, Middleton and Bhattacharya [93].

unbinding of dislocation pairs leads to a transition from a state of (quasi) long-range order to one with short-range order. This transition is called the Kosterlitz-Thouless transition[1].

As far as driven CDWs are concerned, it has been proposed that close to the depinning transition, the system is unstable under proliferation of unbound dislocation pairs (loops) in $d = 2$ ($d = 3$)[2]. As a consequence, a new length scale ξ_D is introduced that determines the density of dislocations of one sign through

$$n_D \sim \xi_D^{-d}. \tag{5.14}$$

As long as ξ_D satisfies $\xi_D < \xi$, where ξ denotes the correlation length of the condensate in the absence of dislocations, ξ_D sets the relevant length scale for the correlations. This scenario can be realized in the strong-pinning limit.

Working in the weak-pinning limit ($\xi_D > \xi$), we argue that the qualitative behavior of the dislocation density n_D (and hence the structure factor) can be understood as follows. In the absence of thermal fluctuations, the generation of dislocations must depend on the number density of pinned sites n_p and on the local strain rate. In addition, the annihilation of dislocations depends on the mobility D and n_D. In mean-field theory, the rates for generation and annihilation of topological defects are given by

$$R^G \sim n_p \cdot v \text{ and } R^A \sim D \cdot n_D. \tag{5.15}$$

Velocity of the CDW enters in R^G since the local strain rate is proportional to the local velocity. Using the above expressions, the mean-field steady-state concentration of dislocations is simply

$$n_D \sim n_p \cdot v. \tag{5.16}$$

Next, we shall use scaling arguments to relate n_D to E, in the limits $E \to E_c$ and $E \gg E_c$.

Let us consider the case $E \to E_c$ first. Using scaling arguments[3] we can write the velocity of a CDW as

$$v \sim (E - E_c)^\theta, \tag{5.17}$$

[1] Kosterlitz and Thouless [72]; Kosterlitz [74].
[2] Coppersmith [90]; Coppersmith [91]; Coppersmith and Millis [91]; Balents and Fisher [95].
[3] Fisher [83]; Fisher [85].

the number of pinning sites as

$$n_p \sim (E - E_c)^{-\nu}, \tag{5.18}$$

and using Eq. (5.16) the number density of dislocations as

$$n_D \sim (E - E_c)^{\theta-\nu}. \tag{5.19}$$

The exponents for a phase-only model introduced by D.S. Fisher[1] are given in an epsilon expansion in $d = 4 - \epsilon$, by $\theta = 1 - \epsilon/6 + O(\epsilon^2)$ and $\nu = 1/2$. Therefore, we expect that

$$n_D \sim (E - E_c)^{1/6}, \tag{5.20}$$

in $d = 2$ in this limit, i.e., n_D is an increasing function of E. This argument supports the idea that dislocations unbind close to E_c. In principle, this argument can be used as a consistency check for models of CDW depinning: as long as $\theta - \nu \geq 0$, dislocations will appear, and hence they should be taken into account. However, it should be kept in mind that the above is based on mean-field arguments, and in particular, the exponents are based on phase-only models exhibiting dynamical critical phenomena. Proliferation of dislocations is likely to destroy the critical behavior, and in the cases where the exponents can be measured, we expect that

$$n_D \sim (E - E_c)^{\theta'}, \tag{5.21}$$

where $\theta' \neq \theta = 1/6$. We have not estimated θ' from our simulations.

Now, let us discuss the limit $E \gg E_c$. Far away from the depinning threshold the velocity will be proportional to the driving force. Consider the case when the strengths of the impurities are drawn from a Gaussian distribution. Let $x \equiv V_i$. The probability that the strength x of a given impurity site is enough to pin the phase locally (neglecting local elasticity) under the influence of an applied force of strength E is given by

$$P(x|x \geq E) \propto \int_E^\infty \mathrm{dx}\; e^{-\frac{x^2}{2V_0^2}}. \tag{5.22}$$

By changing variables we obtain

$$P(x|x \geq E) \propto \int_{E/(\sqrt{2}V_0)}^\infty \mathrm{dx}\; e^{-x^2} = \mathrm{erfc}\left(\frac{E}{\sqrt{2}V_0}\right) = 1 - \mathrm{erf}\left(\frac{E}{\sqrt{2}V_0}\right). \tag{5.23}$$

[1] Fisher [83]; Fisher [85]; Narayan and Fisher [93].

Figure 5.4: Schematic illustration of the behavior of the dislocation density as a function of the driving force. Close to E_c the behavior is describe by a power law, and the at large E the dislocation density decays as $\exp(-E^2)$.

We note that this approximation overestimates the probability due to the neglect of elastic interactions.

To obtain the total number of pinned sites, n_p, and thus the dislocation density, we have to multiply $P(x|x \geq E)$ by the total number of impurities N, thus

$$n_D \sim v \cdot n_p \cdot P(x|x \geq E) = E \cdot n_p \cdot P(x|x \geq E) = n_p \cdot E \left[1 - \mathrm{erf}\left(\frac{E}{\sqrt{2}V_0}\right)\right]. \quad (5.24)$$

The limits of the error function are $\mathrm{erf}(0) = 0$ and $\mathrm{erf}(\infty) = 1$. The error function is exponential and decays much faster than any power of E. For small arguments the error function can be written as

$$\mathrm{erf}(x) = \frac{2}{\sqrt{\pi}} e^{-x^2} \left(z + \frac{2x^3}{1 \cdot 3} + \frac{4x^5}{1 \cdot 3 \cdot 5} + \ldots\right), \quad (5.25)$$

and for large arguments

$$\mathrm{erf}(x) = 1 - \frac{1}{\sqrt{\pi}x} e^{-x^2} \left(1 - \frac{1}{2x^2} + \frac{1 \cdot 3}{(2x^2)^2} - \ldots\right). \quad (5.26)$$

Thus

$$\lim_{E \to \infty} n_D = 0. \quad (5.27)$$

We will compare the predictions of the mean-field theory to the numerical simulations of the MSH model in Section 5.6.

5.5 *Numerical implementation and simulation parameters*

To simulate Eq. (5.6), we discretized it in time and space. We have used the Euler integration scheme for the time derivative. Since the MSH equation has periodic

solutions, Δx must be smaller than the wavelength (we have $q_c = 1$). In addition, a good rule of thumb is that a wavelength should include at least 8 points. Therefore we set $\Delta x = 2\pi/8$. We used the von Neumann stability analysis to ensure Δx is sufficiently small, in order to avoid numerical instabilities. The simulations were done in a 2D square lattice with $L = 256$, $dt = 0.05$ and $dx = 0.78$. The control parameter, ϵ, was varied between 0.1 and 1.2, and the rms magnitude of the quenched impurities, V_0, was varied between 0.2 and 1.0. Unless otherwise mentioned, the structure factors and dislocation densities were averaged over 10 samples.

5.6 *Numerical results*

Having established the equivalence between the two approaches, we now turn to numerical analysis of our model. First, we will take a look at snapshots of the system under different conditions. Fig. 5.5 shows the system in the weak pinning regime, when the intensity of the quenched noise and the driving force are being varied. The snapshots reveal several qualitative features of the model, the most important being: *i)* the effect of quenched disorder on the ground state and the existence of dislocations in large length scales, i.e., $\xi \gg \xi_D$, and *ii)* generation of dislocations in the presence of a non-zero driving force. We will discuss these aspects in the following.

In Fig. 5.5a, the system is not driven ($E = 0$), and it is let to relax to one of its metastable states. As the figure shows, there is a small but finite number of dislocations present. In Fig. 5.5b we have added a small ($E > E_T$) driving force. A comparison with Fig. 5.5a shows, that now the dislocations appear in different locations; they are generated dynamically due to interaction between the elastic forces and the pinning forces. In addition, the number of dislocations is larger than as compared to the case when $E = 0$. In Figs. 5.5c and 5.5d, we decreased the rms magnitude of the random pinning. The driving force was zero, and the impurity configuration is exactly the same is in the previous two figures. As V_0 is lowered, the number of dislocations diminishes, and a further decrease (Fig. 5.5d) in V_0 leads to the disappearance of dislocations.

These observations are consistent with the mean-field theory. As Figs. 5.5c and 5.5d show, dislocations are present at long length scales in the absence of a driving

force, and they are dynamically generated due to increasing and non-uniform distribution of local strains in the system. Due to the finite system size, the exponential tail in the number density of dislocations in Fig. 5.4 now has a cut-off. This is why the dislocations disappear at a finite value of V_0. The features discussed above are generic to the model. As long as we ensure that we are in the weak pinning limit, the behavior as described above does not depend on fine tuning the parameters. We tested this by varying the simulation parameters. A similar comment applies also to the strong pinning limit. The physically interesting regime is, however, between the two limits.

5.6.1 *Dynamical generation of dislocations*

The mean-field theory discussed in Section 5.4.1 in predicts that in the limit $L \to \infty$, dislocations will always emerge when the driving force is non-zero. To make the above discussion more concrete, we have computed the dislocation densities in the simulations. In practice, it is rather difficult to estimate the exact number of dislocations; their periodic appearance at different locations upon changing driving force makes the procedure tedious. However, it is possible to use the local gradient as a criterion for finding a dislocations at point x. This can be done by counting the number of areas in the system where the local gradient $|\nabla\psi| \geq 2 \times |\nabla\psi^*|_{max}$, where ψ^* denotes the undistorted condensate profile. We stress that, although our method is accurate in estimating the number of dislocations only up to a constant, the relative numbers are accurate. The criterion was checked by comparing snapshots of the system at different moments, impurity configurations and driving forces. We will now compare the qualitative predictions of the mean field theory to the simulations of the MSH model.

In Fig. 5.6, we show the dependence of the number of dislocations on external driving force normalized by the maximum dislocation density. The data is in good qualitative agreement with our mean-field arguments. The errors in estimating n_D/n_{max} in Figs. 5.6, 5.7 and 5.8 are of order 5% near the peak, and larger (of order 10 %) in the tails. We are only interested in qualitative trends in the dislocation density, so a detailed estimate of error is not necessary. A general feature of the dislocation densities is the non-zero value at $E = 0$. That also suggests, that the role of ampli-

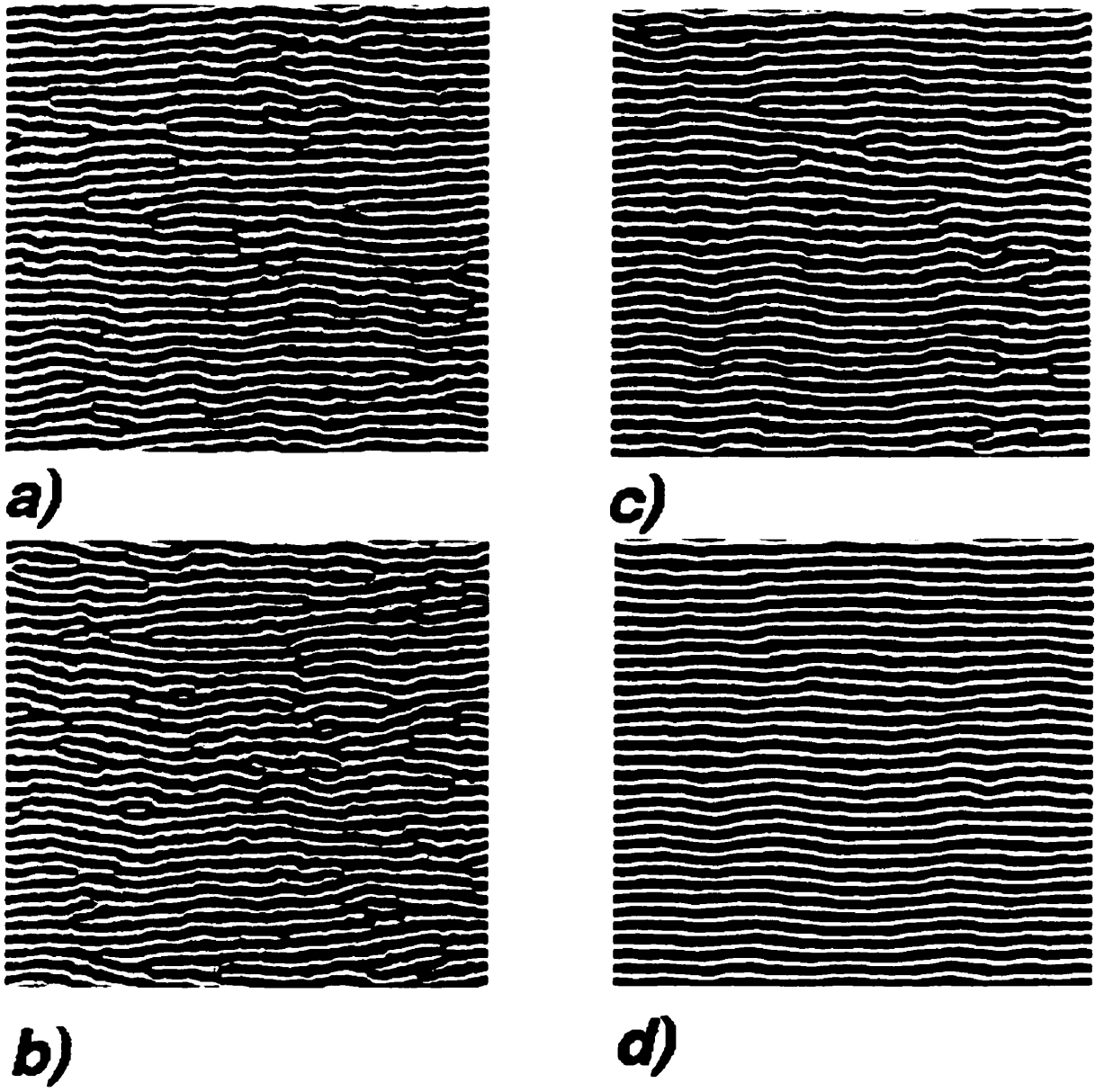

Figure 5.5: Snapshots of simulations of the Modified Swift-Hohenberg equation. In all the figures we are in the weak pinning limit. The concentration of impurities is kept equal in all of the snapshots. The driving force and the intensity of the quenched noise is varied as follows: a) $E = 0$ and $V_0 = 0.4$, b) $E = 0.03$ and $V_0 = 0.4$ c), $E = 0$ and $V_0 = 0.3$, d) $E = 0$ and $V_0 = 0.1$. Panels a) and b) show that the numbers of defects, and thus, the disorder, increases upon increasing driving force. When panels a) is compared to c) and d) it is seen that as the intensity of the quenched noise decreases, the system becomes gradually more ordered.

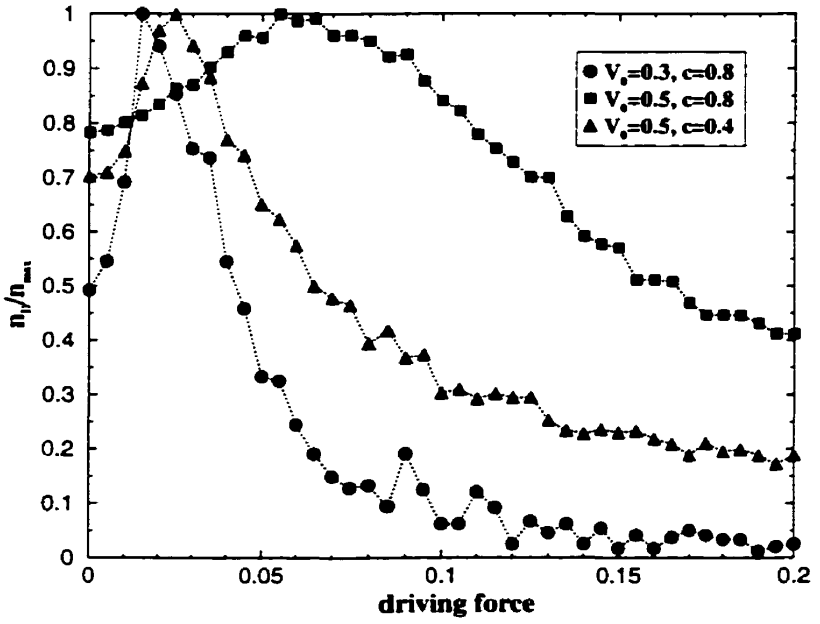

Figure 5.6: Dislocation density as a function of the driving force for different impurity concentrations (c) and rms magnitudes (V_0) of the impurity pinning.

tude fluctuations may be important for $E \neq 0$. Moreover, recent theoretical studies by Zeng, Leath and Fisher [99] in $d = 2$ indicate that dislocations proliferate in the presence of quenched disorder even at $E = 0$. This is in agreement with the general features observed in Fig. 5.6.

The dislocation density can be used to see qualitative differences in the behavior between the weak and strong pinning limits. Roughly speaking, the two regimes can be distinguished by the correlation length ξ. In the strong pinning limit, $\xi \sim O(c^{-1/2})$ and in the weak pinning limit $\xi \gg c^{-1/2}$, where $c^{-1/2}$ denotes the average distance between pinning centers. To study this, we applied the driving force as increasing from zero to higher values ($E \gg E_T$), and compared the results to the case when the driving force was switched off at a high value ($E \gg E_T$). Fig. 5.7 shows the relative dislocation densities for both forward and reverse driving forces at the weak pinning limit. The curves are almost identical except in the area between $E = 0$ and the value where n_D reaches its maximum. This difference is due to existence of many metastable states[1]. As the driving force is increase from zero, dislocations start to appear, but the CDW remains pinned. There are many possible metastable states

[1] See also the work of Tang et al. [87] and Bak, Tang and Wiesenfeld [87]

in which the CDW can be trapped. If thermal noise is added, the relaxation of the system becomes an activated process — there exists an activation barrier between the metastable states, and fluctuations can carry the system over the barrier. Locally, the activation barrier may be reduced due to higher than average strains. Since the system is (apart from dislocations) coupled elastically, relaxation is a collective process. Including thermal fluctuations would lead to similar behavior in the low E limit. However, it has no effect on the position of n_{max}.

Next, we decrease the concentration of impurities, thus moving away from the weak pinning limit toward strong pinning. Formally, we can define a dimensionless parameter $\kappa \equiv \epsilon^{1/2}c/V_0$ to distinguish between the weak and strong pinning limits. $\kappa \to 0$ corresponds to strong pinning and $\kappa \to \infty$ to weak pinning. Fig. 5.8 shows the simulations with both increasing and decreasing driving force (the arrows indicate the direction). The low E limit shows similar behavior as before, although the difference is now clearer than in the previous case. What is important, however, is the difference in the peak positions of the two curves. As discussed above, the peak position indicates depinning. Thus, the lower value of E for n_{max} using the decreasing driving force indicates that the collective CDW conduction extends to lower E as with increasing driving force; the depinning transition takes place at different values of E depending on the direction of the driving force. This is a signature of hysteresis, and in the I-V characteristics it is displayed as switching.

To see more clearly how the depinning transition, or switching as indicated by Fig. 5.8, takes place, we compare two configurations of the same system at different time steps around the depinning threshold. The configurations were taken 500 time steps apart, and then they were deducted from each other. This is shown in Fig. 5.9. The darker areas indicate where the changes are the largest, the color scale is the same in all the snapshots to make comparisons possible. The panels a)-c) show a snapshot from a system exhibiting switching. Just below the threshold there is hardly any movement in the system. As the driving force is increased to E_T, a conducting channel appears, and as the the E is increased to a slightly higher value, the system depins almost at once. The lower panels d)-f) show the system in the weak pinning regime. Even below threshold there are domains that moving. Domain formation

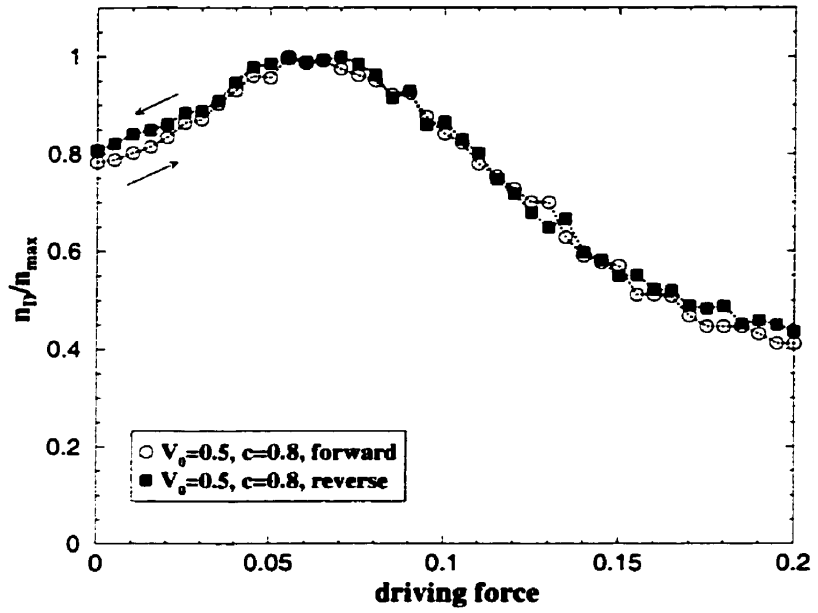

Figure 5.7: The relative number of dislocations as a function of the driving force in the weak pinning case. Within the accuracy of our study, the two curves are identical. The arrows indicate how the driving force was applied.

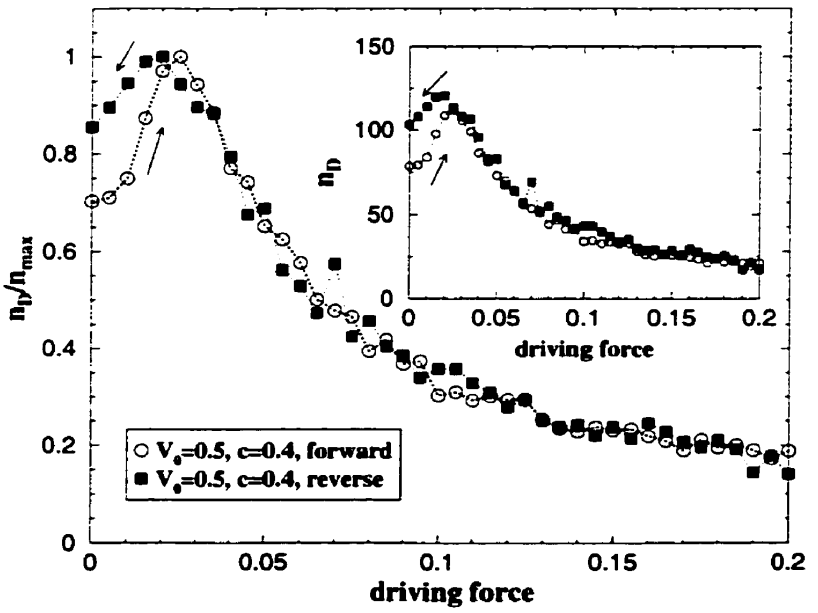

Figure 5.8: The relative number of dislocations as a function of the driving force. The arrows indicate how the driving force was applied. The inset shows the same plot in absolute numbers. At the high field limit the two curves are almost identical. The discrepancy at the $E \to 0$ limit is due to the activated nature of the relaxation process. What is remarkable, is the difference in the position of n_{max}. This shows that the depinning of the CDW condensate occurs at a different value of E depending on the direction of the applied driving force, i.e., the behavior of the CDW is hysteretic.

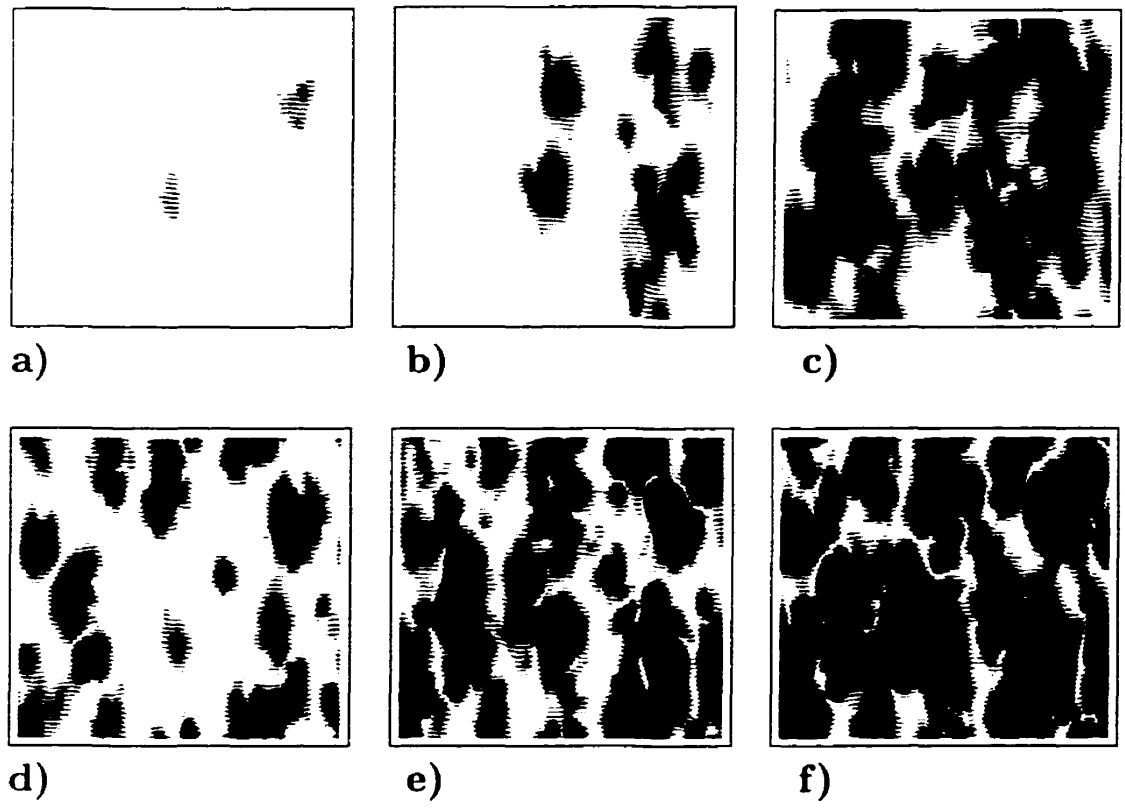

Figure 5.9: The behavior of the system near the depinning threshold. Each of the snapshots is a difference between two configurations 500 time steps a part. The black areas indicate where the changes occur, i.e., which areas are moving The color range is the same in all the pictures. Figures a)-c): $V_0 = 0.5$, $c = 0.4$; a) at $E = 0.020$, b) $E = 0.025$, and c) $E = 0.030$. d)-f): $V_0 = 0.5$, $c = 0.8$; a) at $E = 0.050$, b) $E = 0.060$, and c) $E = 0.070$. Figs. 5.8 and 5.7 show the corresponding dislocation densities.

is a general feature of the system in the weak pinning regime. However, the CDW remains pinned, and stresses are relieved by periodically-appearing phase slips. At E_T, the system depins. Depinning involves almost the whole system, and a slight increase in driving force leads to a more coherent motion.

5.6.2 *Structure factor measurements*

In order to distinguish between the different dynamic phases we calculated the spherically averaged (static) structure factor $S(q)$, defined as

$$S(q) = \left\langle |\hat{\psi}(\vec{q}')|^2 \right\rangle_{|\vec{q}'|=q}, \tag{5.28}$$

In the above, $\hat{\psi}$ denotes the Fourier transform of ψ, an overline denotes an angular average over one configuration, and $\langle \cdots \rangle_{|\vec{q}'|=q}$ denotes an average over all configurations and Fourier modes with $|\vec{q}'| = q$. A typical structure factor is shown in Fig. 5.10

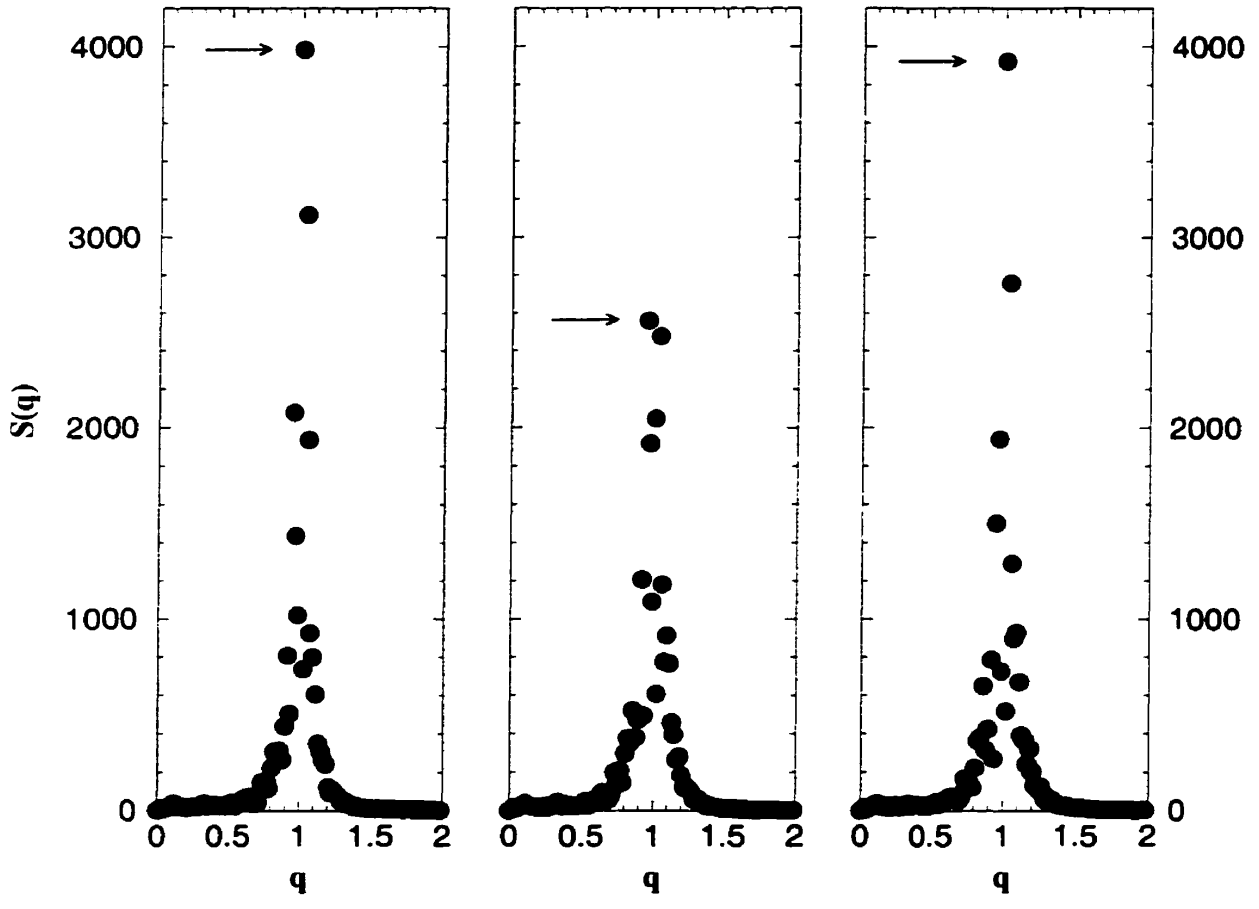

Figure 5.10: Spherically averaged structure factors, $V_0 = 0.5$ and $c = 0.8$. a) The system was driven above E_T, the field was switched off, and the system was let to relax, b) $E = 0.075(> E_T)$, and c) $E = 0.09$. The arrows indicate the maxima.

for a small and a large value of the external drive. It can be seen that for a driving force $E > E_T$, the peak of the structure factor is lower than that of the relaxed state, i.e., when the drive is switched off and the system is let to relax to its ground state. Correspondingly, the half width at half maximum (HWHM) value increases. This implies that the condensate is more disordered in the presence of an external drive and the phase-phase correlation length decreases. However, upon further increasing the drive we observe a sharpening of the peak, i.e., the phase-phase correlation length increases. In what follows, we will demonstrate that the observed behavior is due to dynamically generated dislocations.

In very recent dynamical x-ray scattering experiments Ringland et al. [99b] discovered that when the sliding charge-density wave relaxes from the sliding state to

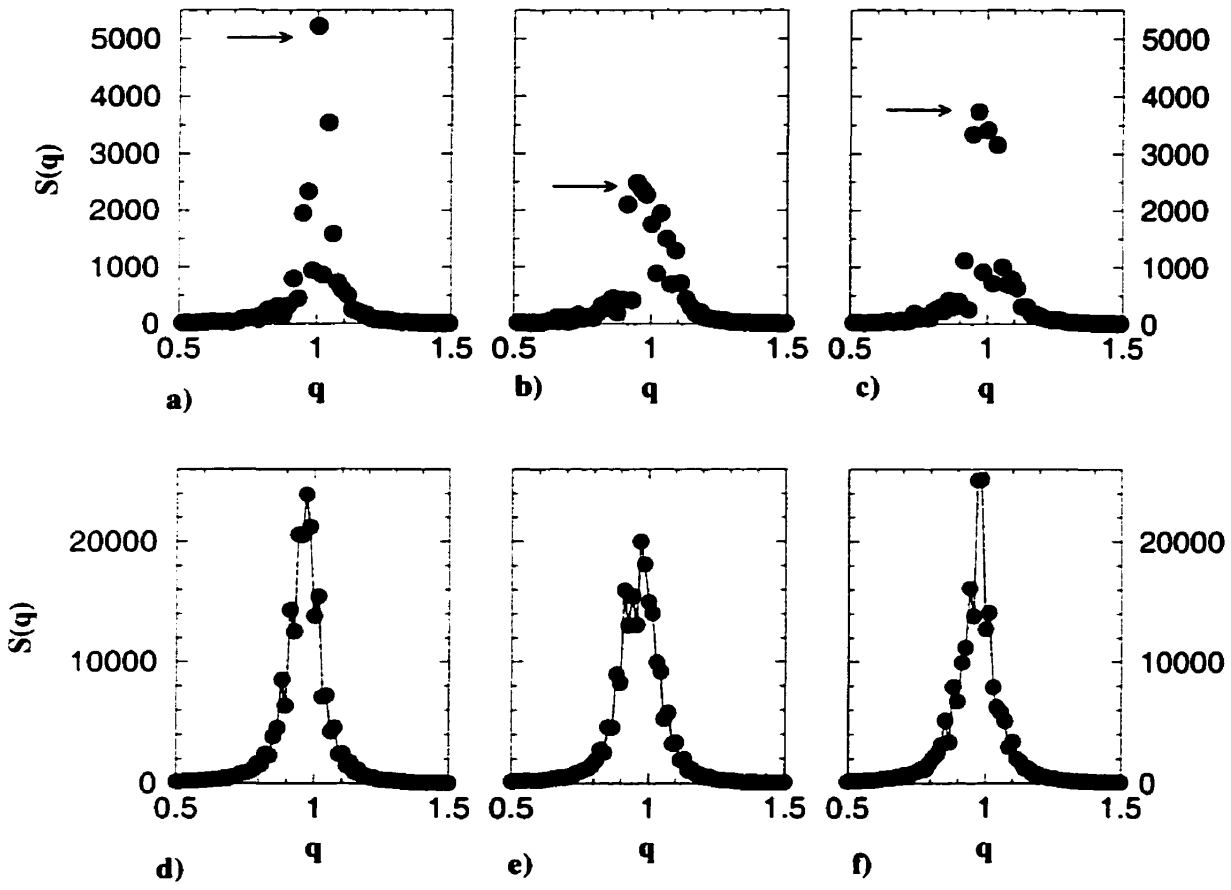

Figure 5.11: Upper panel: Spherically averaged structure factors, $V_0 = 0.4$ and $c = 0.8$. a) The system was driven above E_T, the field was switched off, and the system was let to relax, b) $E = 0.025(> E_T)$, and c) $E = 0.05$. The arrows indicate the maxima. Lower panel: Structure factors in transverse direction. Parameters in d)-f) correspond to those in a)-c).

the pinned state, it becomes more *ordered*. They observed this behavior in the weak pinning regime. This is contrary to what one would intuitively expect; the elastic approach and models based on interface propagation suggest that as the medium depins, it should become more ordered, i.e., the moving interface sees the quenched noise effective thermal noise. This novel behavior has not been observed before, and it is contrary to the predictions of the Fukuyama-Lee-Rice theory — to our knowledge, no existing model can explain this behavior. However, our simulations using the MSH model produce exactly the same qualitative behavior: when the driven state ($E > E_T$) is relaxed ($E = 0$), the resulting state is more ordered than sliding state. Fig. 5.10 demonstrates this behavior. Fig. 5.11 shows both spherically averaged structure factor and a 1D transverse structure factor for a different set of parameters to

demonstrate that the behavior is a generic feature of the model.

We explain this behavior as a manifestation of the proliferation of dynamically generated dislocations. At the relaxed state, the system has settled to its ground state and its energy is minimized. However, even at the ground state there exists a finite number of dislocations[1]. As the driving force is increased, amplitude fluctuations increase, rendering the system more disordered. This leads to decreasing phase-phase correlation length. Upon a further increase of the driving force the dislocations start unbind. Their subsequent motion and annihilation leads to increasing order. This is also visible in the snapshots in Figs. 5.5a and 5.5b. The recent x-ray scattering experiments by Ringland et al. [99a] on sliding CDWs suggest similar qualitative behavior.

5.7 *Conclusion*

In conclusion, we have introduced a novel approach to study the dynamics of driven charge-density waves. We have shown that our approach is equivalent to the conventional Ginzburg-Landau approach close to the Peierls transition. Moreover, we demonstrated by measuring the structure factors that the appearance of phase slips leads to a more disordered structure. However, at very high fields, the system becomes more ordered. In principle, this should be observable. It may well be, however, that this regime is difficult to access experimentally since applying higher driving forces leads to Joule heating, reduction of the gap energy, and finally to the disappearance of the charge-density wave state.

Our results, although of qualitative nature, are able to explain some recent experimental results. By studying the appearance of phase slips as a function of the driving force, we found that the structure factor of the CDW condensate became more ordered as the driving field ($E > E_T$) is switched off and the CDW system is allowed to relax. This is agreement with recent results from dynamical x-ray measurements of Ringland et al. [99b]. We explain this by the dynamical generation of dislocations: non-zero driving force leads to increasing strains and proliferation of dislocations. As the system relaxes to its ground state, it becomes more ordered. This result is also

[1] This is in agreement with the results of Zeng, Leath and Fisher [99].

in qualitative agreement with earlier theoretical expectations[1].

In addition, the interplay between the pinning forces and the internal interactions can lead to hysteresis and switching in the current-voltage characteristics. It is interesting to note that the hysteretic behavior of the dislocation density is closely related to a similar hysteretic behavior in the current-voltage characteristics of the system. This is known as "switching", and it is a generic feature of low-temperature charge-density waves[2]. This behavior, generic in our model, is in qualitative agreement with recent transport measurements of Lemay et al. [99]. Interestingly, this behavior has not been seen in any of the previously studied theoretical models[3]. Since our approach contains both the weak and strong pinning limits, it can be used to study the nature of the depinning transition. In particular, it still remains unsolved if, and when, the transition can be treated as a dynamical critical phenomenon. Our preliminary results suggest the existence of two distinct limits at the transition, namely critical and discontinuous[4].

[1] Coppersmith [90]; Coppersmith [91]; Coppersmith and Millis [91]; Balents and Fisher [95].
[2] Lemay et al. [99]; Zettl and Grüner [82]; Hall and Zettl [84]; Hall, Hundley and Zettl [88].
[3] Littlewood [89]; Sibani and Littlewood [90]; Middleton [92]; Chen et al. [96].
[4] Karttunen et al. [99c].

6

Conclusion

In the first part of this thesis we studied the nonequilibrium properties of driven quasi-one dimensional superconducting rings. The system was subjected to a constant electromotive force. The constant electromotive force induced an acceleration of the supercurrent. At the critical current, the system had to make a transition to a state of lower current. As we discussed, this transition was from a point of instability involving periodic generation of topological defects. This behavior is akin to instabilities in pumped lasers and accelerated solidification fronts. Our results showed that the state selection process depends intimately on the external driving force, i.e., the rate at which the system is driven, its internal properties such as fluctuations, and on the onset of dissipation (Ohmic resistance).

The problem of state selection is generic in all pattern formation problems. However, when the selection is from a point of instability, as in our case, there is one severe obstacle: no well developed formalism exists. We studied the system using linear stability analysis and numerical simulations. This revealed the highly non-linear nature of the system, and breakdown of linear analysis. We argued that, physically, as the Ohmic resistance becomes higher, the generic non-linearities are enhanced by the effects of charge imbalance in the superconducting ring, and the time scales related to its relaxation.

In the second part of this thesis, we proposed a new model for driven charge-density waves. Our model is a phenomenological one, based on a pattern formation approach. We used general symmetry properties of the system, to derive an equation motion for it. Our results demonstrated how symmetry breaking and the occurrence of instabilities led to novel and intriguing behavior, such as hysteresis, bistability and dynamical generation of topological defects, not previously captured by existing

models for charge-density wave dynamics. The model is based on the Swift-Hohenberg equation. We showed that, in the proper limits, our model reduced to the commonly used Ginzburg-Landau approach. A remarkable feature of this approach, absent in the commonly used elastic approximation, is that it includes both amplitude and phase fluctuations of the charge-density wave condensate.

Our results clearly demonstrated that, above the global depinning threshold, phase slips appear and lead to an even more disordered structure, in agreement with recent experimental results[1]. Far away from the threshold the system became more ordered. Evidence of this has been seen in recent x-ray scattering experiments[2]. Furthermore, our model also displayed switching, i.e., hysteresis, in qualitative agreement with experimental results[3]. This behavior has not been fully captured by other models of charge-density wave dynamics. The generic inclusion of both amplitude and phase fluctuations suggests that this model can be used to study the nature of the depinning transition, i.e., determining the limits of the elastic approach, as well as if the CDW depinning transition is indeed a dynamical critical phenomenon. Finally, we also note that our results are in qualitative agreement with recent Balents-Fisher theory[4] for periodic systems under influence of quenched disorder.

[1] Ringland et al. [99b].
[2] Ringland et al. [99a].
[3] Zettl and Grüner [82]; Hall and Zettl [84]; Hall, Hundley and Zettl [86]; Sherwin, Zettl and Hall [88]; Lemay et al. [99].
[4] Balents and Fisher [95].

REFERENCES

ABRAHAMS, E. AND TSUNETO, T. [66]. Time variation of the Ginzburg-Landau order parameter. *Phys. Rev.*, **152**(1), 416 (1966).

ADELMAN, T. L., ZAITSEV-ZOTOV, S. V., AND THORNE, R. E. [95]. Field-effect modulation of charge-density-wave transport in $NbSe_3$ and TaS_3. *Phys. Rev. Lett.*, **74**(26), 5264 (1995).

ALAVA, M., KARTTUNEN, M. E. J., AND NISKANEN, K. J. [95]. Residual stresses in plastic random systems. *Europhys. Lett.*, **32**, 143 (1995).

ANDERSON, P. W. [84]. *Basic Notions of Condensed Matter Physics.* Addison-Wesley, Redwood City, CA, 1984.

ANDERSON, P. W., WERTHAMER, N. R., AND LUTTINGER, J. M. [65]. An additional equation in the phenomenology of superconductivity: Resistive effects. *Phys. Rev.*, **138**(4A), A1157 (1965).

BAK, P., TANG, C., AND WIESENFELD, K. [87]. Self-organized criticality: An explanation of the 1/f noise. *Phys. Rev. Lett.*, **59**, 381 (1987).

BALENTS, L. AND FISHER, M. P. A. [95]. Temporal order in dirty driven periodic media. *Phys. Rev. Lett.*, **75**, 4270 (1995).

BARABÁSI, A.-L. AND STANLEY, H. E. [95]. *Fractal Concepts in Surface Growth.* Cambridge University Press, Cambridge, UK, 1995.

BARDEEN, J. [41]. Theory of superconductivity. *Phys. Rev.*, **59**, 928 (1941). Possibility for CDW formation in connection to superconductivity.

BEN-JACOB, E., BRAND, H., DEE, G., KRAMER, L., AND LANGER, J. S. [85]. Pattern propagation in nonlinear dissipative systems. *Physica D*, **14**, 348 (1985).

BHATTACHARYA, S., HIGGINS, M. J., AND STOKES, J. P. [89]. Harmonic generation and scaling behavior in sliding-charge-density-wave conductors. *Phys. Rev. Lett.*, **63**(14), 1503 (1989).

BHATTACHARYA, S., STOKES, J. P., ROBBINS, M. O., AND KLEMM, R. A. [85]. Origin of broadband noise in charge-density-wave conductors. *Phys. Rev. Lett.*, **54**(22), 2453 (1985).

BLOOM, I., MARLEY, A. C., AND WEISSMAN, M. B. [94]. Correlation between broadband noise and frequency fluctuations of narrow-band noise in the charge-density wave in $NbSe_3$. *Phys. Rev. B*, **50**(16), 12218 (1994).

BROCK, J. D., FINNEFROCK, A. C., RINGLAND, K. L., AND SWEETLAND, E. [94]. Detailed structure of a charge-density wave in a quenched random field. *Phys. Rev. Lett.*, **73**(26), 3588 (1994).

BYERS, N. AND YANG, C. N. [61]. Theoretical considerations concerning quantized magnetic flux in superconducting cylinders. *Phys. Rev. Lett.*, **7**(2), 46 (1961).

CAROLI, B., CAROLI, C., AND ROULET, B. [92]. Instabilities of planar solidification fronts. In Godrèche, C., editor, *Solids Far from Equilibrium*, page 155. Cambridge University Press, Cambridge.

CHEN, L. W., BALENTS, L., FISHER, M. P. A., AND MARCHETTI, M. C. [96]. Dynamical transition in sliding charge-density wave with quenched disorder. *Phys. Rev. B*, **54**(18), 12798 (1996).

COPPERSMITH, S. N. [90]. Phase slips and the instability of the Fukuyama-Lee-Rice model of charge-density waves. *Phys. Rev. Lett.*, **65**, 1044 (1990).

COPPERSMITH, S. N. [91]. Pinning energies and phase slips in weakly pinned charge-density waves. *Phys. Rev. B*, **44**, 2887 (1991).

COPPERSMITH, S. N. AND LITTLEWOOD, P. B. [86]. Interference phenomena and mode locking in the model of deformable sliding charge-density waves. *Phys. Rev. Lett.*, **57**(15), 1927 (1986).

COPPERSMITH, S. N. AND MILLIS, A. J. [91]. Diverging strains in the phase-deformation model of sliding charge-density waves. *Phys. Rev. B*, **44**, 7799 (1991).

CROSS, M. C. AND HOHENBERG, P. C. [93]. Pattern formation outside of equilibrium. *Rev. Mod. Phys.*, **65**(3), 851 (1993).

DE GENNES, P. G. [66]. *Superconductivity of Metals and Alloys*. Addision-Wesley, Reading, MA, 1966.

DICARLO, D., MCCARTEN, J., ADELMAN, T. L., MAHER, M. P., AND THORNE, R. E. [94a]. Narrow-band-noise generation in charge-density-wave compounds. *Phys. Rev. B*, **49**(20), 14722 (1994).

DICARLO, D., THORNE, R. E., SWEETLAND, E., SUTTON, M., AND BROCK, J. D. [94b]. Charge-density-wave structure in $NbSe_3$. *Phys. Rev. B*, **50**, 8288 (1994).

DOLAN, G. J. AND JACKEL, L. D. [77]. Voltage measurements within the nonequilibrium region near phase-slip centers. *Phys. Rev. Lett.*, **39**(25), 1628 (1977).

DOMINQUEZ-LERMA, M. A., CANNELL, D. S., AND AHLERS, G. [86]. Eckhaus boundary and wave-number selection in rotating Couette-Taylor flow. *Phys. Rev. A*, **34**(6), 4956 (1986).

ECKHAUS, W. [65]. *Studies in Non-Linear Stability Theory*, volume 6 of *Springer Tracts in Natural Philosophy*. Springer-Verlag, New York, 1965.

EFETOV, K. B. AND LARKIN, A. I. [77]. Charge-density wave in random potential. *Sov. Phys.-JETP*, **45**, 1236 (1977).

ELDER, K. R., VINĀLS, J., AND GRANT, M. [92]. Dynamic scaling and quasiordered states in the two-dimensional Swift-Hohenberg equation. *Phys. Rev. A*, **46**(12), 7618 (1992).

FISHER, D. S. [83]. Threshold behavior of charge-density waves pinned by impurities. *Phys. Rev. Lett.*, **50**, 1486 (1983).

FISHER, D. S. [85]. Sliding charge-density waves as a dynamical critical phenomenon. *Phys. Rev. B*, **31**, 1396 (1985).

FISHER, D. S., FISHER, M. P. A., AND HUSE, D. A. [91]. Thermal fluctuations, quenched disorder, phase transitions, and transport in type-II superconductors. *Phys. Rev. B*, **43**(1), 130 (1991).

FLEMING, R. M. AND GRIMES, C. C. [79]. Sliding-mode conductivity in $NbSe_3$: Observation of a threshold electric field and conduction noise. *Phys. Rev. Lett.*, **42**, 1423 (1979).

FRÖHLICH, H. [54]. On the theory of superconductivity: The one-dimensional case. *Proc. Roy. Soc. A*, **223**, 296 (1954).

FUKUYAMA, H. [76]. Pinning in Peierls-Fröhlich state and conductivity. *J. Phys. Soc. Japan*, **41**(2), 513 (1976).

FUKUYAMA, H. AND LEE, P. A. [78]. Dynamics of charge density wave. I. Impurity pinning in a single chain. *Phys. Rev. B*, **17**(2), 535 (1978).

GARDINER, C. [90]. *Handbook of Stochastic Methods.* Springer-Verlag, Berlin, 2nd edition, 1990.

GILL, J. C. [81]. Transient non-linear phenomena and metastable states of charge-density waves in niobium triselenide. *Solid State Comm.*, **39**, 1203 (1981).

GOLDENFELD, N. [92]. *Lectures on Phase Transitions and the Renormalization Group.* Addison-Wesley, Reading, MA, 1992.

GORKOV, L. P. [58]. On the energy spectrum of superconductors. *Sov. Phys. - JETP*, **7**, 505 (1958).

GORKOV, L. P. AND GRÜNER, G., EDITORS [89]. *Charge Density Waves in Solids.* Elsevier Science Publishers B.V., The Netherlands, 1989.

GRAHAM, R. [73]. Generalized thermodynamic potential for the convection instability. *Phys. Rev. Lett.*, **31**(25), 1479 (1973).

GRAHAM, R. [74]. Hydrodynamic fluctuations near the convection instability. *Phys. Rev. A*, **10**(5), 1762 (1974).

GRÜNER, G. [88]. The dynamics of charge-density waves. *Rev. Mod. Phys.*, **60**, 1129 (1988).

GRÜNER, G. [94]. *Density waves in solids.* Addison-Wesley, Reading, MA, 1994.

GRÜNER, G., ZAWADOWSKI, A., AND CHAIKIN, P. M. [81]. Nonlinear conductivity and noise due to charge-density-wave depinning in $NbSe_3$. *Phys. Rev. Lett.*, **46**(7), 511 (1981).

GRÜNER, G. AND ZETTL, A. [85]. Charge density wave conduction: A novel collective transport phenomenon in solids. *Phys. Rep.*, **119**, 117 (1985).

HALL, R. P., HUNDLEY, M. F., AND ZETTL, A. [86]. Switching and phase-slip centers in charge density-wave conductors. *Phys. Rev. Lett.*, **56**(22), 2399 (1986).

HALL, R. P., HUNDLEY, M. F., AND ZETTL, A. [88]. Switching and charge-density-wave transport in $NbSe_3$. I. dc characteristics. *Phys. Rev. B*, **38**(18), 13002 (1988).

HALL, R. P. AND ZETTL, A. [84]. Charge density wave depinning and switching in $NbSe_3$. *Solid State Comm.*, **50**(9), 813 (1984).

HERNÁNDEZ-GARCÍA, E., VIÑALS, J., TORAL, R., AND SAN MIGUEL, M. [93]. Fluctuations and pattern selection near an Eckhaus instability. *Phys. Rev. Lett.*, **70**, 3576 (1993).

HIGGINS, M. J., MIDDLETON, A. A., AND BHATTACHARYA, S. [93]. Scaling near mode locking in a charge density wave conductor. *Phys. Rev. Lett.*, **70**(24), 3784 (1993).

HU, J. AND WESTERVELT, R. M. [95]. Collective transport in two-dimensional magnetic bubble arrays. *Phys. Rev. B*, **51**(23), 17279 (1995).

IMRY, Y. AND MA, S. [75]. Random-field instability of the ordered state of continuous symmetry. *Phys. Rev. Lett.*, **35**, 1399 (1975).

KARDAR, M., PARISI, G., AND ZHANG, Y. C. [86]. Dynamic scaling of growing interfaces. *Phys. Rev. Lett.*, **56**, 889 (1986).

KARTTUNEN, M., ELDER, K. R., TARLIE, M., AND GRANT, M. [99a]. Nonequilibrium behavior of driven quasi-one-dimensional superconducting wires. *In preparation*, (1999).

KARTTUNEN, M., HAATAJA, M., ELDER, K. R., AND GRANT, M. [99b]. Model of driven charge-density waves. *Submitted to Phys. Rev. Lett.*, (1999).

KARTTUNEN, M., HAATAJA, M., ELDER, K. R., AND GRANT, M. [99c]. Theory of dynamics of driven CDWs. *In preparation*, (1999).

KARTTUNEN, M., PROVATAS, N., ALA-NISSILA, T., AND GRANT, M. [98]. Nucleation, growth, and scaling in slow combustion. *J. Stat. Phys.*, **90**(3/4), 1401 (1998).

KEDVES, F. J., MÉSZÁROS, S., VAD, K., HALÁSZ, G., KESZEI, B., AND MIHÁLY, L. [87]. Estimation of maximum electrical resistivity of high T_c superconducting ceramics by the Meissner effect. *Solid State Comm.*, **63**(11), 991 (1987).

KESSLER, D. A., LEVINE, H., AND TU, Y. [91]. Interface fluctuations in random media. *Phys. Rev. B*, **43**(8), 4551 (1991).

KOSCHMIEDER, E. L. [66]. On convection on a uniformly heated plane. *Beitr. Phys. Atmos.*, **39**, 1 (1966).

KOSHELEV, A. E. AND VINOKUR, V. M. [94]. Dynamic melting of the vortex lattice. *Phys. Rev. Lett.*, **73**(26), 3580 (1994).

KOSTERLITZ, J. [74]. The critical properties of the two-dimensional XY model. *J. Phys. C*, **7**, 1046 (1974).

KOSTERLITZ, J. M. AND THOULESS, D. J. [72]. Long range order and metastability in two dimensional solids and superfluids. *J. Phys. C*, **5**, L124 (1972).

KRAMER, L. AND BARATOFF, A. [77]. Lossless and dissipative current-carrying states in quasi-one-dimensional superconductors. *Phys. Rev. Lett.*, **38**(9), 518 (1977).

KRAMER, L. AND RANGEL, R. [84]. Structure and properties of the dissipative phase-slip state in narrow superconducting filaments with and without inhomogeneities. *J. Low. Temp. Phys.*, **57**(3/4), 391 (1984).

KRAMER, L., SCHOBER, H. R., AND ZIMMERMANN, W. [88]. Pattern competition and the decay of unstable patterns in quasi-one-dimensional systems. *Physica D*, **31**, 212 (1988).

KRAMER, L. AND ZIMMERMANN, W. [85]. On the Eckhaus instability for spatially periodic patterns. *Physica D*, **16**(221) (1985).

KRUG, J. AND SPOHN, H. [90]. Kinetic roughening of growing surfaces. In Godrèche, C., editor, *Solids Far From Equilibrium: Growth, Morphology and Defects*, chapter Ch. 6, page 479. Cambridge University Press, Cambridge.

KUITTU, M.-P., HAATAJA, M., PROVATAS, N., AND ALA-NISSILA, T. [98]. Dynamics of driven interfaces near isotropic percolation transition. *Phys. Rev. E*, **58**(2), 1514 (1998).

LANGER, J. S. [80]. Instabilities and pattern formation in crystal growth. *Rev. Mod. Phys.*, **52**, 1 (1980).

LANGER, J. S. AND AMBEGAOKAR, V. [67]. Intrinsic resistive transition in narrow superconducting channels. *Phys. Rev.*, **164**(2), 498 (1967).

LEE, P. A. AND RICE, T. M. [79]. Electric field depinning of charge density waves. *Phys. Rev. B*, **19**(8), 3970 (1979).

LEE, P. A., RICE, T. M., AND ANDERSON, P. W. [74]. Conductivity from charge or spin density waves. *Solid State Comm.*, **14**, 703 (1974).

LEMAY, S. G., THORNE, R. E., LI, Y., AND BROCK, J. D. [99]. Evidence for quasi-periodic collective creep in charge-density-wave systems. *preprint*, (1999).

LEVY, J., SHERWIN, M. S., ABRAHAM, F. F., AND WIESENFELD, K. [92]. Unified model of switching and nonswitching charge-density-wave dynamics. *Phys. Rev. Lett.*, **68**(19), 2968 (1992).

LITTLE, W. A. [67]. Decay of persistent currents in small superconductors. *Phys. Rev.*, **156**(2), 396 (1967).

LITTLEWOOD, P. [89]. Computer simulations of CDW dynamics. In Gorkov, L. P. and Grüner, G., editors, *Charge Density Waves in Solids*, chapter Ch. 8. Elsevier, Amsterdam.

LITTLEWOOD, P. B. [86]. Sliding charge-density waves: A numerical study. *Phys. Rev. Lett.*, **33**(10), 6694 (1986).

MATSUKAWA, H. [86]. Static and dynamic properties of charge-density-waves described by the Fukuyama-Lee-Rice model. I. Perturbational analysis on the dc+ac combined phenomena. *J. Phys. Soc. Jpn.*, **56**, 1522 (1986).

MATSUKAWA, H. AND TAKAYAMA, H. [86a]. Numerical study of statics and dynamics of charge-density-waves based on Fukuyama-Lee-Rice model. *Physica B*, **143**, 80 (1986).

MATSUKAWA, H. AND TAKAYAMA, H. [86b]. Static and dynamic properties of charge-density-waves described by the Fukuyama-Lee-Rice model. I. Perturbational analysis and dc nonlinear properties. *J. Phys. Soc. Jpn.*, **56**, 1507 (1986).

MCCUMBER, D. E. [68]. Intrinsic resistive transition in thin superconductive wires driven from current sources. *Phys. Rev.*, **172**(3), 427 (1968).

MCCUMBER, D. E. AND HALPERIN, B. I. [70]. Time scale of intrinsic resistive fluctuations in thin superconductive wires. *Phys. Rev. B*, **1**(3), 1054 (1970).

MIDDLETON, A. A. [92]. Asymptotic uniqueness of the sliding state for charge-density waves. *Phys. Rev. Lett.*, **68**, 670 (1992).

MIDDLETON, A. A. AND FISHER, D. S. [91]. Critical behavior of pinned charge-density waves below the threshold of sliding. *Phys. Rev. Lett.*, **66**, 92 (1991).

MIDDLETON, A. A. AND FISHER, D. S. [93]. Critical behavior of charge-density waves below threshold: Numerical and scaling analysis. *Phys. Rev. B*, **47**(7), 3530 (1993).

MONCEAU, P., EDITOR [85a]. *Electronic properties of inorganic quasi-one-dimensional compounds. Part I - Theoretical.* D. Reidel Publishing Company, Dordrecht, 1985.

MONCEAU, P., EDITOR [85b]. *Electronic properties of inorganic quasi-one-dimensional compounds. Part II - Experimental.* D. Reidel Publishing Company, Dordrecht, 1985.

MONCEAU, P., ONG, N. P., PORTIS, A. M., MEERSCHAUT, A., AND ROUXEL, J. [76]. Electric field breakdown of charge-density-wave-induced anomalies in $NbSe_3$. *Phys. Rev. Lett.*, **37**(10), 602 (1976).

MONCEAU, P., RICHARD, J., AND RENARD, M. [80]. Interference effects of the charge-density-wave motion in $NbSe_3$. *Phys. Rev. Lett.*, **45**(1), 43 (1980).

MYERS, C. R. AND SETHNA, J. P. [93a]. Collective dynamics in a model of sliding charge-density waves. I. Critical behavior. *Phys. Rev. B*, **47**(17), 11171 (1993).

MYERS, C. R. AND SETHNA, J. P. [93b]. Collective dynamics in a model of sliding charge-density waves. II. Finite-size effects. *Phys. Rev. B*, **47**(17), 11194 (1993).

NARAYAN, O. AND FISHER, D. S. [93]. Threshold critical dynamics of driven interfaces in random media. *Phys. Rev. B*, **48**(10), 7030 (1993).

NAYFEH, A. H. [81]. *Introduction to Perturbation Techniques.* John Wiley, New York, 1981.

NELSON, D. R. AND TONER, J. [81]. Bond-orientational order, dislocation loops, and melting of solids and smectic-a liquid crystals. *Phys. Rev. B*, **24**(1), 363 (1981).

NEWELL, A. C., PASSOT, T., AND LEGA, J. [93]. Order parameter equations for patterns. *Ann. Rev. Fluid Mech.*, **25**, 399 (1993).

ONG, N. P., VERMA, G., AND MAKI, K. [84]. Vortex-array model for charge-density-wave conduction noise. *Phys. Rev. Lett.*, **52**, 663 (1984).

ONSAGER, L. AND MACHLUP, S. [53]. Fluctuations and irreversible processes. *Phys. Rev.*, **91**(6), 1505 (1953).

PEIERLS, R. [30]. Zur Theorie der elektrischen und thermischen Leitfähigkeit von Metallen. *Ann. Phys. (Leipzig)*, **4**, 121 (1930).

PEIERLS, R. E. [55]. *Quantum Theory of Solids*. Oxford University Press, New York, 1955.

PINES, D. AND NOZIÉRES, P. [66]. *The Theory of Quantum Liquids*, volume I, Normal Fermi Liquids. W.A. Benjamin, Inc., New York, 1966.

POMEAU, Y. AND MANNEVILLE, P. [79]. Stability and fluctuations of a spatially periodic convective flow. *J. Physique Lett. (Paris)*, **23**, L–609 (1979).

PROVATAS, N., ALA-NISSILA, T., GRANT, M . ELDER, K. R., AND PICHÉ, L. [95]. Scaling, propagation and kinetic roughening of flame fronts in random media. *J. Stat. Phys.*, **81**, 737 (1995).

RAMAKRISHNA, S. [93]. Phase slip and current flow in finite samples of charge-density-wave materials. *Phys. Rev. B*, **48**, 5025 (1993).

RAMAKRISHNA, S., MAHER, M. P., AMBEGAOKAR, V., AND ECKERN, U. [92]. Phase slip in charge-density-wave systems. *Phys. Rev. Lett.*, **68**, 2066 (1992).

RIEGER, T., SCALAPINO, D. J., AND MERCEREAU, J. E. [72]. Time-dependent superconductivity and quantum dissipation. *Phys. Rev. B*, **6**(5), 1734 (1972).

RINGLAND, K. L., FINNEFROCK, A. C., LI, Y., BROCK, J. D., LEMAY, S. G., AND THORNE, R. E. [99a]. Observation of scaling in sliding charge-density waves. *Preprint*, (1999).

RINGLAND, K. L., FINNEFROCK, A. C., LI, Y., BROCK, J. D., LEMAY, S. G., AND THORNE, R. E. [99b]. Scaling in charge-density-wave relaxation: Time resolved x-ray scattering measurements. *Phys. Rev. Lett.*, **82**, 1923 (1999).

ROBBINS, M. O., STOKES, J. P., AND BHATTACHARYA, S. [85]. Charge-density-wave depinning: A dynamical critical phenomenon? *Phys. Rev. Lett.*, **55**(25), 2822 (1985).

ROSS JR., J. H., WANG, Z., AND SLICHTER, C. P. [90]. NMR studies of $NbSe_3$: Electronic structures, static charge-density-wave measurements, and observations of the moving charge-density waves. *Phys. Rev. B*, **41**(5), 2722 (1990).

SCHMID, A. [66]. A time dependent Ginzburg-Landau equation and its application to the problem of resistivity in the mixed state. *Phys. Kond. Mat.*, **5**, 302 (1966).

SHERWIN, M. AND ZETTL, A. [85]. Complete charge-density-wave mode locking and freeze-out of fluctuations in $NbSe_3$. *Phys. Rev. B*, **32**(8), 5536 (1985).

SHERWIN, M. S., ZETTL, A., AND HALL, R. P. [88]. Switching and charge-density-wave transport in $NbSe_3$. III. Dynamical instabilities. *Phys. Rev. B*, **18**(38), 13028 (1988).

SIBANI, P. AND LITTLEWOOD, P. B. [90]. Critical dynamics of a pinned elastic medium in two and three dimensions: A model for charge-density waves. *Phys. Rev. Lett.*, **64**(11), 1305 (1990).

SKOCPOL, W. J., BEASLEY, M. R., AND TINKHAM, M. [74]. Phase-slip centers and nonequilibrium processes in superconducting tin microbridges. *J. Low Temp. Phys.*, **16**, 145 (1974).

SNEDDON, L., CROSS, M. C., AND FISHER, D. S. [82]. Sliding conductivity of charge-density-waves. *Phys. Rev. Lett.*, **49**(4), 292 (1982).

STEPHEN, M. J. AND SUHL, H. [64]. Weak time dependence in pure superconductors. *Phys. Rev. Lett.*, **13**(26), 797 (1964).

SWIFT, J. AND HOHENBERG, P. C. [77]. Hydrodynamic fluctuations at the convective instability. *Phys. Rev. A*, **15**, 319 (1977).

TANG, C., WIESENFELD, K., BAK, P., COPPERSMITH, S., AND LITTLEWOOD, P. [87]. Phase organization. *Phys. Rev. Lett.*, **58**(12), 1161 (1987).

TARLIE, M. B. AND ELDER, K. R. [98]. Metastable state selection in one-dimensional systems with a time-ramped control parameter. *Phys. Rev. Lett.*, **81**(1), 18 (1998).

TARLIE, M. B. AND MCKANE, A. J. [98]. Unstable decay and state selection. *J. Phys. A*, **31**(3), L71 (1998).

TIDECKS, R. [90]. *Current Induced Nonequilibrium Phenomena in Quasi-One-Dimensional Superconductors*, volume 121 of *Springer Tracts in Modern Physics*. Springer-Verlag, Berlin, 1990.

TILLEY, D. R. AND TILLEY, J. [90]. *Superfluidity and Superconductivity*. Graduate Student Series in Physics. Institute of Physics Publishing, London, 3rd edition, 1990.

TINKHAM, M. [96]. *Introduction to Superconductivity*. International Series in Pure and Applied Physics. McGraw-Hill, New York, 2nd edition, 1996.

TORRENT, M. C. AND SAN MIGUEL, M. [88]. Stochastic-dynamics characterization of delayed laser threshold instability with swept control parameter. *Phys. Rev. A*, **38**(1), 245 (1988).

TUCKERMAN, L. S. AND BARKLEY, D. [90]. Bifurcation analysis of the Eckhaus instability. *Physica D*, **46**, 57 (1990).

TÜTTÖ, I. AND ZAWADOWSKI, A. [85]. Quantum theory of local perturbation of the charge-density wave by an impurity: Friedel oscillations. *Phys. Rev. B*, **32**, 2449 (1985).

WEBB, W. W. AND WARBURTON, R. J. [68]. Intrinsic quantum fluctuations in uniform filamentary superconductors. *Phys. Rev. Lett.*, **20**(9), 461 (1968).

ZENG, C., LEATH, P. L., AND FISHER, D. S. [99]. Absence of Bragg glass. *Phys. Rev. Lett.*, **82**, 1935 (1999).

ZETTL, A. AND GRÜNER, G. [82]. Onset of charge-density-wave conduction: Switching and hysteresis in $NbSe_3$. *Phys. Rev. B*, **26**, 2298 (1982).